Dynamic combinatorial chemistry for the multiplexed identification of glyco-dyn[n]arenes in an anti-adhesive strategy against Pseudomonas aeruginosa

Fanny Demontrond, Yoann Pascal, Marion Donnier-Maréchal, Corentin Raillon, Baptiste Luton, Clara de la Tramblais, Laurent Vial, David Gueyrard, Wessam Galia, Emmanuelle Berger, et al.

Dynamic combinatorial chemistry for the multiplexed identification of glyco-dyn[n]arenes in an anti-adhesive strategy against *Pseudomonas aeruginosa*

Fanny Demontrond,[a] Yoann Pascal,[a] Marion Donnier-Maréchal,[a] Corentin Raillon,[a] Baptiste Luton,[b] Clara De la Tramblais,[c] Laurent Vial,[a] David Gueyrard,[a] Wessam Galia,[b] Emmanuelle Berger,[b] Alain Géloën,[b] Benoit Cournoyer,[b] Julien Leclaire,[a] and Sébastien Vidal[a,c]*

[a] *Institut de Chimie et Biochimie Moléculaires et Supramoléculaires, UMR 5246, CNRS, Université Claude Bernard Lyon 1, Université de Lyon, INSA Lyon, CPE Lyon, Villeurbanne, 69622, France*

[b] *UMR Ecologie Microbienne, CNRS 5557, INRAE 1418, Research Group «Bacterial Opportunistic Pathogens and Environment», VetAgro Sup, Aisle 3, 1st Floor, 69280 Marcy L'Etoile, France*

[c] *Institut de Chimie des Substances Naturelles, UPR 2301, CNRS, Université Paris-Saclay, Gif-sur-Yvette, 91198, France, sebastien.vidal@cnrs.fr*

This article is dedicated to Sir James Fraser Stoddart and Prof Jeremy K. M. Sanders who have inspired this work through their pioneering studies in supramolecular chemistry.

Abstract: Carbohydrate-protein interactions are of prime importance in cell-cell communication, signal transduction, cancer, bacterial or viral infection. Chemists have designed multivalent systems to mimick these recognition phenomena and provide potent ligands of these proteins with foreseen therapeutic applications. Dynamic combinatorial chemistry provides access to a library of chemical species in equilibrium through reversible covalent bonds. This strategy can be readily applied to the rapid and efficient identification of multivalent glycoclusters by introducing a protein into the equilibrating library for the selection of the fittest glycocluster for this protein. 1,4-Dithiophenols conjugated to monosaccharides were equilibrated into dynamic combinatorial libraries providing a diverse mixture of glycoclusters. Selection of the best ligand for different lectins (ConA, LecA and LecB from *Pseudomonas aeruginosa*) could increase the concentration of glyco-dyn[3]arenes and glyco-dyn[4]arenes. A key aspect of this strategy is that multiplexing can be readily achieved by using two building blocks (galactosylated and fucosylated 1,4-dithiophenols) to interrogate several lectins at once in a single experiment. These macrocyclic glycoclusters could be synthesized, isolated, then evaluated as ligands of the lectins and displayed nanomolar dissociation constants. Furthermore, while no toxicity could be detected against human cells or bacteria, their evaluation as anti-adhesive agents could be confirmed through a virulence assay on human A549 lung epithelial cells.

Introduction

Carbohydrates are present at the cell surface and are taking part to the cell's communication with other healthy cells.[1-4] But they are also involved in the recognition by pathogens (bacteria, viruses) for the very first step of infection, i.e. adhesion to the host cell.[5-7] Bacteria will take advantage of a series of proteins (lectins or adhesins) present at their membrane, at the tip of their flagellum or pili to recognize specific oligosaccharidic structures at the host cell surface. When adhesion is secured, the bacteria will be internalized and deliver their cytotoxins or will reach a density that will trigger an

accumulation of quorum sensing molecules (e.g. homoserinelactones), then hasten their cell division, generate a biofilm, release toxins and become problematic or fatal to the host cells. The carbohydrate-lectin interactions are usually quite weak in terms of affinity, typically in the millimolar range.[8-9] Such interactions in nature are governed by multivalent interactions through lectin clustering at the cell surface, most of lectins being multimeric as the assembly of four and up to six monomeric units. Such multivalent interactions can provide a stronger carbohydrate-lectin interaction through multivalency. Chemists have designed a series of biomimetic strategies to tackle bacterial infections through two approaches.[10-12] The first one resides on a "medicinal chemistry" strategy in which the structure of the lectin and its natural ligand are known. The chemist and biochemist would then team up to generate a series of carbohydrate analogues of the natural ligand, largely termed as glycomimetics, and identify the most potent ligand of the lectin through intensive structure-activity relationship studies. This approach has been successfully applied for the design of potent FimH ligands against *Escherichia coli* urinary tract infections,[13-19] or targeting Galectin-3 in pulmonary fibrosis.[20-24] Another competitive strategy for the design of high affinity ligands of lectins is based on multivalency, meaning the design of multivalent glycoconjugates displaying multiple copies of the same and simple monosaccharide on a central core. The multivalent glycoconjugates can be based on small organic molecules (e.g. calixarene, pillararene, fullerene, porphyrin, peptide) and will be called a glycocluster.[11-12, 25] Several glycoclusters have been demonstrated as protective against bacterial infection up to the animal model and are very promising approaches.[26-28] While antibiotics are killing the bacteria and create a selection of the most resistant bacterial strains during a medical treatment, multivalent glycoconjugates are limiting the bacterial infection through anti-adhesion of the bacteria to the host cell, thus avoiding selective pressures on the bacterial strain and the emergence of resistance phenotypes.[29-32] For these reasons, glycoscientists have designed a large series of multivalent systems for interfering with bacterial adhesion. Nevertheless, like in every drug design process, the synthesis of each candidate with subtle structural variations can be time consuming prior a production of the additional datasets required to progress from a "hit" to a "lead" candidate.

This is where dynamic combinatorial chemistry (DCC) comes into play, offering the possibility to reversibly assemble simple building blocks into multivalent architectures under mild conditions.[33] In dynamic combinatorial libraries (DCLs), thermodynamic control implies that altering experimental conditions can induce changes in library composition. In theory, DCLs are sensitive to many external influences, such as temperature, pressure or light.[34] In practice, the response of libraries to a template target has been the most studied. Introducing a template (*e.g.*, a protein) within a thermodynamically-controlled library of multivalent ligands was shown to shift the equilibrium towards the best binder(s), in an amplification process that is, after all, the way in which biomolecules have evolved their sophisticated functions.[35-36] If amplification is selective for the compound(s) that binds most strongly to the template, then DCC conveniently enables both the detection and the isolation of hit candidate(s).

A scarce number of examples of dynamic combinatorial chemistry applied for the identification of lectin ligands have been reported (Figure 1). The very first study by Ramström and Lehn used glycoside appended with a thiol-functionalized linker arm.[37] The disulfide exchange DCL was analyzed by reverse phase HPLC through UV absorption of the aromatic aglycon. Selection of the bis-mannoside ligand was observed when adding a sepharose-bound Concanavalin A (ConA), a lectin binding to mannose epitopes. While a valency of only two carbohydrate epitopes could be reached in the latter study, a follow-up investigation by the same group took advantage of acyl-hydrazone reversible covalent bond formation to explore higher valencies based on benzaldehyde aglycons and mono- di- or tri-hydrazide core scaffolds.[38] DCLs of up to 474 constituents were generated and the identification of the best ligand for ConA was performed through a novel assay involving an enzyme-linked lectin assay (ELLA). This

assay was implemented in a 96-well plate and dynamic deconvolution was applied based on the removal of a single building block from the complete library. A trivalent ligand with micromolar affinity towards ConA was finally identified through this strategy. A few years later, Reeh and de Mendoza designed a DCL library of glycoclusters based on Fe(II)-bipyridine complexes providing valencies of six carbohydrate epitopes.[39] Analysis of the DCL was readily performed by reverse phase HPLC through UV absorption of the bipyridine moiety. Sepharose-bound ConA was incorporated into the equilibrating DCLs and a hexa-mannoside glycocluster was clearly identified as the best ligand for ConA. Fulton et al. have used a polyacrylamide appended with benzaldehyde groups for the reversible covalent condensation with hydrazide-functionalized carbohydrates.[40] DCLs were studied by ^{1}H NMR and the incorporation of galactose or mannose moieties was analyzed in the presence of either ConA (for mannose) or *Escherichia coli* heat labile toxin (LTB, for galactose). The best binding polymers could be isolated and their association constants with lectins evaluated.

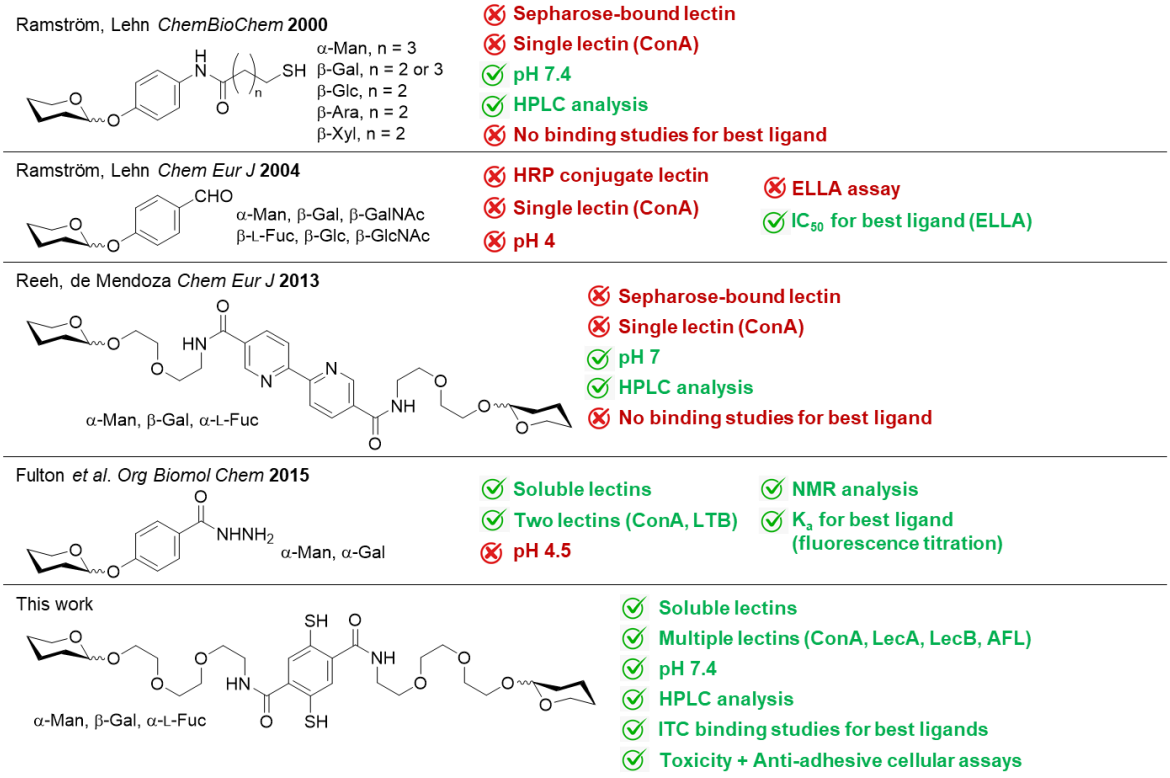

Figure 1. Pioneering studies on dynamic combinatorial chemistry with glycosylated architectures and their conditions and results

These precedents have paved the way to further studies in the context of dynamic combinatorial chemistry applied to the rapid and efficient identification of glycoclusters as high affinity ligands of lectins. Nevertheless, they suffer from a few drawbacks such as the use of sepharose-bound lectins which does not allow for an easy analysis of a large array of lectins since these are not always commercially available either as pure biomaterials or as polymer-supported. The best ligands identified were not always assayed against the lectin to clearly demonstrate their improved binding properties. The only lectin studied was thus the model lectin ConA which is typically used as a proof of concept but has no therapeutic implications, and a rather tedious ELLA assay was required to fully deconvolute the properties of the glycoclusters in the DCLs.[38] Acyl-hydrazone exchange is typically performed at pH 4.0-4.5 and is not always perfectly compatible with the stability of the lectin.[38, 40]. Spontaneous disulfide bond formation and exchange take place in aqueous solutions within pH range 7 to 9, and can be halted by reducing the pH below the pKa of the thiols involved. This inherent

thermodynamic sensitivity has been harnessed by researchers such as Prof Jeremy K. M. Sanders[41-43] and others[44-45] to create intricate molecular architectures and receptors in aqueous media. In this world of disulfide exchange-based DCC,[46] some also explored and developed over the last decade a new family of dynamic cyclophanes named dyn[n]arenes, which are based on mono- to tetra-functionalized 1,4-dithiophenol units linked by disulfide bridges.[47] We have recently demonstrated that a set of driving forces such as templating, folding and stacking lead to the selection and amplification of dyn[n]arenes of different composition, size and stereochemistry.[48-51] Furthermore, the unraveling of interactions involved in the dyn[n]arenes assembly processes not only led to the identification of novel physicochemical phenomena like the hydrophilic effect,[52] but also to innovative applications such as chiroptical sensing of biomolecules.[53]

Here, we describe an innovative approach for the design of high affinity lectin ligands through dynamic combinatorial chemistry which will address drawbacks reported before (Figure 2). The reversible covalent bond is a disulfide exchange of 1,4-dithiophenols that can equilibrate in buffer solution compatible with lectins stability and at neutral pH. Our approach reconsidered several aspects of the experimental setup developed so far to provide improved DCL conditions and generate novel outputs for glycoscience applications (Figure 1). The lectins used in the assays were not bound to sepharose or other polymer, nor conjugated to a horse radish peroxidase (HRP) for ELLA assay, but rather used in their native form in buffer solutions. Multiple lectins were readily used in the present study with a possibility for multiplexing several lectins with a single reference DCL for a rapid identification of the best glycoclusters in a single experimental process. Lectins of therapeutic interest from Pseudomonas aeruginosa have been studied and very high affinity glycoclusters could be identified, isolated and assayed against the lectin by ITC for a confirmation of their nanomolar affinities and also in a cellular assay to monitor their anti-adhesive properties.

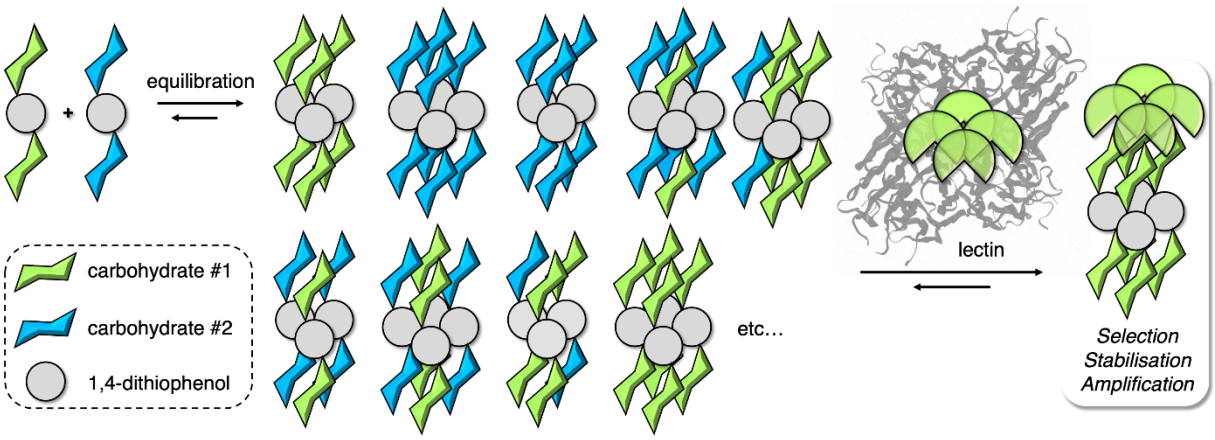

Figure 2. Schematic representation of the 1,4-dithiophenol equilibration of dynamic combinatorial libraries of glycosylated dyn[n]arenes and influence of a lectin on the composition of the library

Results and Discussion

Synthesis of 1,4-dithiophenol building blocks

The glycosylated 1,4-dithiophenol building blocks were obtained through amide bond formation between an amino-functionalized glycoside and a protected dicarboxylic acid (Scheme 1). 1,4-dithiophenol-2,5-dicarboxylic acid **1**[54] required a protection of the thiols with 2-cyanoethyl to the bis-carboxylic acid **2** to provide a robust and reproducible amidation. Previous attempts of amidation with the bis-thiocarbamates protected thiols afforded only low yields for the desired amides. Then, the

azido-functionalized glycoside precursor was initially conjugated with the bis-acid **2** under Staudinger-Villarasa conditions but with only low yields (20-30%) and concomitant formation of partially deacetylated byproducts. The azido moiety was then reduced into the amine but further amidation again produced up to 15% of deacetylated byproducts very difficult to separate from the desired amine. To avoid deacetylation, an ammonium tosylate intermediate **4** was obtained by reduction of the azido-carbohydrates **3** under hydrogenation conditions with a stoichiometric amount of *p*-toluenesulfonic acid (TsOH).[55] The subsequent amidation using the diacid **2** afforded the desired glycosylated 1,4-dithiophenol intermediates **5** in good yields and high purity. The simultaneous deprotection of acetate esters on the carbohydrate moiety and the 2-cyanoethyl groups at the thiophenol was performed in a single step using cesium hydroxide[56] to afford the desired fully deprotected glycosylated 1,4-dithiophenol building blocks **6**.

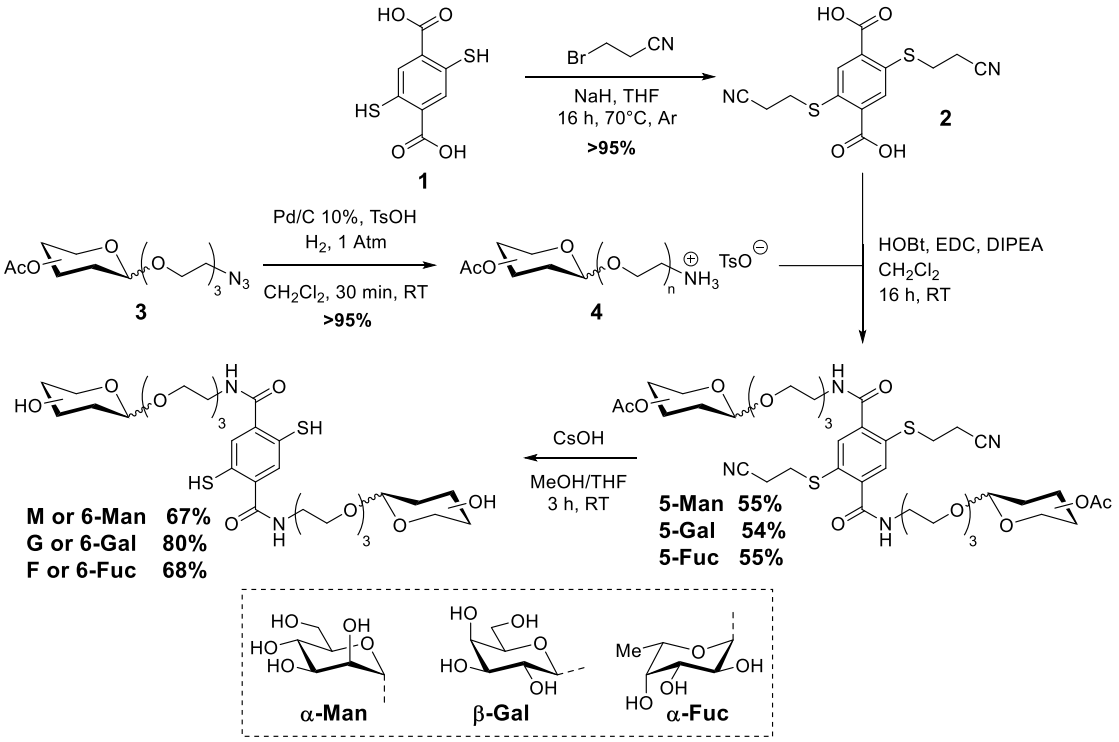

Scheme 1. Synthesis of the glycosylated 1,4-dithiophenol building blocks

Equilibration and study of dynamic combinatorial libraries (DCLs)

Disulfides are prone to oligomerization under neutral pH in solution, and oxidation can occur with the assistance of oxygen dissolved in the solvent. 1,4-Dithiophenols will similarly generate linear oligomers in solution with two residual thiophenols which can trigger cyclization for trimers, tetramers, or pentamers and so on (Figure 3). One reason is that dihedral angle around the S-S bond is typically close to 90° creating a helicoidal-type conformation bringing the residual thiophenols in close vicinity thus favoring the ring closing of such oligomers. Equilibration is in general considered as complete when the composition of the DCL is not evolving anymore and can be analyzed by reverse phase UHPLC using the UV absorbance of the aromatic 1,4-dithiophenol core.

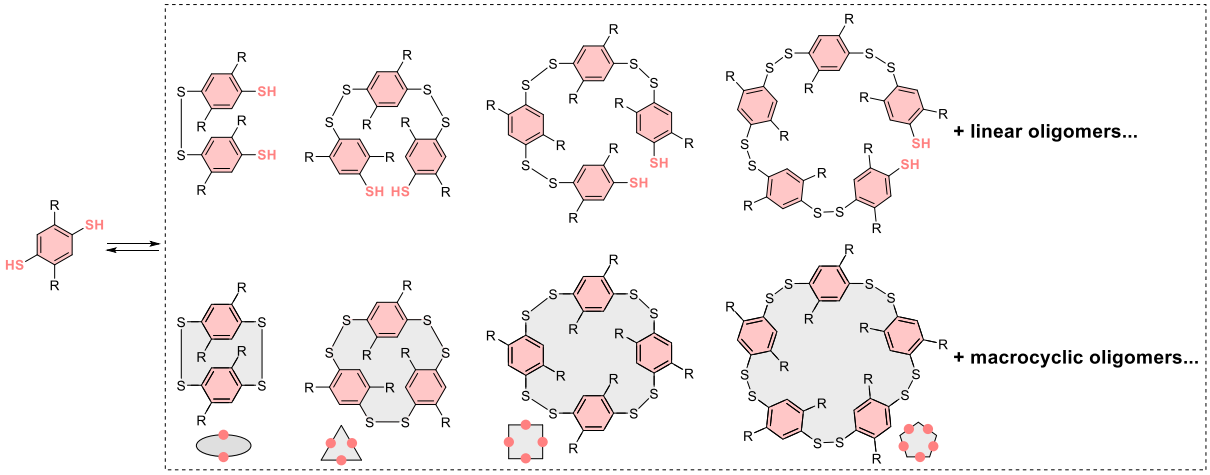

Figure 3. Schematic representation of the oligomerization process for 1,4-dithiophenols in the DCLs

The DCL equilibration was studied using the fucosylated 1,4-dithiophenol building block **F** alone in solution with a particular attention for the determination of the operating conditions (Figure 4). Stirring rate of the solution did not influence the equilibration of the **F**-DCL (Figure 4a), nor did the addition of NaCl and $CaCl_2$ since most lectins require exogenous Ca^{2+} for proper binding (Figure 4b) or the type of buffer used (Figure 4c, Tris or PBS). Concentration of **F** in solution had a strong influence on the DCL equilibration since at low concentration (0.4 mM) a large proportion of the **F** building block was oxidized to sulfenic (RSOH) or sulfinic acids (RSO_2H) with characteristic mass spectrometry *m/z* values of M+16 or M+32 (Figure 4d). The oxidation into two sulfenic acids on both thiols or one thiol remaining with a sulfinic acid could not be distinguished. This is problematic since oxidized **F** species cannot participate to the DCL equilibration as they are not thiols anymore and hence their presence must be reduced to the lowest proportion as possible. This was readily achieved by using higher concentration (4 mM) of 1,4-dithiophenol **F** in the DCL solution. Thus, the amount of oxygen dissolved in the solvent was much less important in comparison to the concentration of the equilibrating **F** building block and the oxidized species were limited to less than 5% in relative quantity. Finally, temperature of equilibration of the DCL did not have a major impact other than extending the time required for equilibration (3 h at 22°C, 72 h at 4°C) but the low temperature conditions allowed the complete removal of oxidized species (Figure 4e). A typical DCL equilibration was finally performed at room temperature in a few hours, using the required buffer solution for the lectin and at 4 mM concentration of 1,4-dithiophenol the building block with stirring.

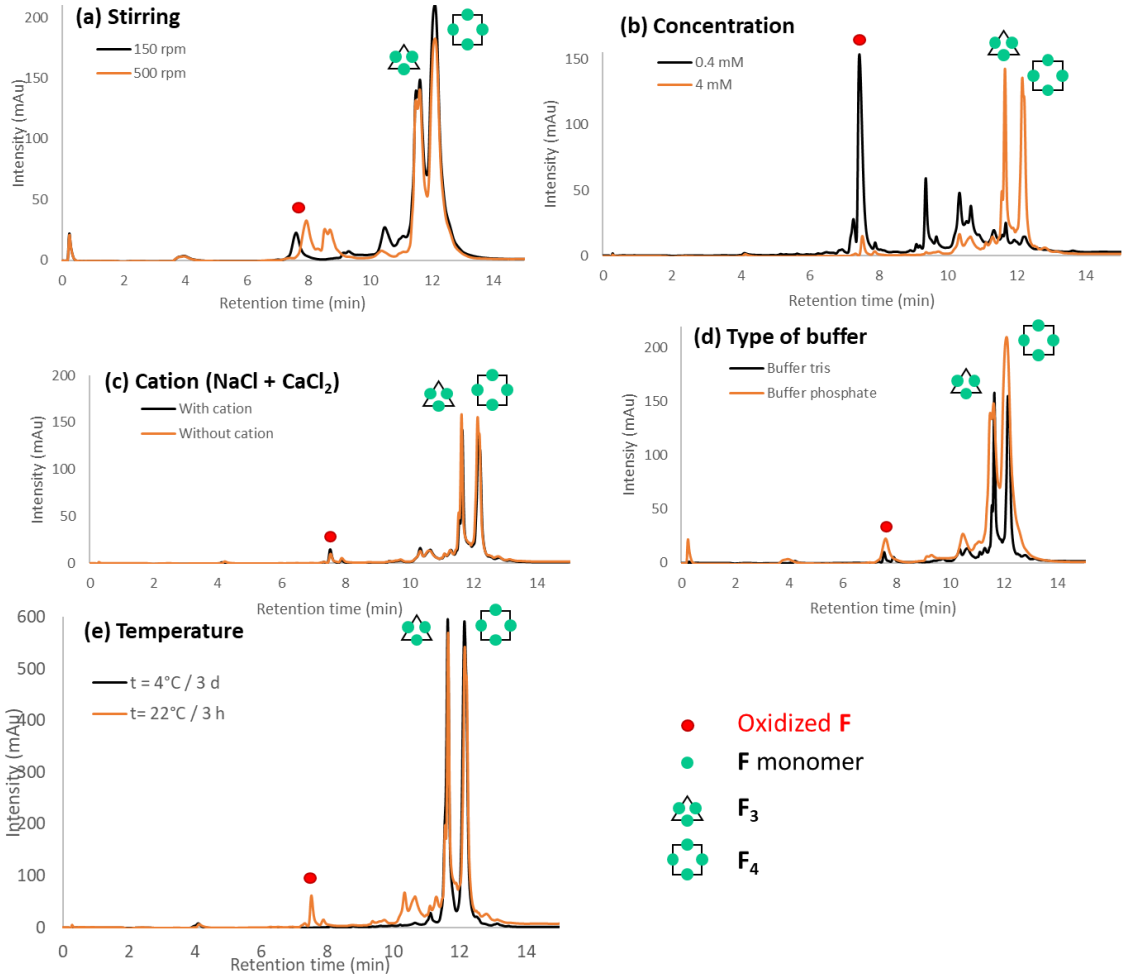

193

194 **Figure 4.** Influence of several parameters on an equilibrated DCL of **F** after > 7 h. (a) stirring ([**F**] = 4
195 mM, 200 mM PBS, 22°C), (b) addition of Na^+ or Ca^{2+} ([**F**] = 4 mM, 200 mM Tris, 22°C, 100 mM NaCl, 100
196 µM $CaCl_2$), (c) type of buffer ([**F**] = 4 mM 200 mM PBS or 200 mM Tris, 22°C), (d) concentration ([**F**] =
197 0.4 or 4 mM, 200 mM Tris, 22°C), or (e) temperature ([**F**] = 4 mM, 200 mM Tris, 4°C or 22°C).

198 The kinetic analysis of the DCL equilibration was performed with the mannosylated 1,4-dithiophenol
199 **M** (Figure 5). At t=0, the monomer **M** can be observed at ca. 7 min retention time (RT) with a very tiny
200 amount of oligomerized species (ca. 10 min at RT). Equilibration then takes place in a few hours to
201 reach the disappearance of the monomer **M** after 3.5 h. After 0.5 h, a portion of oxidized **M** species
202 appeared and stayed constant over the course of the equilibration. Oligomeric species are growing
203 over the course of the equilibration of the DCL and appear at ca. 10 min at RT and are mainly composed
204 of macrocyclic $\mathbf{M_3}$ and $\mathbf{M_4}$. The retention times had enough difference to clearly identify these species
205 and their mass spectrometry data were matching their molecular formula and composition. Therefore,
206 DCLs can be readily equilibrated at room temperature in a buffer solution and the equilibrium can be
207 reached within 3 to 4 hours. The DCL composition can be determined from UHPLC-MS data and a series
208 of macrocyclic oligomers are typically observed.

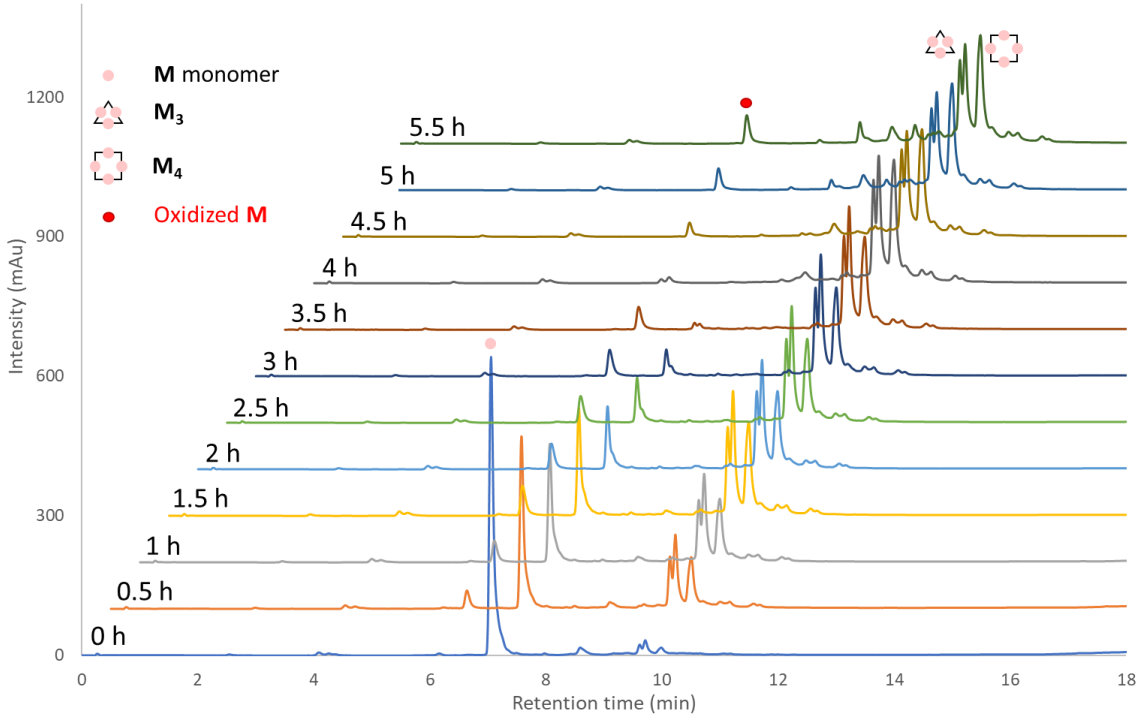

Figure 5. UHPLC-MS analysis of the DCL using the **M** building block (RT, [**M**] = 4 mM, 200 mM Tris buffer)

*Study of DCL composed of **M** and **F** building blocks in the presence of ConA*

DCLs containing two different 1,4-dithiophenol building blocks have been studied. Their equilibration with and without lectin will provide information about the identification of the best ligand for that lectin in solution if the proportion of one of these species is increased. A (**M**+**F**)-DCL containing equimolar amounts of each building block at a total concentration of 4 mM (2 mM each) was equilibrated to reach equilibrium within a few hours. The resulting DCL composition was determined by UHPLC-MS analysis (Figure 6). The first important observation is that all possible heteroglycoclusters based on trimers and tetramers can be observed and characterized in the UHPLC-MS data. They all appeared at different retention times from 5 to 15 minutes, due to the difference in polarity between the mannose and fucose moieties: fucose building block **F** being more apolar than the mannosylated one **M**, the retention time increased with the increasing number of **F** in the macrocycles.

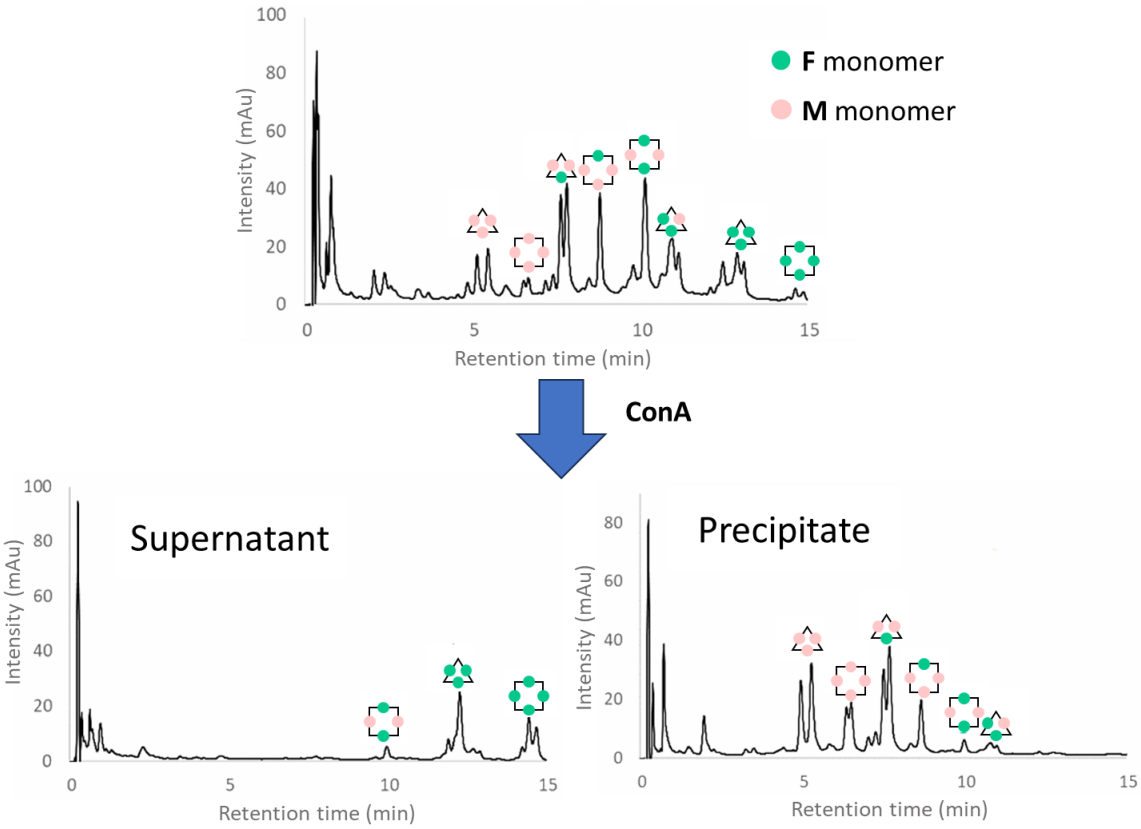

Figure 6. Equilibration of DCLs composed of **M** and **F** building blocks and influence of ConA on the composition. **M**:**F** (1:1, 4 mM), ConA (4 mM) in buffer Tris 200 mM, NaCl 100 mM, $CaCl_2$ 100 µM, at RT

The same (**M**+**F**)-DCL equilibration was performed in the presence of ConA in the solution. A reference (**M**+**F**)-DCL was equilibrated during 3.5 h at room temperature and with a concentration of 4 mM (to minimize oxidation of the thiols). After that, this reference DCL was aliquoted into a new DCL and diluted 10x with buffer to reach 0.4 mM concentration of **M**+**F**. The lectin (ConA, 0.4 mM) was then added and the DCL equilibrated for an additional 2.5 h and a precipitate appeared in the solution. The precipitate was recovered by centrifugation and the supernatant separated. The precipitate contained the macrocycles with high affinity to the lectin that created a large three-dimensional network of aggregated proteins and glycoclusters that crushed out of the solution. This precipitate was treated with 1M HCl to unfold the protein and release the glycoclusters in solution that could be analyzed by UHPLC-MS. This precipitate was composed mainly of $\mathbf{M_3}$ and $\mathbf{M_4}$ glycoclusters. As a consequence, the supernatant contained mostly the fucosylated species that could not bind to the mannose-specific ConA lectin.

The relative proportions of each macrocycle can be obtained through the area under the curve (AUC) of the UHPLC chromatograms and allow the monitoring of the increase/decrease of each macrocycle in the (**M**+**F**)-DCL with or without the ConA lectin (Figure 7). The increase of the $\mathbf{M_3}$ can be clearly identified along with an increase in $\mathbf{M_4}$ while the proportion of most of the heteroglycoclusters composed of **M** and **F** building blocks decrease in the DCL. The increased proportion of $\mathbf{M_3}$ and $\mathbf{M_4}$ can be attributed to the selection of these high affinity ligands by the ConA lectin. This will be later confirmed by ITC studies of these glycoclusters with ConA. Hence, ConA triggered the re-organization of the (**M**+**F**)-DCL to favor the organization of the **M** building blocks into homoglycoclusters $\mathbf{M_3}$ and $\mathbf{M_4}$ by decreasing the amount of heteroglycoclusters which displayed a poorer affinity for the lectin. As a consequence, the increased proportion of fucosylated species ($\mathbf{F_3}$ and $\mathbf{F_4}$) could be attributed to the

fact that if the **M** building blocks are brought together by ConA, then the remaining **F** building blocks do not have any other outcome than to assemble together into macrocyclic oligomers $\mathbf{F_3}$ and $\mathbf{F_4}$. ITC binding studies of the fucosylated macrocycles $\mathbf{F_3}$ and $\mathbf{F_4}$ were performed to demonstrate that these compounds have no affinity for the ConA lectin and therefore could not be selected by the lectin in the equilibrating (**M**+**F**)-DCL.

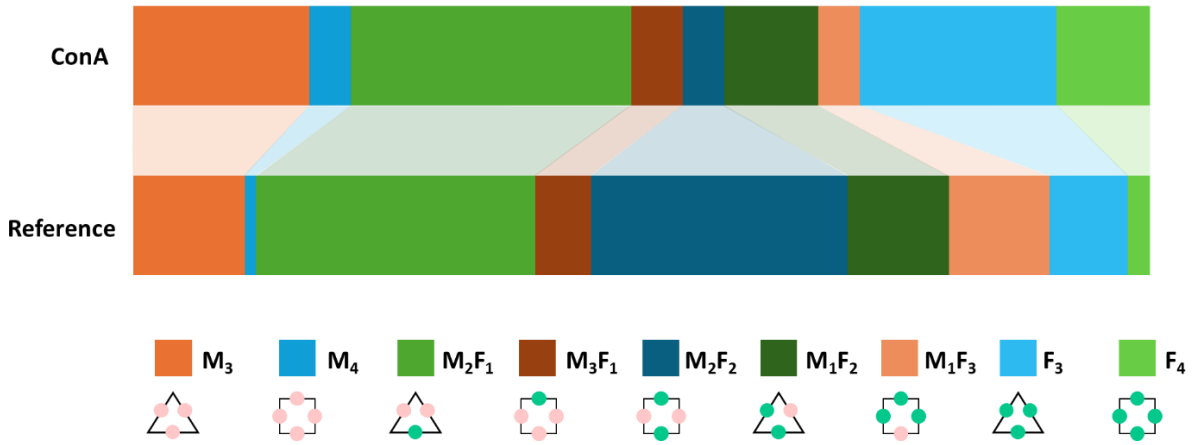

Figure 7. Comparison of the reference DCL to the ConA amplified DCL combining materials from the supernatant and precipitate fractions. Measurements were performed in triplicate and did not differ by more than 5%.

Purification of the macrocyclic glycoclusters $\boldsymbol{X_3/X_4}$

The trimeric and tetrameric macrocycles $\mathbf{X_3/X_4}$ had to be purified from the equilibrated DCLs. For that purpose, DCLs of **M**, **G** or **F** building blocks were equilibrated at low temperature (4°C) during 72 h to limit oxidation, and the resulting DCL composed mostly of $\mathbf{X_3/X_4}$ was purified by preparative HPLC to collect the macrocycles (Figure 8). It is worth pointing out that the macrocycles $\mathbf{X_3}$ and $\mathbf{X_4}$ were obtained pure after preparative HPLC, but rearrangements were always observed during evaporation of solvents from the collected fractions and also after a few hours in solution, preventing ITC studies with lectins. Two sets of peaks were typically observed in the UHPLC chromatogram for each species ($\mathbf{X_3}$ or $\mathbf{X_4}$) and were due to the intrinsic chirality of the S-S bond which provides diastereoisomers for each disulfide linkage.[48] Due to these limitations in reaching pure macrocycles, the mixture of $\mathbf{X_3/X_4}$ was analyzed by ITC and the exact composition of the solution was determined for each individual measurement. The molecular weight of $\mathbf{X_3/X_4}$ was calculated as the ratio of each macrocycle and according to the AUC proportion in the UHPLC chromatogram.

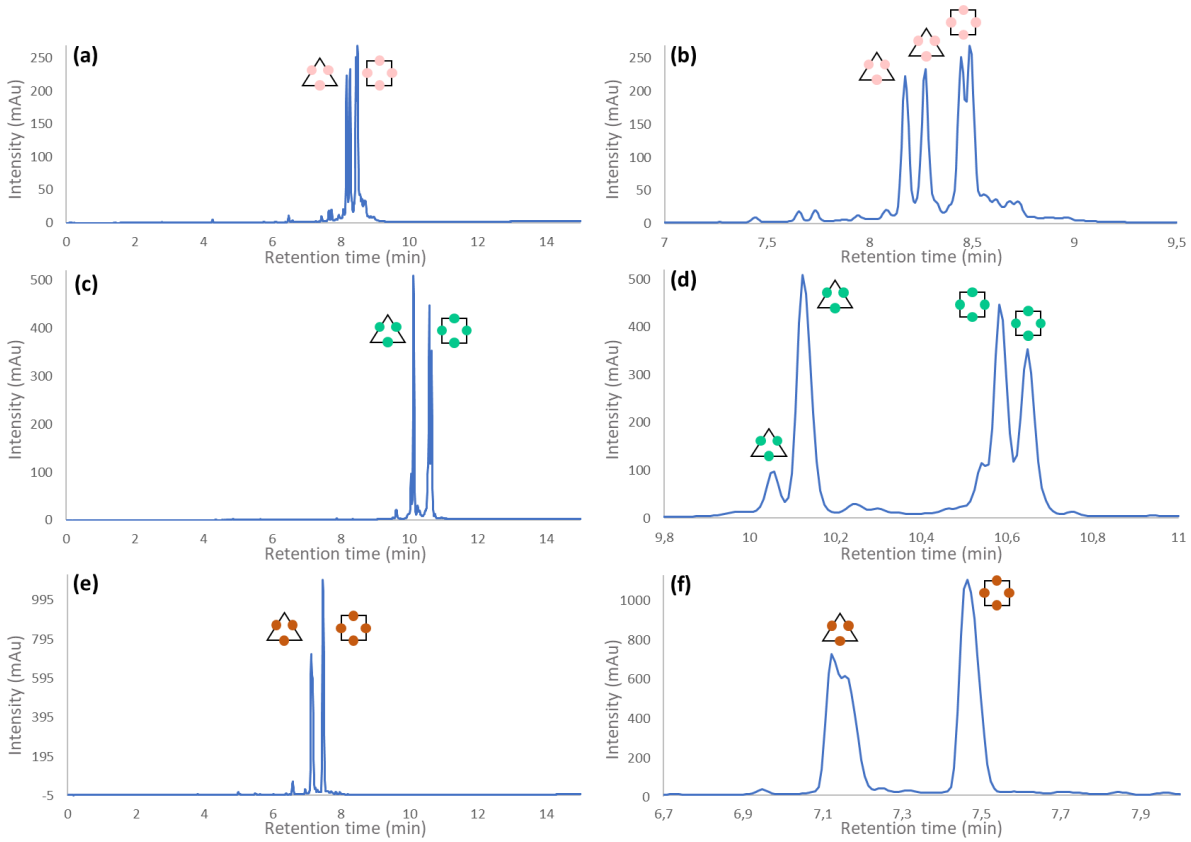

Figure 8. UHPLC chromatograms of glycosylated dyn[n]arenes after typical equilibration and purification by preparative HPLC. (a,b) **M_3/M_4**, (c,d) **F_3/F_4** and (e,f) **G_3/G_4** in buffer Tris 200 mM, NaCl 100 mM, $CaCl_2$ 100 µM, at RT.

ITC binding studies of **M_3/M_4** *with ConA*

The affinity of the mannosylated glycoclusters **M_3/M_4** was verified by isothermal titration microcalorimetry (ITC) to quantify the multivalent interactions between ConA and the ligands. Titration provided a sigmoidal curve which is representative of a strong affinity of the ligands for ConA with a 60-fold improvement of affinity (β) in comparison to the monovalent reference ligand methyl α-D-mannopyranoside (**α-D-ManOMe**) (Figure 9).

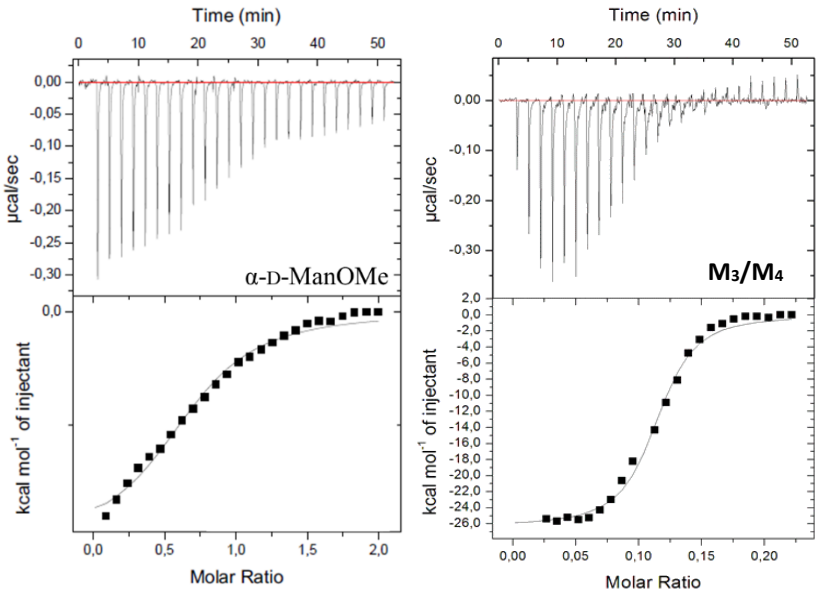

Figure 9. Isothermal titration microcalorimetry (ITC) analysis of the binding properties toward ConA (0.12 mM) for **α-D-ManOMe** (1.8 mM, left panel) and the association titration curve obtained with a 1:1 binding model (lower left panel). ITC data obtained for injections of **M_3/M_4** (0.2 mM, 1:1) into a solution of ConA (0.12 mM) and the associated titration curve (lower right panel).

Analysis of the ITC data (Table 1) also provided information about the stoichiometry of the glycoclusters' complexes with ConA, and the *n* value of 0.09 indicates that, theoretically, up to 11 lectin monomers can be involved in binding events simultaneously with the glycoclusters. Since the valency of **M_3** is of 6 mannose units and 8 for the **M_4** macrocycle, this *n* value indicates that nearly all mannosides are involved in an interaction with ConA, and thus a multivalent interaction is responsible for the improvement of affinity (β). This result indicates that the higher multivalency (6 to 8 valency) reached with the oligomerized **M_3/M_4** is indeed responsible for the sharp increase in affinity (β = 61) towards ConA reaching nanomolar affinity. For comparative purposes, it is to be noted that the affinity of a calixarene-based tetravalent ligand (**Calix-Man_4**, Figure S1) of ConA was reported in the nanomolar range,[26] similar to the macrocycles **M_3/M_4**, meaning that both are high affinity ligands for this lectin.

Table 1. ITC data for the binding properties of glycosylated dyn[n]arenes **M_3/M_4** and tetravalent **Calix-Man_4** towards ConA

Ligand	*n*	-Δ*H* (kJ.mol^{-1})	-TΔ*S* (kJ.mol^{-1})	K_d (nM)	β[a]
α-D-ManOMe	0.67 ± 0.02	8.53 ± 0.06	18.6 ± 0.4	18 000	1
M_3/M_4[b]	0.09 ± 0.02	106.6 ± 24.7	5.8 ± 2.1	294	61
Calix-Man_4	0.25 ± 0.02	104.6 ± 4.2	68.7 ± 3.9	540	33.3

[a] β is the binding potency calculated as the ratio of the monovalent **α-D-ManOMe** reference K_d value to the K_d value of the multivalent compound. [b] Values obtained from four independent measurements.

Multiplexing of DCLs for the simultaneous rapid identification of high affinity ligands of three lectins (LecA, LecB and AFL)

Having demonstrated that 1,4-dithiophenol building blocks could oligomerize in solution and that the resulting DCL could be influenced by the addition of an external stimulus (lectin) to generate the best fit ligands of that protein, the concept was then pushed one step further by designing a multiplexed

experiment in which several lectins were used as external stimuli for the identification of their best ligands, in a single experiment. First, a selection of three lectins from pathogens has been selected. *Pseudomonas aeruginosa* is a bacterium responsible for lung infections and is highly resistant to antimicrobials. Two lectins have been reported as virulence factors in this species, namely LecA which has a strong affinity for galactose ligands, and LecB for fucose. *Aspergillus fumigatus*, a fungus, responsible for lung infections, was also found to bind host cells through an AFL lectin which has affinity for fucose. Both pathogens are significant infectious agents that can benefit from the design of innovative therapeutic approaches. By using the galactosylated and fucosylated building blocks **G** and **F**, respectively, a multiplexed system of DCL can be readily setup for the identification in a single experiment of each high affinity ligand for all three lectins (Figure 10 and Figure S7).

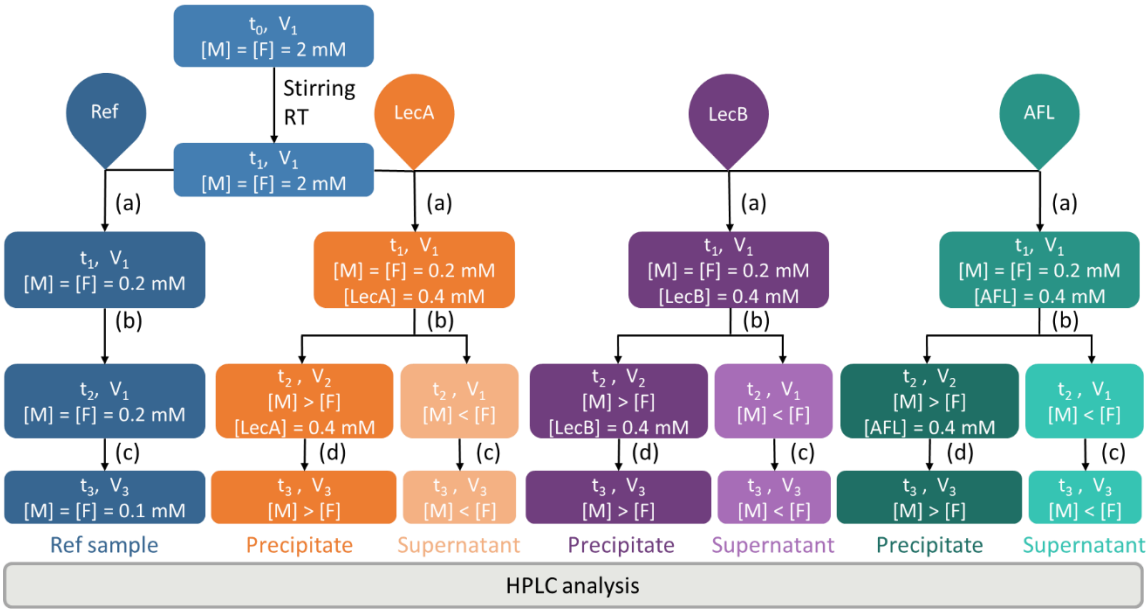

Figure 10. Simultaneous analysis of the DCL equilibration for three different lectins (LecA, LecB and AFL) and comparison to a reference DCL in buffer Tris 200 mM, NaCl 100 mM, $CaCl_2$ 100 µM, at RT. V_1 = 500 µL ; V_2 = 0 µL ; V_3 = 1000 µL; (a) Dilution ×10 - Stirring, RT; (b) Centrifugation; (c) Dilution with HCl 1M; (d) Dilution with HCl 1M, Dilution ×2 Buffer. For complete information, please see supporting information.

A (**G**+**F**)-DCL was equilibrated at 4 mM and the progress of equilibration of monitored by UHPLC. When the amount of **G** and **F** monomers reached less than 15% of the DCL composition, the reference (**G**+**F**)-DCL was diluted 10x then separated into four different 0.4 mM DCLs and each of them were exposed to 0.4 mM of the lectin to be studied (LecA, LecB and AFL) or a reference DCL buffer. The reactions were monitored by UHPLC, and when the **G** and **F** monomers were totally consumed, DCLs were centrifuged to separate the precipitate containing the lectins and the high affinity ligands from the supernatant (containing the non-specific macrocycles). UHPLC-MS analyses were used to quantify the amount of each macrocycle in the respective DCL reactions.

UHPLC-MS analyses of the reference DCL revealed that galactosylated macrocycles could not be detected, but several heteroglycoclusters could be identified clearly as well as homoglycoclusters (Figure 11). Some compounds could not be assigned to any structure (e.g. t = 2.6 min, *m/z* = 661, representing 1.6% in the mixture), and oxidized building block **G** could be observed at a retention time of ca. 4.3 min which represented less than 5% in the DCL constituents.

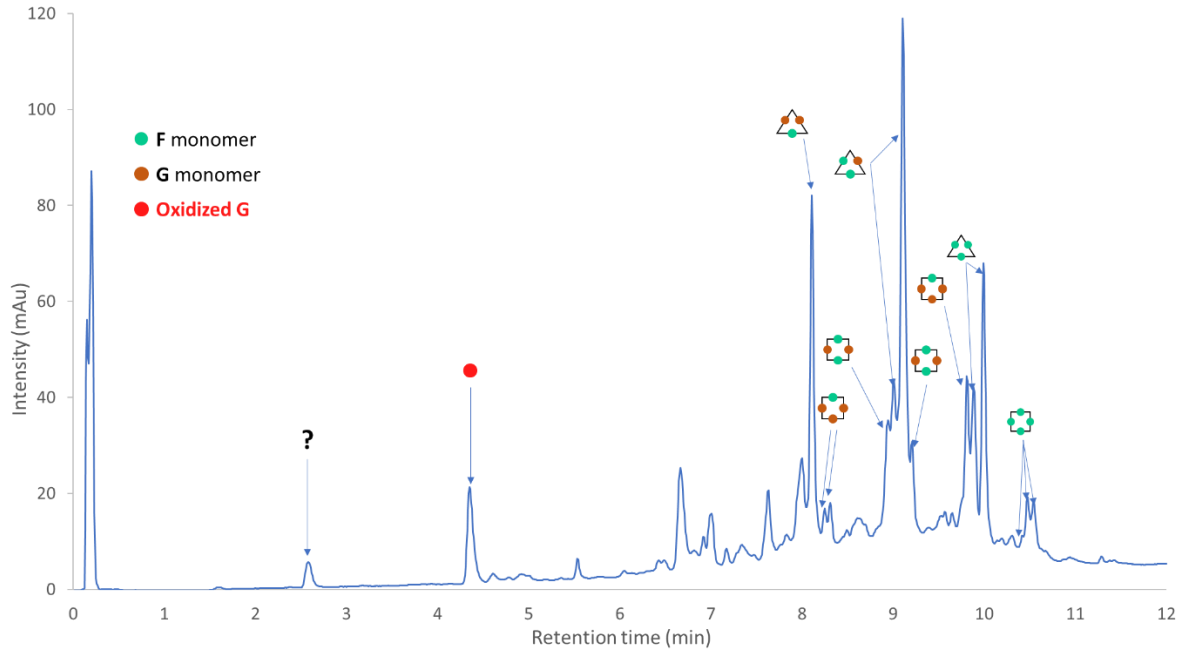

Figure 11. Equilibration of the reference DCL composed of **G/F** building blocks (1:1, 4 mM) in buffer Tris 200 mM, NaCl 100 mM, $CaCl_2$ 100 µM, at RT during 36 h

The LecA-(**G**+**F**)-DCL was analyzed by UHPLC from its precipitate and supernatant samples (Figure 12). The overall composition of the DCL was changed in comparison to the reference DCL. The first observation was an emergence of $\mathbf{G_3}$ and $\mathbf{G_4}$ macrocycles in the precipitate sample. The addition of the LecA lectin therefore modified the distribution of the hetero- and homoglycoclusters with the hetero-species decreasing drastically in proportion and the homoglycoclusters becoming the major species in the DCL. Some changes are important such as the heteroglycocluster $\mathbf{G_2F_2}$ which decreased by ca. 80% in the presence of LecA, but also $\mathbf{G_1F_2}$ (74% decrease) and $\mathbf{G_1F_3}$ (50% decrease) while homoglycoclusters such as $\mathbf{F_3}$ and $\mathbf{F_4}$ have increased by 69% and 174%, respectively (Figure 13). As previously observed in the ConA-DCLs, the addition of the galactose-specific LecA lectin triggered the scrambling of the (**G**+**F**)-DCL favoring the formation of $\mathbf{G_3}$ and $\mathbf{G_4}$ glycoclusters, along with the corresponding $\mathbf{F_3}$ and $\mathbf{F_4}$ macrocycles that would rearrange together. A peak at t = 4.8 min could not be assigned to a compound and displayed a molecular weight of 1159 $g.mol^{-1}$ that represented 20% in the precipitate sample (Figure 12a). In the supernatant, an unknown compound at t = 2.5 min was also observed with a molecular weight of 648 $g.mol^{-1}$ (Figure 12b).

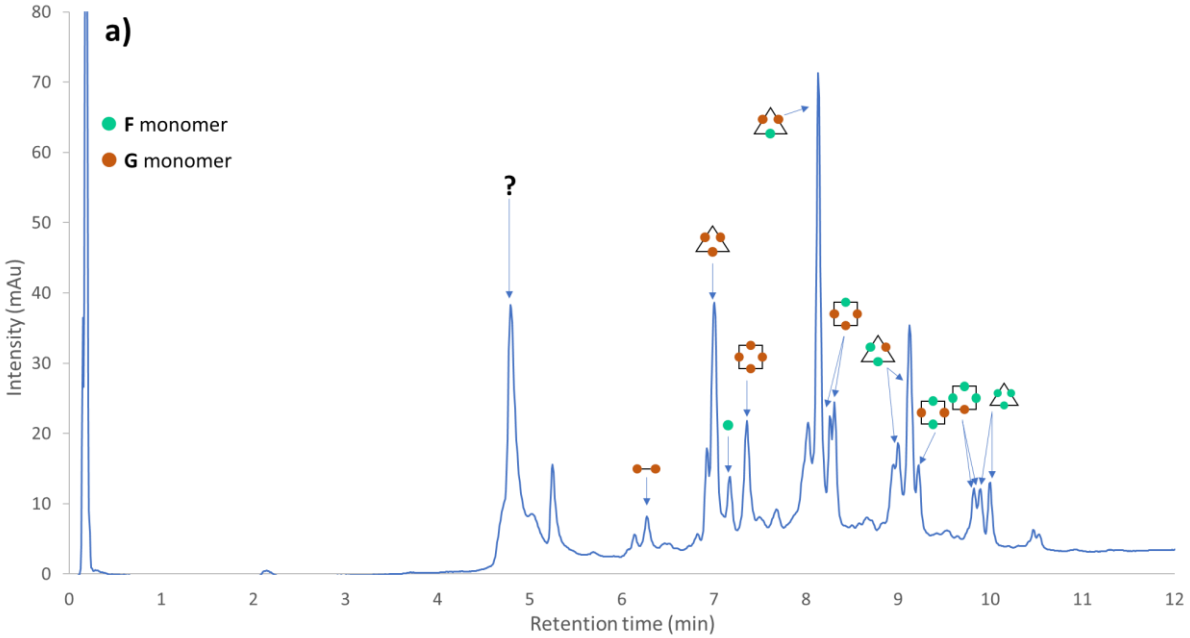

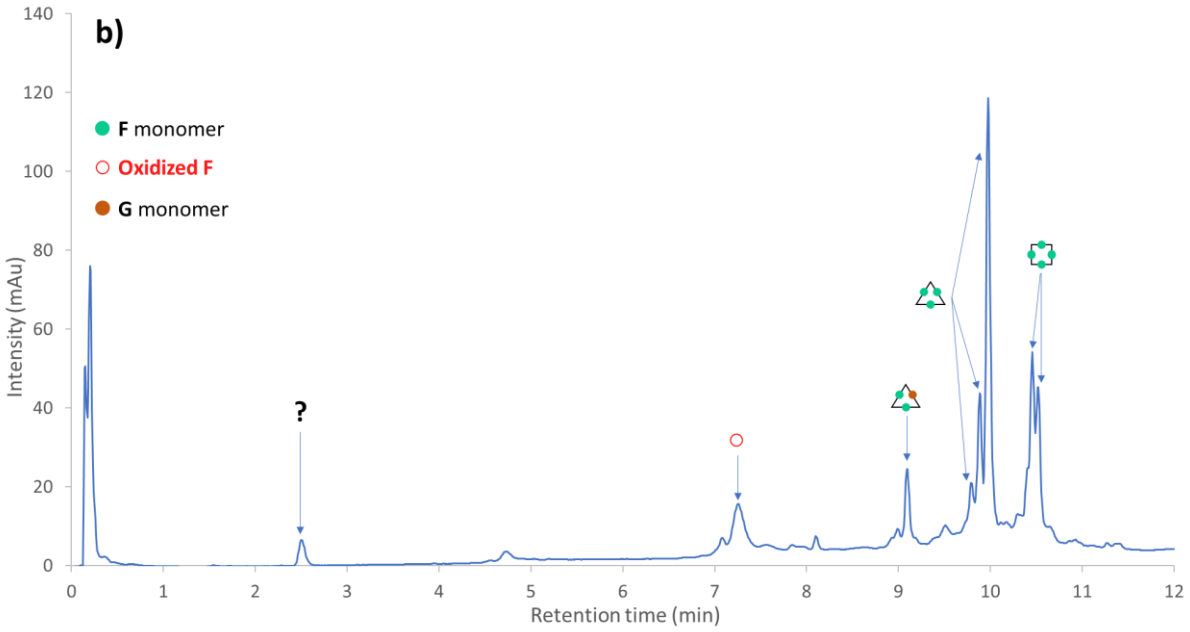

Figure 12. UHPLC analysis of the **G/F** (1:1, 0.4 mM) DCL after incubation with LecA (0.4 mM) with the (a) precipitate and (b) supernatant

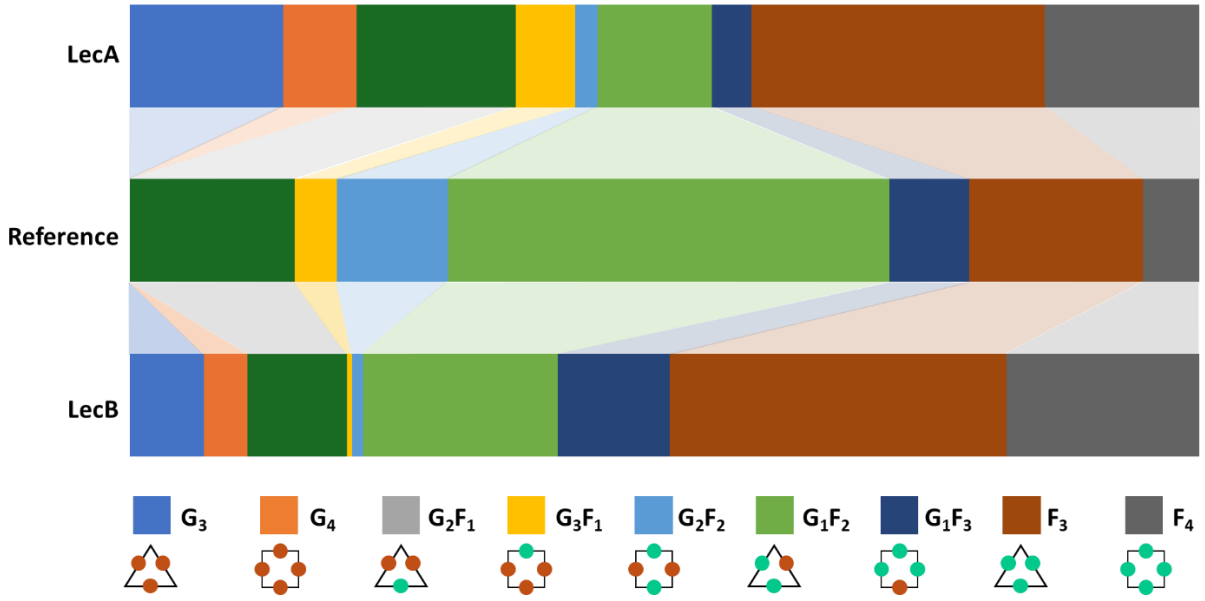

Figure 13. Comparison of the reference **G/F** DCL to the LecA (top) and LecB (bottom) amplified DCL combining materials from the supernatant and precipitate fractions. Measurements were performed in triplicate and did not differ by more than 5%.

The LecB-(**G**+**F**)-DCL was then analyzed similarly by UHPLC-MS (Figure S2) using precipitate and supernatant samples. A modification of the reference DCL composition was clearly observed with the appearance of $\mathbf{G_3}$ and $\mathbf{G_4}$ species in the supernatant as non specific LecB ligands (Figure S2b). Heteroglycoclusters $\mathbf{G_2F}$, $\mathbf{G_3F}$, $\mathbf{G_2F_2}$ and $\mathbf{GF_2}$ decreased quite drastically in the DCL mixture (52%, 79%, 82% and 55% respectively) while the homoglycoclusters $\mathbf{F_3}$ and $\mathbf{F_4}$ increased by 73% 272% respectively (Figure 13). The same unknown compounds at t = 2.6 min (4%) and t = 4.8 minutes (5%) observed with LecA could be detected but at a very limited proportion in the whole DCL (Figure S2b).

Finally, the AFL-(**G**+**F**)-DCL was setup and processed as the other DCLs. Nevertheless, after equilibration and centrifugation, the supernatant tended to further precipitate and lead to suspended matters (Figure S3). A filtration through Amicon filters provided a filtrate but their UHPLC-MS analyses could not provide exploitable data. AFL displayed low nanomolar affinities for the multivalent ligands designed here (see ITC studies, *vide infra*). Therefore, the precipitation of AFL with the multivalent ligands in the DCL library might occur at much lower concentrations in comparison to LecA or LecB rendering the processing of the DCL analysis more complex and unsuccessful so far. The same DCL could have been performed with lower amounts of lectin but a minimum amount of 0.2 mM in lectin was necessary for the proper analysis of the DCLs to reach a reliable signal-to-noise ratio in the UHPLC-MS analyses (data not shown).

ITC binding studies of $\mathbf{G_3}$/$\mathbf{G_4}$ *and* $\mathbf{F_3}$/$\mathbf{F_4}$ *with LecA, LecB and AFL*

The $\mathbf{G_3}$/$\mathbf{G_4}$ macrocycles could be purified by preparative UHPLC and then assayed by ITC to determine their binding properties towards LecA, the galactose-specific lectin from *Pseudomonas aeruginosa* (Figure S4, Table 2). The stoichiometry of the $\mathbf{G_3}$/$\mathbf{G_4}$ to LecA complexes was measured as n = 0.10. This value indicates that up to ten lectin monomers can interact simultaneously with the glycoclusters. The maximum valency of the $\mathbf{G_4}$ glycocluster was 8 which would suggest a stoichiometry of n = 0.125. This n value suggested that nearly all galactose ligands were interacting with a lectin. This slight difference could be explained by the low precipitation observed in the ITC titration experiment within the last

injections of the titration (Figure S4). A dissociation constant of 185 nM was measured which represented an increase in affinity (β) of 378 in comparison to the monovalent LecA ligand reference methyl β-D-galactopyranoside (**β-D-GalOMe**). This high affinity was very much comparable to the **Calix-Gal$_4$** (Figure S1) that displayed nanomolar affinity for LecA. A negative control was measured with the **F$_3$/F$_4$** glycoclusters that did not display any binding to LecA with a titration curve that was totally flat (Figure S4). The strong binding to LecA observed for the **G$_3$/G$_4$** glycoclusters was indeed due to the specific binding of galactoside epitopes since the core framework of the glycocluster of **F$_3$/F$_4$** glycoclusters did not interact with the lectin.

Table 2. ITC data for the binding properties of glycosylated dyn[n]arenes **G$_3$/G$_4$** towards LecA

Ligand	*n*	-Δ*H* (kJ.mol^{-1})	-TΔ*S* (kJ.mol^{-1})	K$_d$ (nM)	β[a]
β-D-GalOMe[b]	0.80	39.0	15.0	70 000	1
G$_3$/G$_4$[c]	0.10 ± 0.01	158.3 ± 8.3	119.7	185	378
Calix-Gal$_4$[d]	0.24 ± 0.01	104 ± 1	65.0	176	398

[a] β is the binding potency calculated as the ratio of the monovalent **β-D-GalOMe** reference K$_d$ value to the K$_d$ value of the multivalent compound. [b] Values obtained from the literature.[57] [c] Values obtained from duplicate measurements. [d] Values obtained from the literature.[26]

The similar ITC study was then performed with the **F$_3$/F$_4$** glycoclusters towards LecB (Figure S5, Table 3). The affinity measured was in the low nanomolar range (K$_d$ = 90 nM) and does compare very favorably with the previously reported high affinity ligands for LecB such as the **Calix-Fuc$_4$** glycocluster (Figure S1). The increase in affinity observed was more moderate for LecB than for LecA since the β value was of only 6 for the **F$_3$/F$_4$** glycoclusters. This was already the case for the **Calix-Fuc$_4$** glycocluster and was explained by the LecB organization which harbors distant multimeric binding sites too far apart to interact simultaneously with two fucoside epitopes in a chelate binding mode.[12] Similarly, the negative control measurement was performed with the **G$_3$/G$_4$** glycocluster which did not display any affinity towards LecB (Figure S5).

Table 3. ITC data for the binding properties of glycosylated dyn[n]arenes **F$_3$/F$_4$** towards LecB

Ligand	*n*	-Δ*H* (kJ.mol^{-1})	-TΔ*S* (kJ.mol^{-1})	K$_d$ (nM)	β[a]
α-L-FucOMe[b]	1.00 ± 0.07	31.5 ± 0.8	-6.2	555	1
F$_3$/F$_4$[c]	0.10 ± 0.01	225.8 ± 6.3	184.1	90	6
Calix-Fuc$_4$[b]	0.32 ± 0.02	89.6 ± 2.1	47.8	48	11.6

[a] β is the binding potency calculated as the ratio of the monovalent **α-L-FucOMe** reference K$_d$ value to the K$_d$ value of the multivalent compound. [b] Values obtained from the literature.[26] [c] Values obtained from triplicate measurements.

The **F$_3$/F$_4$** glycoclusters were then assayed against AFL, another fucose-specific lectin from the *Aspergillus fumigatus* fungal pathogen.[58] This lectin is a hexamer displaying six fucose binding sites in a propeller-like spatial arrangement. The cooperativity in binding to several binding sites simultaneously has been demonstrated by the group of Renaudet using a cyclic peptide scaffold with six fucoside epitopes (Figure S6).[59] The affinity towards LecB was in the low nanomolar range (Table 4) and these ligands displayed the highest affinity ligands for AFL reported to date. A similar approach was reported by Gouin *et al.* with octavalent glycoclusters displaying fucoside epitopes on a silsesquioxane core scaffold (Figure S6).[60] Again, the K$_d$ value of 40 nM (Table 4) ranked this type of glycocluster in the highest affinity for AFL.

The **F_3/F_4** glycoclusters displayed a K_d value of 38 nM (Figure S7, Table 4) which is in line with the multivalent glycoclusters previously reported. The negative control with **G_3/G_4** glycoclusters confirmed that no non-specific binding could be attributed to the macrocyclic core scaffolds.

Table 4. ITC data for the binding properties of glycosylated dyn[n]arenes **F_3/F_4** towards AFL

Ligand	*n*	-Δ*H* (kJ.mol^{-1})	-TΔ*S* (kJ.mol^{-1})	K_d (nM)	β[a]
α-L-FucOMe[b]	2.98	32.8	7.7	40 300	1
F_3/F_4[b]	0.11 ± 0.03	335.0 ± 0.0	292.5 ± 0.5	38	1060
Cyclodecapeptide[c]	0.77 ± 0.01	154.5 ± 3.5	109.5	18.5	2178
Silsesquioxane[d]	0.71 ± 0.04	-247.2 ± 16.0	205.0 ± 16.2	40	1007

[a] β is the binding potency calculated as the ratio of the monovalent **α-L-FucOMe** reference K_d value to the K_d value of the multivalent compound. [b] Values obtained from duplicate measurements. [c] Values obtained from the literature.[59] [d] Values obtained from the literature.[60]

As a conclusion for these ITC binding studies, the **X_3/X_4** glycoclusters identified after lectin-selection in the equilibrating DCLs could be purified and their binding properties studied by ITC. All these dynarene glycoclusters displayed high affinity for their respective lectins and can be considered as candidates to prevent or reduce bacterial interactions with epithelial cells. They were found to have binding affinities similar to those of the calixarene-based glycoclusters that were demonstrated as efficient bio-mimetics reducing mouse lung infection by *Pseudomonas aeruginosa*.[26] Similarly, the fucosylated glycoclusters **F_3/F_4** appeared as valuable candidates to reduce the outcome of A*spergillus fumigatus* lung infections (in immuno-compromised patients), based on their high affinity for the AFL lectin. Given the potential of these compounds for biological applications, their toxicity and anti-adhesive properties against *Pseudomonas aeruginosa* were evaluated on A549 lung epithelial cells.

Incidence of dynarenes on Pseudomonas aeruginosa PAO1 cells and lung epithelial cells

The toxicity of the designed **X_3/X_4** glycoclusters was evaluated against *P. aeruginosa* strain PAO1 (the main strain model used in virulence studies) using two different assays. The growth of PAO1 was not inhibited by the exposure to the **X_3/X_4** dynarenes (up to 10 mM) on Muller-Hinton agar plates. In parallel, a Live-Dead assay monitoring dead cells (through their permeability to propidium iodide) indicated that no toxicity could be observed against PAO1 for the **X_3/X_4** dynarenes used up to 10 mM, over incubation times of 4 hours.

Aggregation bacterial cell assays

The absence of toxicity on *P. aeruginosa* allowed to test the abilities of **X_3/X_4** dynarenes to induce the formation of PAO1 cell aggregates. The presence of LecA, LecB or other adhesins at the surface of the bacterial cells can trigger their aggregation in the presence of the multivalent **X_3/X_4** dynarenes acting as cross-linking agents between cells through carbohydrate-lectin interactions. Our previously reported procedure[61] was used to test the formation of cellular aggregates induced by multivalent **X_3/X_4** dynarenes ligands. This procedure was slightly modified by performing an analysis of the relative numbers of aggregates through a Malvern mastersizer 3000 diffraction laser system (Figure 14) rather than flow cytometry. A shoulder is observed at 6 µm suggesting the presence of aggregates of about 3 cells in the control experiment with PBS. The blue and green curves showed the impact of adding mannosylated dynarenes **M_3/M_4** (100 or 250 µM) generating larger aggregates of a few tens of microns with nearly no influence of the concentration used.

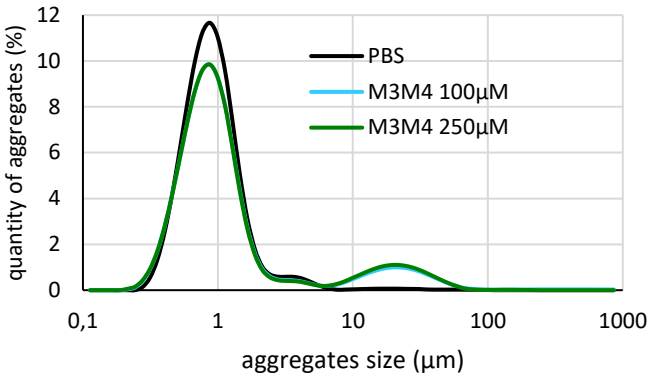

Figure 14. Illustration of aggregate size distribution patterns observed in a *P. aeruginosa* PAO1 cell broth exposed to two concentrations (100 µM, 250 µM) of mannosylated dynarenes. Two cell categories can be defined through the analysis of the cell size distribution patterns: (1) planktonic PAO1 cells (< 3 µm), and (2) aggregated PAO1 cells (> 3 µm).

The aggregation assays clearly showed the ability of multivalent **X_3/X_4** dynarenes at inducing the formation of PAO1 cell aggregates (Figure 15). The glycosylated dynarene aggregation potential was compared with those of glycosylated calixarenes which have been reported as highly efficient multivalent ligands for inducing the formation of PAO1 cell aggregates.[26] Interestingly, these aggregation levels were correlated to an anti-adhesive effect reducing the formation of aggregates when PAO1 cells are exposed to glyco-conjugate concentrations above 1 mM.[26] This anti-adhesive effect was considered to result from a saturation of adhesins at the bacterial cell surface preventing interactions with the neighboring cells. Mannosylated (**M_3/M_4**) and galactosylated (**G_3/G_4**) dynarenes were found to generate as much aggregates than the calixarene-based glycoclusters (Figure S1, cFUC, cGAL, cMAN) but not the fucosylated (**F_3/F_4**) dynarenes (Figure 15).

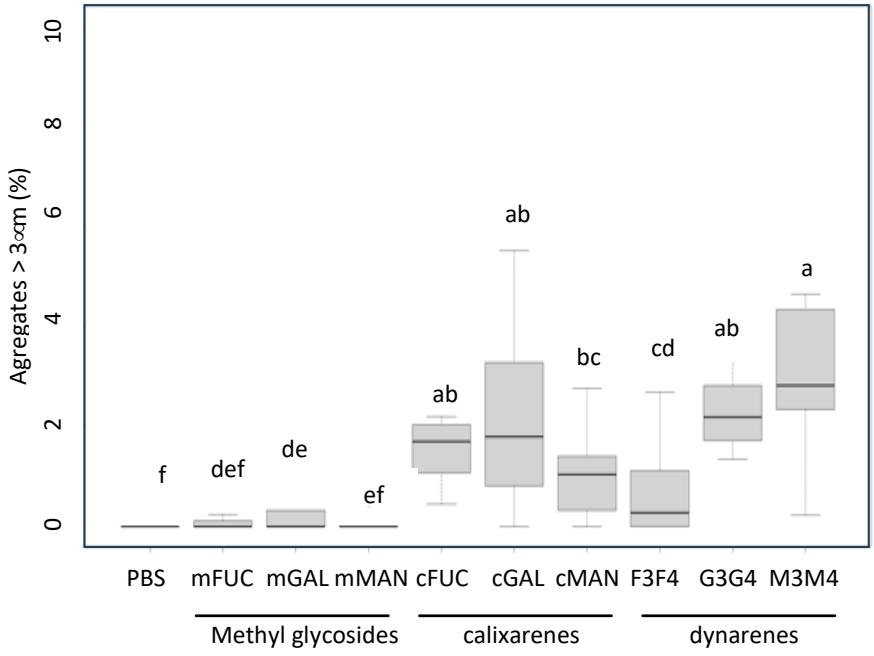

Figure 15. Boxplot of *P. aeruginosa* PAO1 cells aggregation levels induced through interactions with 100 µM of methyl glycosides (monovalent ligands – mFUC = methyl α-L-fucopyranoside, mGAL = methyl β-D-galactopyranoside, mMAN = methyl α-D-mannopyranoside), tetravalent calixarene-based glycoclusters (cFUC, cGAL, cMAN) and the multivalent **X_3/X_4** dynarene glycoclusters**.** Size of the aggregates were estimated using a Malvern MasterSizer. Boxplots were used to show the minimum,

first quartile (Q1), median, third quartile (Q3), and maximum relative abundances for PAO1 aggregates with a size > 3 µm among a cell population. 100 µM of all compounds were used per assay. Boxplots with distinct letter codes showed significant differences (p-values < 0.05 using Kruskal-Wallis (KW) Dunn tests). Aggregates observed among control PAO1 cells in PBS were subtracted from the results; PBS values were thus transformed into zero. At least three independent aggregation assays were performed per assay, and more than five technical Mastersizer readings were performed per replicate.

Similar results were obtained with the bpoe6656 strain[61-62] which belongs to the PA14 clade of *P. aeruginosa* expressing ExoU-based virulence behaviors rather than ExoS-based ones of the PAO1 clade (Figure 16). Aggregation of these PA14 bpoe6656 cells was found higher with the galactosylated **G_3/G_4** dynarene (Figure 16B) than the mannosylated **M_3/M_4** dynarenes (Figure 16A). Interestingly, a positive linear response between the number of aggregates and the concentrations of **M_3/M_4** dynarenes could be observed with these two strains but was less significant with the **G_3/G_4** dynarenes. This confirmed the trends reported on Figure 15 where mannosylated **M_3/M_4** dynarenes induced the formation of a greater number of aggregates.

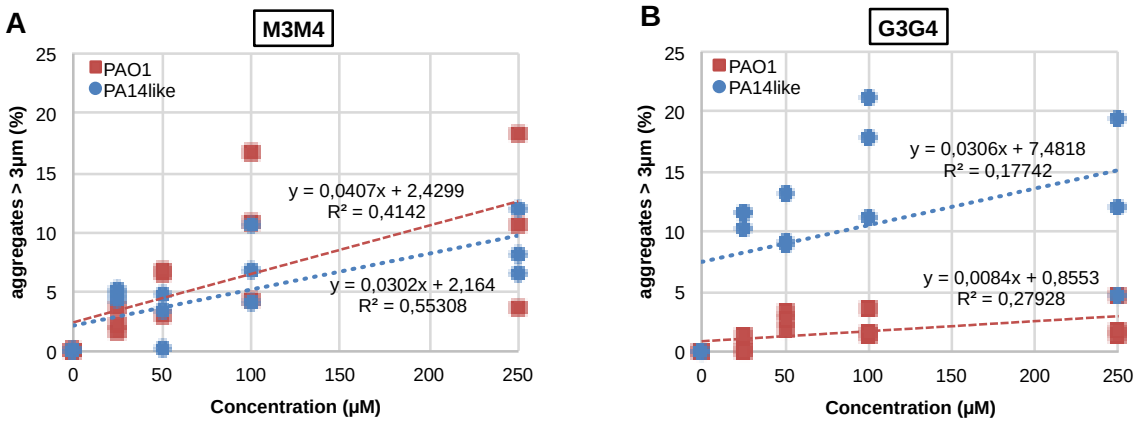

Figure 16. Linear regression analysis of the effect of **M_3/M_4** and **G_3/G_4** dynarene concentrations (µM) on the relative number of aggregates > 3µm in cell populations of PAO1 and PA14-like strain bpoe6656. (A) Mannosylated dynarene **M_3/M_4** and (B) galactosylated dynarene **G_3/G_4**. The linear model fitting the observed relation is indicated on the curve with its R^2 value of goodness-of-fit. R^2 indicates the percentage of the response variable explained by the model. Three independent aggregation assays were performed per dynarene concentration (matching the coloured square or circles), and more than five technical Mastersizer readings were performed per replicate.

P. aeruginosa virulence cell assays using A549 lung epithelial cells

In our previous study,[26] calixarene-based glycoclusters were found to inhibit PAO1 adhesion on A549 epithelial cells after 3 hours of co-culture. We have now optimized these virulence assays to evaluate the protective effects of multivalent **X_3/X_4** dynarene glycoclusters against PAO1 virulence. xCELLigence monitorings, using E96-microtiter plates harboring gold electrodes (Acea Biosciences, San Diego, USA) were implemented to test the changes in PAO1 virulence properties triggered by **X_3/X_4** dynarenes. These monitorings implied real-time analyses (RTCA) of impedance changes over time for epithelial cell monolayers, which are expressed as cell index (CI) arbitrary units. These cell index values are reflecting changes in A549 epithelial cell adhesion forces over the electrodes which are triggered by morphological and A549 cell number changes over time. Cell indexes were normalized at time of treatments (i.e. presented as delta cell indexes).

To perform these RTCA, the toxicity of **X_3/X_4** dynarene glycoclusters on A549 epithelial cells was first investigated. No toxicity effect on the A549 was observed using dynarenes (data not shown).

Experiments testing the incidence of **X_3/X_4** dynarenes on the PAO1 infection of A549 cells monitored by the xCELLigence system were then undertaken. PAO1 cells were grown as reported above, washed with PBS, and pre-incubated for 15 min with the **X_3/X_4** dynarene glycocclusters (1 mM) as performed in our previous study.[26] These PAO1 cells were then diluted to obtain a multiplicity of infection (MOI) of 10 according to the number of A549 cells prepared for the RTCA in the culture media without antibiotics.

The impact of **X_3/X_4** dynarene glycoclusters on *P. aeruginosa* virulence was tested on A549 cell monolayers after 2 hours of co-cultures. Since dynarenes did not exert any significant toxicity on PAO1 cells, their high proliferation rate (approx. 40 min.) could interfere with pre-treated bacteria. In order to avoid excess PAO1 proliferation, remaining PAO1 cells in suspension were removed after 2 hours of co-culture and replaced by fresh cell culture media in order to amplify the effect of adherent bacteria (Figure 17A).

In comparison to control A549 cells, PAO1 adhesion to epithelial cells induced a drastic reduction of cell index according to time with respect of high alteration of A549 cell number, adhesion force and/or morphology (Figure 17A). This effect was significantly counterbalanced in co-cultures with PAO1 pre-exposed to either three **X_3/X_4** dynarenes, suggesting that PAO1 adherence and/or virulence was altered by **X_3/X_4** dynarene glycoclusters. In order to test whether PAO1 adhesion to epithelial cells was involved in alteration of epithelial cell index, a second approach was used to monitor A549 cell adhesion rate by RTCA of cells in suspension loaded onto the E-Plate. During this adhesion phase, the cell index (normalized to media alone) increases according to cell adhesion at the bottom of plate wells, which occurs within a few hours.[63] Since at MOI10, **X_3/X_4** dynarenes are present in the co-culture media at 4.13 μM, their toxicity was checked on A549 cells in suspension and they did not alter cell adhesion rate and/or force (Figure 17B). Pre-incubation of A549 cells in suspension with PAO1 (MOI10) was found to drastically affect epithelial cell adhesion (Figure 17C). Pre-incubation of PAO1 with **X_3/X_4** dynarenes (1 mM on MOI100) was found to exert a protective effect against this alteration of epithelial cell adhesion. In order to analyze the mechanisms involved in PAO1 virulence, at the end of experiment (3-4 hours), A549 cells were fixed in a 5% PBS formalin solution and kept at least 1 hour at 4°C. Then they were labeled with PBS 0.1% Triton containing Phalloïdin-Atto488 for cytoskeleton labeling, DAPI for cell nuclei counts and dihydroxyrhodamine (DHR) to evaluate stress induced reactive oxygen species (ROS) during five minutes then washed twice in PBS and analyzed through automated image analyses (×4) (Figure 17D). PAO1 adhesion/infection was found to affect A549 cell adhesion by reducing the number of adherent cells and induction of oxidative stress (i.e. increased intracellular ROS). Image acquisitions at higher magnification (×20) with identical parameters highlight morphological changes such as reduction of adhesion surfaces (spheric cells) and loss of phalloïdin fluorescence intensity reflecting destabilization of actin polymerization (Figure 17E). These data are in accordance with the effect of PAO1 adhesion on oxidative stress and consequent alteration of cell adhesion.[64] All **X_3/X_4** dynarene glycoclusters protect at least partially (**G_3/G_4**) or to a large extent (**F_3/F_4**) A549 cells from the anti-adhesive activity of PAO1 in RTCA experiments confirmed by the counterbalancing effect on cell number adhesion, ROS induction and morphological alterations.

In conclusion, **X_3/X_4** dynarene glycoclusters could be demonstrated to exert a protective effect against PAO1 virulence on lung epithelial cells. The exact mechanism of protection is still to be further investigated but it is probably through inhibition of their adhesion on epithelial cells by inducing bacterial aggregation.

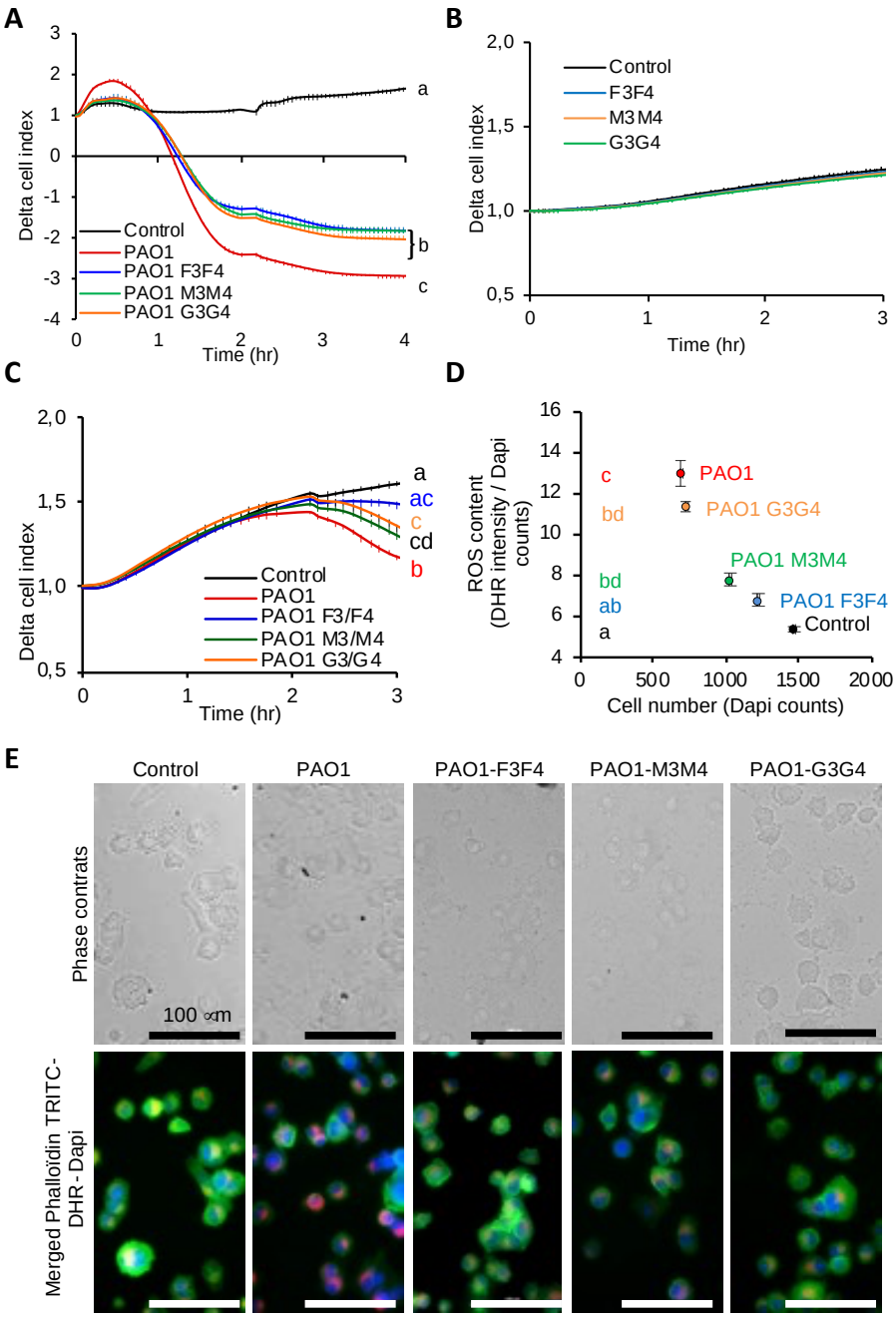

Figure 17. *Pseudomonas aeruginosa* PAO1 anti-adhesive assays using **X_3/X_4** dynarene glycoclusters and A549 epithelial cells. (A) Real-time monitoring of A549 cell monolayer in co-culture with PAO1 pre-treated with **X_3/X_4** dynarenes (1 mM). Co-cultures were washed out after 2 hours and replaced by fresh culture media then monitored during 2 hours. Data were obtained with 8 replicates of 3 independent preparations of each PAO1-**X_3/X_4** dynarenes. (B) Real-time monitoring of A549 cell adhesion after pre-incubation with **X_3/X_4** dynarenes (4.13 µM) and (C) with PAO1 pre-treated with **X_3/X_4** dynarene (1 mM) (n= 8 replicates). (D-E) After PAO1 exposure, A549 cells were fixed and labeled with either DAPI (blue color) for nuclei counts, phalloidin-Atto488 (green color) for cytoskeleton and dihydroxyrhodamine (DHR, red color) for reactive oxygen species (ROS). (D) Cell number (i.e. DAPI counts) and mean ROS content per cell (i.e. DHR intensity normalized to DAPI counts) were obtained by automated analysis of at least 16 images (magnification ×4). (E) Phase contrast and merged fluorescence images at objective ×20. Data are presented as mean values +/-SEM, different letters represent significant differences according to Kruskal Wallis followed by Mann Whitney (Wilcoxon) tests ($p<0.05$).

Conclusion

Carbohydrates are decorated at the surface of cells and play a major role in biological processes more specifically in several diseases. The very first step of bacterial or viral infection is the attachment of the pathogen to the cell surface through carbohydrate-lectin interactions, carbohydrates being present at the host cell surface in the glycocalyx and proteins being used by pathogens for infection. The design of multivalent glycoconjugates to lure pathogens and prevent adhesion to host cells is a general strategy that has found several illustrations over the past decades. The design and synthesis of multivalent glycoconjugates as potent ligands of such proteins has required intensive research work from chemists and biochemists to identify drug candidates. One main drawback is the synthesis of a large panel of analogues in a family of compounds for the structure-activity relationship study and to reach the best candidate after testing all compounds separately in a time and material consuming process. Dynamic combinatorial chemistry can provide a rapid and efficient access to a large variety of multivalent glycoconjugates and speed up drastically the process of drug discovery in this context. One major advantage is to setup an equilibrating dynamic combinatorial library of glycoclusters and then introduce a lectin for the *in situ* selection of the fittest ligand of the protein. Glycosylated 1,4-dithiophenols were equilibrated through disulfide exchange to reach a library of glycoclusters. A model study was performed with concanavalin A (ConA) to demonstrate the selection of the best ligands in this dynamic combinatorial library. More importantly, this strategy allowed the identification of the best ligands for more than one lectin in a single experimental setup by using two simple 1,4-dithiophenols building blocks. High affinity glycoclusters could be amplified in the equilibrating mixtures using LecA or LecB, leading to glyco-dyn[3]arenes and glyco-dyn[4]arenes. The glycoclusters could then be synthesized, isolated for their evaluation as lectin ligands and anti-adhesive agents against *Pseudomonas aeruginosa*. Dissociation constants in the nanomolar range could be measured by ITC which places these compounds in the same range of "classical" calixarene-based glycoclusters which among the best ligands for these pathogenic lectins. These glyco-dynarenes did not display any toxicity towards neither human cells, nor *Pseudomonas aeruginosa*. Their evaluation as anti-adhesive agents could be validated in a virulence assay on human A549 lung epithelial cells which indicated that glyco-dynarenes could perform similarly to our previous calixarene-based glycoclusters model.

Acknowledgements

The authors thank the Université Lyon 1 and the CNRS for financial support. This work was supported by the Agence Nationale de la Recherche (DynaSweet ANR-17-CE07-0054). Dr Florian Albrieux, Dr Alexandra Berlioz-Barbier, Christian Duchamp, and Antoine Vauchez are gratefully acknowledged for UHPLC-MS analyses at the Centre Commun de Spectrométrie de Masse of Université Lyon 1, along with Dr Nathalie Hue and Vincent Steinmetz at the ICSN mass spectrometry department.

References

1. Barchi, J. J., *Comprehensive Glycoscience, 2nd Edition*. Elsevier: 2021.
2. Bertozzi, C. R.; Kiessling; L., L., Chemical Glycobiology. *Science* **2001,** *291* (5512), 2357-2364.

3. Gabius, H.-J.; Cudic, M.; Diercks, T.; Kaltner, H.; Kopitz, J.; Mayo, K. H.; Murphy, P. V.; Oscarson, S.; Roy, R.; Schedlbauer, A.; Toegel, S.; Romero, A., What is the Sugar Code? *ChemBioChem* **2022,** *23* (13), e202100327.
4. Varki, A.; Cummings, R. D.; Esko, J. D.; Stanley, P.; Hart, G. W.; Aebi, M.; Mohnen, D.; Kinoshita, T.; Packer, N. H.; Prestegard, J. J.; Schnaar, R. L.; Seeberger, P. H., *Essentials of Glycobiology, 4th edition*. Cold Spring Harbor New York, 2022.
5. Cummings, R. D., Stuck on sugars – how carbohydrates regulate cell adhesion, recognition, and signaling. *Glycoconj. J.* **2019,** *36* (4), 241-257.
6. Mason, C. P.; Tarr, A. W., Human Lectins and Their Roles in Viral Infections. *Molecules* **2015,** *20* (2), 2229-2271.
7. Meiers, J.; Siebs, E.; Zahorska, E.; Titz, A., Lectin antagonists in infection, immunity, and inflammation. *Curr. Opin. Chem. Biol.* **2019,** *53*, 51-67.
8. Lee, Y. C.; Lee, R. T., Carbohydrate-Protein Interactions: Basis of Glycobiology. *Acc. Chem. Res.* **1995,** *28* (8), 321-327.
9. Lis, H.; Sharon, N., Lectins: Carbohydrate-Specific Proteins That Mediate Cellular Recognition. *Chem. Rev.* **1998,** *98* (2), 637-674.
10. Valverde, P.; Ardá, A.; Reichardt, N.-C.; Jiménez-Barbero, J.; Gimeno, A., Glycans in drug discovery. *MedChemComm* **2019,** *10* (10), 1678-1691.
11. Bernardi, A.; Jimenez-Barbero, J.; Casnati, A.; De Castro, C.; Darbre, T.; Fieschi, F.; Finne, J.; Funken, H.; Jaeger, K.-E.; Lahmann, M.; Lindhorst, T. K.; Marradi, M.; Messner, P.; Molinaro, A.; Murphy, P. V.; Nativi, C.; Oscarson, S.; Penades, S.; Peri, F.; Pieters, R. J.; Renaudet, O.; Reymond, J.-L.; Richichi, B.; Rojo, J.; Sansone, F.; Schaffer, C.; Turnbull, W. B.; Velasco-Torrijos, T.; Vidal, S.; Vincent, S.; Wennekes, T.; Zuilhof, H.; Imberty, A., Multivalent glycoconjugates as anti-pathogenic agents. *Chem. Soc. Rev.* **2013,** *42* (11), 4709-4727.
12. Cecioni, S.; Imberty, A.; Vidal, S., Glycomimetics versus Multivalent Glycoconjugates for the Design of High Affinity Lectin Ligands. *Chem. Rev.* **2015,** *115* (1), 525-561.
13. Mousavifar, L.; Roy, R., Recent development in the design of small 'drug-like' and nanoscale glycomimetics against Escherichia coli infections. *Drug Discov. Today* **2021,** *26* (9), 2124-2137.
14. Mousavifar, L.; Touaibia, M.; Roy, R., Development of Mannopyranoside Therapeutics against Adherent-Invasive Escherichia coli Infections. *Acc. Chem. Res.* **2018,** *51* (11), 2937-2948.
15. Chalopin, T.; Alvarez Dorta, D.; Sivignon, A.; Caudan, M.; Dumych, T. I.; Bilyy, R. O.; Deniaud, D.; Barnich, N.; Bouckaert, J.; Gouin, S. G., Second generation of thiazolylmannosides, FimH antagonists for E. coli-induced Crohn's disease. *Org. Biomol. Chem.* **2016,** *14* (16), 3913-3925.
16. Schönemann, W.; Cramer, J.; Mühlethaler, T.; Fiege, B.; Silbermann, M.; Rabbani, S.; Dätwyler, P.; Zihlmann, P.; Jakob, R. P.; Sager, C. P.; Smieško, M.; Schwardt, O.; Maier, T.; Ernst, B., Improvement of Aglycone π-Stacking Yields Nanomolar to Sub-nanomolar FimH Antagonists. *ChemMedChem* **2019,** *14* (7), 749-757.
17. Kleeb, S.; Jiang, X.; Frei, P.; Sigl, A.; Bezençon, J.; Bamberger, K.; Schwardt, O.; Ernst, B., FimH Antagonists: Phosphate Prodrugs Improve Oral Bioavailability. *J. Med. Chem.* **2016,** *59* (7), 3163-3182.
18. Kleeb, S.; Pang, L.; Mayer, K.; Eris, D.; Sigl, A.; Preston, R. C.; Zihlmann, P.; Sharpe, T.; Jakob, R. P.; Abgottspon, D.; Hutter, A. S.; Scharenberg, M.; Jiang, X.; Navarra, G.; Rabbani, S.; Smiesko, M.; Lüdin, N.; Bezençon, J.; Schwardt, O.; Maier, T.; Ernst, B., FimH Antagonists: Bioisosteres To Improve the in Vitro and in Vivo PK/PD Profile. *J. Med. Chem.* **2015,** *58* (5), 2221-2239.
19. Tomašić, T.; Rabbani, S.; Gobec, M.; Raščan, I. M.; Podlipnik, Č.; Ernst, B.; Anderluh, M., Branched α-d-mannopyranosides: a new class of potent FimH antagonists. *MedChemComm* **2014,** *5* (8), 1247-1253.
20. Romero, A.; Gabius, H.-J., Galectin-3: is this member of a large family of multifunctional lectins (already) a therapeutic target? *Exp. Opin. Ther. Patents* **2019,** *23* (10), 819-828.
21. Zetterberg, F. R.; MacKinnon, A.; Brimert, T.; Gravelle, L.; Johnsson, R. E.; Kahl-Knutson, B.; Leffler, H.; Nilsson, U. J.; Pedersen, A.; Peterson, K.; Roper, J. A.; Schambye, H.; Slack, R. J.; Tantawi, S., Discovery and Optimization of the First Highly Effective and Orally Available Galectin-3 Inhibitors for Treatment of Fibrotic Disease. *J. Med. Chem.* **2022,** *65* (19), 12626-12638.

22. Bum-Erdene, K.; Collins, P. M.; Hugo, M. W.; Tarighat, S. S.; Fei, F.; Kishor, C.; Leffler, H.; Nilsson, U. J.; Groffen, J.; Grice, I. D.; Heisterkamp, N.; Blanchard, H., Novel Selective Galectin-3 Antagonists Are Cytotoxic to Acute Lymphoblastic Leukemia. *J. Med. Chem.* **2022,** *65* (8), 5975-5989.
23. Bratteby, K.; Torkelsson, E.; L'Estrade, E. T.; Peterson, K.; Shalgunov, V.; Xiong, M.; Leffler, H.; Zetterberg, F. R.; Olsson, T. G.; Gillings, N.; Nilsson, U. J.; Herth, M. M.; Erlandsson, M., In Vivo Veritas: 18F-Radiolabeled Glycomimetics Allow Insights into the Pharmacological Fate of Galectin-3 Inhibitors. *J. Med. Chem.* **2020,** *63* (2), 747-755.
24. Mahanti, M.; Pal, K. B.; Kumar, R.; Schulze, M.; Leffler, H.; Logan, D. T.; Nilsson, U. J., Ligand Sulfur Oxidation State Progressively Alters Galectin-3-Ligand Complex Conformations To Induce Affinity-Influencing Hydrogen Bonds. *J. Med. Chem.* **2023,** *66* (21), 14716-14723.
25. Renaudet, O.; Roy, R., Multivalent scaffolds in glycoscience: an overview. *Chem. Soc. Rev.* **2013,** *42* (11), 4515-4517.
26. Boukerb, A. M.; Rousset, A.; Galanos, N.; Méar, J.-B.; Thépaut, M.; Grandjean, T.; Gillon, E.; Cecioni, S.; Abderrahmen, C.; Faure, K.; Redelberger, D.; Kipnis, E.; Dessein, R.; Havet, S.; Darblade, B.; Matthews, S. E.; de Bentzmann, S.; Guéry, B.; Cournoyer, B.; Imberty, A.; Vidal, S., Antiadhesive Properties of Glycoclusters against *Pseudomonas aeruginosa* Lung Infection. *J. Med. Chem.* **2014,** *57* (24), 10275-10289.
27. Ligeour, C.; Vidal, O.; Dupin, L.; Casoni, F.; Gillon, E.; Meyer, A.; Vidal, S.; Vergoten, G.; Lacroix, J.-M.; Souteyrand, E.; Imberty, A.; Vasseur, J.-J.; Chevolot, Y.; Morvan, F., Mannose-centered aromatic galactoclusters inhibit the biofilm formation of *Pseudomonas aeruginosa*. *Org. Biomol. Chem.* **2015,** *13* (31), 8433-8444.
28. Reymond, J.-L.; Bergmann, M.; Darbre, T., Glycopeptide dendrimers as Pseudomonas aeruginosa biofilm inhibitors. *Chem. Soc. Rev.* **2013,** *42* (11), 4814-4822.
29. Sharon, N., Carbohydrates as future anti-adhesion drugs for infectious diseases. *Biochim. Biophys. Acta* **2006,** *1760* (4), 527-537.
30. Pera, N. P.; Pieters, R. J., Towards bacterial adhesion-based therapeutics and detection methods. *MedChemComm* **2014,** *5* (8), 1027-1035.
31. Imberty, A.; Chabre, Y. M.; Roy, R., Glycomimetics and Glycodendrimers as High Affinity Microbial Anti-adhesins. *Chem. Eur. J.* **2008,** *14* (25), 7490-7499.
32. Sattin, S.; Bernardi, A., Glycoconjugates and Glycomimetics as Microbial Anti-Adhesives. *Trends Biotechnol.* **2016,** *34* (6), 483-495.
33. Corbett, P. T.; Leclaire, J.; Vial, L.; West, K. R.; Wietor, J.-L.; Sanders, J. K. M.; Otto, S., Dynamic Combinatorial Chemistry. *Chem. Rev.* **2006,** *106* (9), 3652-3711.
34. Li, J.; Nowak, P.; Otto, S., Dynamic Combinatorial Libraries: From Exploring Molecular Recognition to Systems Chemistry. *J. Am. Chem. Soc.* **2013,** *135* (25), 9222-9239.
35. Frei, P.; Hevey, R.; Ernst, B., Dynamic Combinatorial Chemistry: A New Methodology Comes of Age. *Chem. Eur. J.* **2019,** *25* (1), 60-73.
36. Canal-Martín, A.; Pérez-Fernández, R., Protein-Directed Dynamic Combinatorial Chemistry: An Efficient Strategy in Drug Design. *ACS Omega* **2020,** *5* (41), 26307-26315.
37. Ramström, O.; Lehn, J.-M., In Situ Generation and Screening of a Dynamic Combinatorial Carbohydrate Library against Concanavalin A. *ChemBioChem* **2000,** *1* (1), 41-48.
38. Ramström, O.; Lohmann, S.; Bunyapaiboonsri, T.; Lehn, J.-M., Dynamic Combinatorial Carbohydrate Libraries: Probing the Binding Site of the Concanavalin A Lectin. *Chem. Eur. J.* **2004,** *10* (7), 1711-1715.
39. Reeh, P.; de Mendoza, J., Dynamic Multivalency for Carbohydrate–Protein Recognition through Dynamic Combinatorial Libraries Based on FeII–Bipyridine Complexes. *Chem. Eur. J.* **2013,** *19* (17), 5259-5262.
40. Mahon, C. S.; Fascione, M. A.; Sakonsinsiri, C.; McAllister, T. E.; Bruce Turnbull, W.; Fulton, D. A., Templating carbohydrate-functionalised polymer-scaffolded dynamic combinatorial libraries with lectins. *Org. Biomol. Chem.* **2015,** *13* (9), 2756-2761.
41. Ponnuswamy, N.; Cougnon, F. B. L.; Clough, J. M.; Pantoş, G. D.; Sanders, J. K. M., Discovery of an Organic Trefoil Knot. *Science* **2012,** *338* (6108), 783-785.

42. Otto, S.; Furlan, R. L. E.; Sanders, J. K. M., Selection and Amplification of Hosts From Dynamic Combinatorial Libraries of Macrocyclic Disulfides. *Science* **2002,** *297* (5581), 590-593.
43. Brisig, B.; Sanders, J. K. M.; Otto, S., Selection and Amplification of a Catalyst from a Dynamic Combinatorial Library. *Angew. Chem. Int. Ed.* **2003,** *42* (11), 1270-1273.
44. Gianga, T.-M.; Audibert, E.; Trandafir, A.; Kociok-Köhn, G.; Pantoş, G. D., Discovery of an all-donor aromatic [2]catenane. *Chem. Sci.* **2020,** *11* (35), 9685-9690.
45. Adamski, P.; Eleveld, M.; Sood, A.; Kun, Á.; Szilágyi, A.; Czárán, T.; Szathmáry, E.; Otto, S., From self-replication to replicator systems en route to de novo life. *Nat. Rev. Chem.* **2020,** *4* (8), 386-403.
46. Orrillo, A. G.; Furlan, R. L. E., Sulfur in Dynamic Covalent Chemistry. *Angew. Chem. Int. Ed.* **2022,** *61* (26), e202201168.
47. Vial, L.; Perret, F.; Leclaire, J., Dyn[n]arenes: Versatile Platforms To Study the Interplay between Covalent and Noncovalent Bonds. *Eur. J. Org. Chem.* **2022**, e202101274.
48. Skowron, P.-T.; Dumartin, M.; Jeamet, E.; Perret, F.; Gourlaouen, C.; Baudouin, A.; Fenet, B.; Naubron, J.-V.; Fotiadu, F.; Vial, L.; Leclaire, J., On-Demand Cyclophanes: Substituent-Directed Self-Assembling, Folding, and Binding. *J. Org. Chem.* **2016,** *81* (2), 654-661.
49. Donnier-Maréchal, M.; Septavaux, J.; Jeamet, E.; Héloin, A.; Perret, F.; Dumont, E.; Rossi, J.-C.; Ziarelli, F.; Leclaire, J.; Vial, L., Diastereoselective Synthesis of a Dyn[3]arene with Distinct Binding Behaviors toward Linear Biogenic Polyamines. *Org. Lett.* **2018,** *20* (8), 2420-2423.
50. Dumartin, M.; Septavaux, J.; Donnier-Maréchal, M.; Jeamet, E.; Dumont, E.; Perret, F.; Vial, L.; Leclaire, J., The dark side of disulfide-based dynamic combinatorial chemistry. *Chem. Sci.* **2020,** *11* (31), 8151-8156.
51. Zhang, Y.; Ourri, B.; Skowron, P.-T.; Jeamet, E.; Chetot, T.; Duchamp, C.; Belenguer, A. M.; Vanthuyne, N.; Cala, O.; Dumont, E.; Mandal, P. K.; Huc, I.; Perret, F.; Vial, L.; Leclaire, J., Self-assembly of achiral building blocks into chiral cyclophanes using non-directional interactions. *Chem. Sci.* **2023,** *14* (26), 7126-7135.
52. Jeamet, E.; Septavaux, J.; Héloin, A.; Donnier-Maréchal, M.; Dumartin, M.; Ourri, B.; Mandal, P.; Huc, I.; Bignon, E.; Dumont, E.; Morell, C.; Francoia, J.-P.; Perret, F.; Vial, L.; Leclaire, J., Wetting the lock and key enthalpically favours polyelectrolyte binding. *Chem. Sci.* **2019,** *10* (1), 277-283.
53. Vial, L.; Dumartin, M.; Donnier-Maréchal, M.; Perret, F.; Francoia, J.-P.; Leclaire, J., Chirality sensing and discrimination of lysine derivatives in water with a dyn[4]arene. *Chem. Commun.* **2016,** *52* (99), 14219-14221.
54. Vial, L.; Ludlow, R. F.; Leclaire, J.; Pérez-Fernández, R.; Otto, S., Controlling the Biological Effects of Spermine Using a Synthetic Receptor. *J. Am. Chem. Soc.* **2006,** *128* (31), 10253-10257.
55. Mével, M.; Bouzelha, M.; Leray, A.; Pacouret, S.; Guilbaud, M.; Penaud-Budloo, M.; Alvarez-Dorta, D.; Dubreil, L.; Gouin, S. G.; Combal, J. P.; Hommel, M.; Gonzalez-Aseguinolaza, G.; Blouin, V.; Moullier, P.; Adjali, O.; Deniaud, D.; Ayuso, E., Chemical modification of the adeno-associated virus capsid to improve gene delivery. *Chem. Sci.* **2020,** *11* (4), 1122-1131.
56. Kimura, T.; Yamamoto, A.; Namauo, T., Preparation of Octakis (methylthio)octaethylphthalocyaninato Titanium (IV) Benzenedichalcogenolates. *Phosphorus Sulfur Silicon Relat. Elem.* **2010,** *185* (5-6), 1008-1013.
57. Cecioni, S.; Faure, S.; Darbost, U.; Bonnamour, I.; Parrot-Lopez, H.; Roy, O.; Taillefumier, C.; Wimmerová, M.; Praly, J.-P.; Imberty, A.; Vidal, S., Selectivity among Two Lectins: Probing the Effect of Topology, Multivalency and Flexibility of "Clicked" Multivalent Glycoclusters. *Chem. Eur. J.* **2011,** *17* (7), 2146-2159.
58. Houser, J.; Komarek, J.; Kostlanova, N.; Cioci, G.; Varrot, A.; Kerr, S. C.; Lahmann, M.; Balloy, V.; Fahy, J. V.; Chignard, M.; Imberty, A.; Wimmerova, M., A Soluble Fucose-Specific Lectin from Aspergillus fumigatus Conidia - Structure, Specificity and Possible Role in Fungal Pathogenicity. *PLoS One* **2013,** *8* (12), e83077.
59. Goyard, D.; Baldoneschi, V.; Varrot, A.; Fiore, M.; Imberty, A.; Richichi, B.; Renaudet, O.; Nativi, C., Multivalent Glycomimetics with Affinity and Selectivity toward Fucose-Binding Receptors from Emerging Pathogens. *Bioconjugate Chem.* **2018,** *29* (1), 83-88.

60. Lehot, V.; Brissonnet, Y.; Dussouy, C.; Brument, S.; Cabanettes, A.; Gillon, E.; Deniaud, D.; Varrot, A.; Le Pape, P.; Gouin, S. G., Multivalent Fucosides with Nanomolar Affinity for the Aspergillus fumigatus Lectin FleA Prevent Spore Adhesion to Pneumocytes. *Chem. Eur. J.* **2018,** *24* (72), 19243-19249.
61. Boukerb, A. M.; Decor, A.; Ribun, S.; Tabaroni, R.; Rousset, A.; Commin, L.; Buff, S.; Doléans-Jordheim, A.; Vidal, S.; Varrot, A.; Imberty, A.; Cournoyer, B., Genomic Rearrangements and Functional Diversification of lecA and lecB Lectin-Coding Regions Impacting the Efficacy of Glycomimetics Directed against Pseudomonas aeruginosa. *Front. Microbiol.* **2016,** *7*, 811. doi: 10.3389/fmicb.2016.00811.
62. Hauser, A. R., The type III secretion system of Pseudomonas aeruginosa: infection by injection. *Nat. Rev. Microbiol.* **2009,** *7* (9), 654-665.
63. Géloën, A.; Berger, E., Reduced Glutathione Decreases Cell Adhesion and Increases Cell Volume. *Arch. Clin. Biomed. Res.* **2022,** *6*, 880-888.
64. Engel, J.; Balachandran, P., Role of Pseudomonas aeruginosa type III effectors in disease. *Curr. Opin. Microbiol.* **2009,** *12* (1), 61-66.

Dynamic combinatorial chemistry for the multiplexed identification of glyco-dyn[n]arenes in an anti-adhesive strategy against *Pseudomonas aeruginosa*

Fanny Demontrond,[a] Yoann Pascal,[a] Marion Donnier-Maréchal,[a] Corentin Raillon,[a] Baptiste Luton,[b] Clara De la Tramblais,[c] Laurent Vial,[a] David Gueyrard,[a] Benoit Cournoyer,[b] Julien Leclaire,[a] and Sébastien Vidal[a,c]*

[a] *Institut de Chimie et Biochimie Moléculaires et Supramoléculaires, UMR 5246, CNRS, Université Claude Bernard Lyon 1, Université de Lyon, INSA Lyon, CPE Lyon, Villeurbanne, 69622, France*

[b] *UMR Ecologie Microbienne, CNRS 5557, INRAE 1418, Research Group «Bacterial Opportunistic Pathogens and Environment», VetAgro Sup, Aisle 3, 1st Floor, 69280 Marcy L'Etoile, France*

[c] *Institut de Chimie des Substances Naturelles, UPR 2301, CNRS, Université Paris-Saclay, Gif-sur-Yvette, 91198, France, sebastien.vidal@cnrs.fr*

Supporting Information

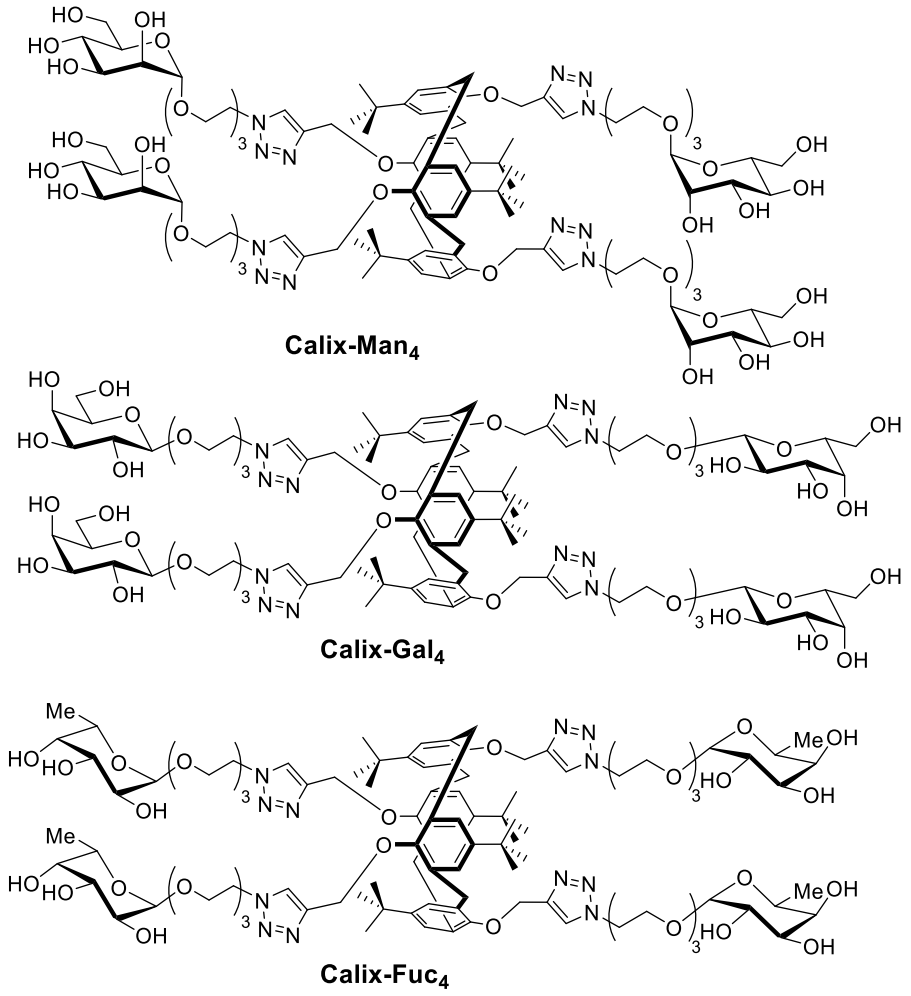

Figure S1. Structure of the tetravalent calixarene-based glycoclusters **Calix-Man$_4$**, **Calix-Gal$_4$** and **Calix-Fuc$_4$**

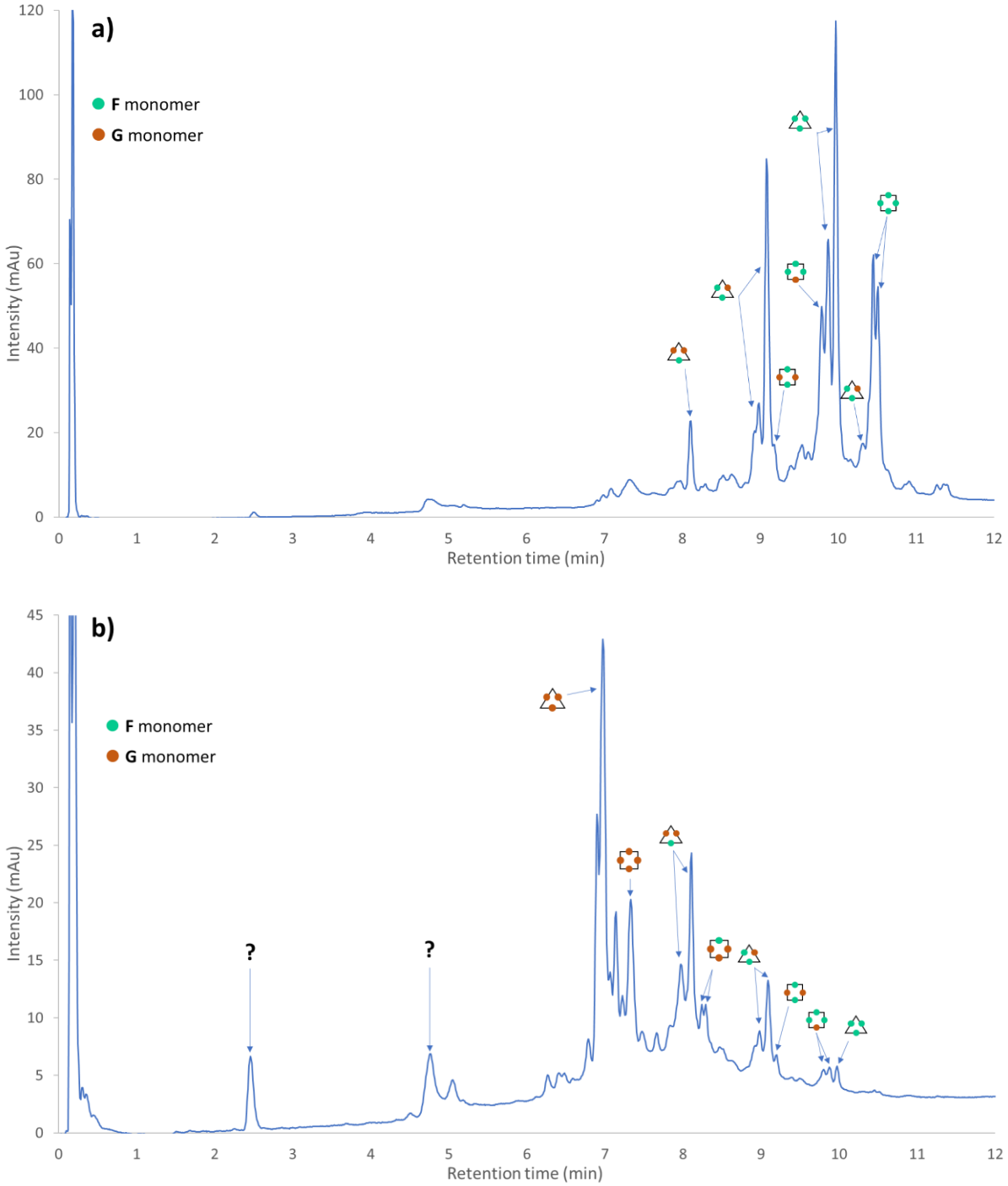

Figure S2. UHPLC analysis of the **G/F** (1:1, 0.4 mM) DCL after incubation with LecB (0.4 mM) with the (a) precipitate and (b) supernatant

Figure S3. Picture of the precipitate and supernatant samples obtained for the AFL-(**G+F**)-DCL

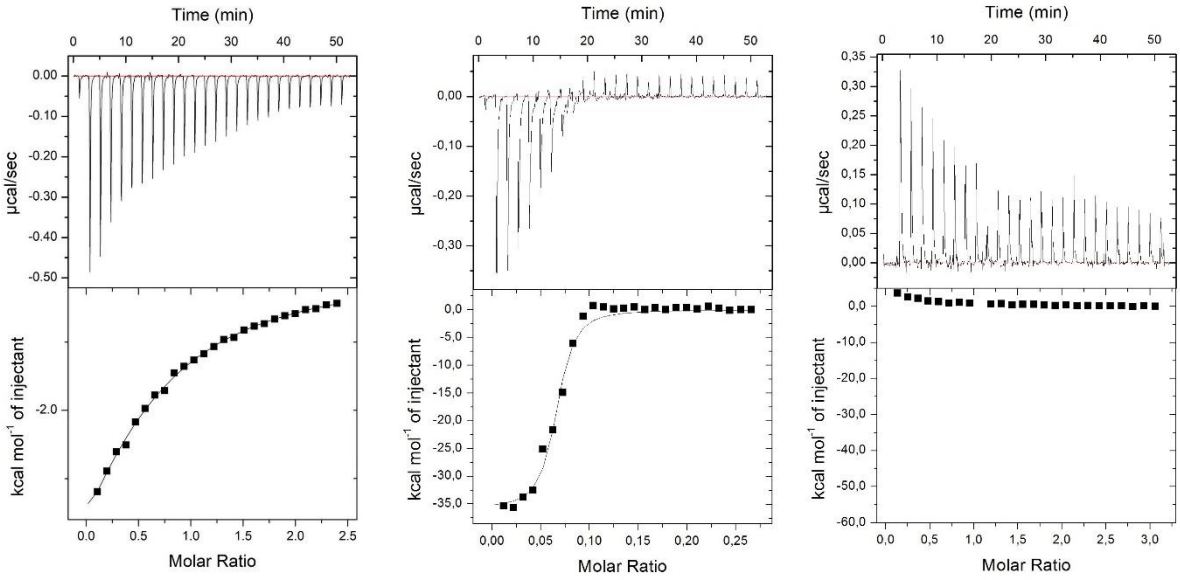

Figure S4. Isothermal titration microcalorimetry (ITC) analysis of the binding properties toward LecA (0.1 mM) for **β-D-GalOMe** (1.8 mM, left panel) and the association titration curve obtained with a 1:1 binding model (lower left panel). ITC data obtained for injections of $\mathbf{G_3/G_4}$ (0.2 mM, 1:1) into a solution of LecA (0.1 mM) and the associated titration curve (center panel). ITC data obtained for injections of $\mathbf{F_3/F_4}$ (0.575 mM, 1:1) into a solution of LecA (0.05 mM) and the associated titration curve (right panel).

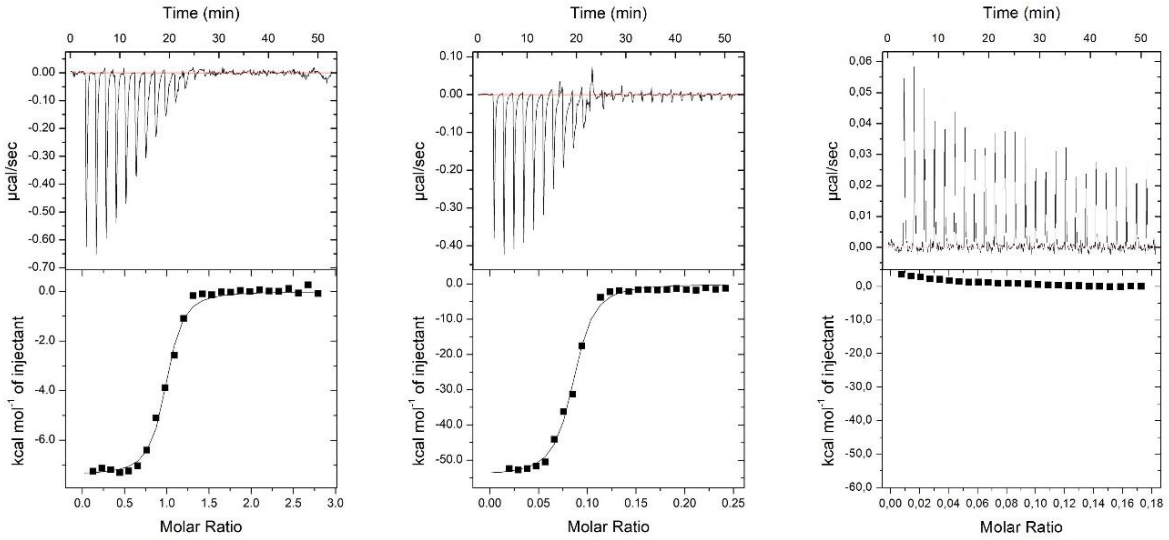

Figure S5. Isothermal titration microcalorimetry (ITC) analysis of the binding properties toward LecB (0.112 mM) for **α-L-FucOMe** (1.67 mM, left panel) and the association titration curve obtained with a 1:1 binding model (lower left panel). ITC data obtained for injections of **F_3/F_4** (0.072 mM, 1:1) into a solution of LecB (0.112 mM) and the associated titration curve (center panel). ITC data obtained for injections of **G_3/G_4** (0.209 mM, 1:1) into a solution of LecB (0.112 mM) and the associated titration curve (right panel).

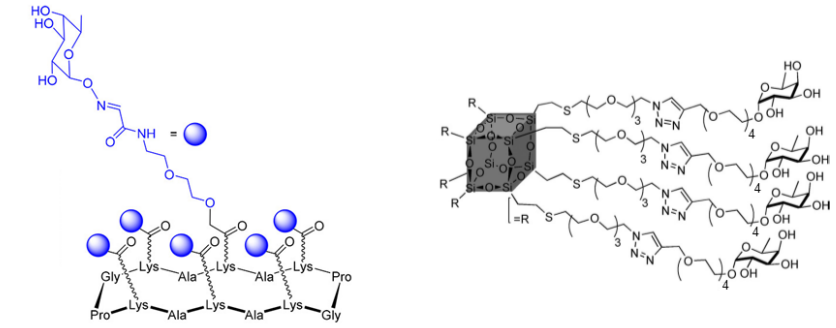

Figure S6. Hexavalent cyclodecapeptide-based and silsesquioxane-based glycoclusters used as a comparison with the **F_3/F_4** fucosylated dyn[n]arenes.

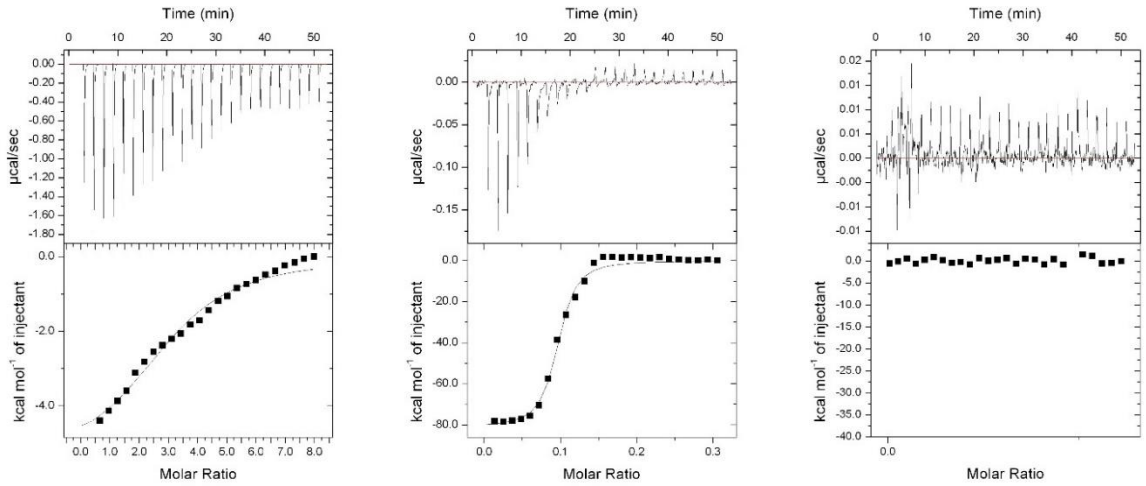

Figure S7. Isothermal titration microcalorimetry (ITC) analysis of the binding properties toward AFL (0.05 mM) for **α-L-FucOMe** (3 mM, left panel) and the association titration curve obtained with a 1:1 binding model (lower left panel). ITC data obtained for injections of **F_3/F_4** (0.012 mM, 1:1) into a solution of AFL (0.05 mM) and the associated titration curve (center panel). ITC data obtained for injections of **G_3/G_4** (0.012 mM, 1:1) into a solution of AFL (0.01 mM) and the associated titration curve (right panel).

Materials and methods

Commercial reagents were used without further purification. Solvents were dried using standard methods. All reactions were carried out under argon. Column chromatography was performed using silica gel (40–63 µm). Reactions were monitored via TLC on a silica gel aluminum plate and visualized under UV light (254 nm).

^{1}H, ^{13}C, DEPT, COSY, HSQC, HMBC experiments were performed on Bruker spectrometers: AV 300, AVL 300, AV 400 and AV 500 at 298K at the CCRMN of the University of Lyon. The chemical shifts are indicated in ppm (parts per million) in reference to the residual solvent peak (*J. Org. Chem.,* **1997**, *62*, 7512-7515). Coupling constants (*J*) are indicated in Hz (Hertz). The abbreviations used for the multiplicity are: s (singlet), b (broad), d (doublet), dd (doublet of doublet), t (triplet), td (triplet of doublet), q (quadruplet), m (multiplet).

Low resolution mass spectrometry was performed on a LCQ advantage (50-20 000 *m/z*) apparatus from Thermofinnigan. High resolution mass spectrometry was performed on a MicrOTOFQ II (50-20 000 *m/z*) apparatus from Bruker. Electrospray ionization was used in all cases.

Lyophilization was carried out in a CHRIST Alpha 2-4 LDPlus apparatus or on a CHRIST Alpha 3-4 LSC Basic system.

C18 Chromatography was performed on automated systems such as CombiFlash Companion system from Serlabo Technologies, Puriflash 5.020 apparatus from Interchim or Pure C-805 from Buchi using C18 Reversed-Phase column cartridges.

Preparative high-performance liquid chromatographies were performed on a Shimadzu LC20 semi-preparative system equipped with a binary pump, a manual injection manifold, dual wavelength UV detector. The chromatographic separation was performed at RT on various columns. The chromatograms were recorded at 210 and 250 nm.

Filtration with membrane could be performed on hydrophilic (0.45 µm pore size, hydrophilic polyethersulfone, 47 mm diameter, ref: HPWP04700) or hydrophobic (Membrane Durapore, PVDF hydrophobic, 0.22 µm pore size, 47 mm diameter, ref: GVHP04700) membranes purchased from Merck Millipore

HPLC analyses were performed on a UHPLC Thermo Scientific Dionex UltiMate 3000 system equipped with a binary pump, an auto-sampler, a variable wavelength UV detector. The chromatographic separation was performed at 30°C on various columns. The chromatograms were recorded at 210 and 254 nm. High resolution mass spectrometry was performed on a QTOF Impact II (50-20 000 *m/z*) apparatus from Bruker. **Column**: Thermo Scientific Accucore C8 80 Å, 2.1×50 mm, 2.6 µm and **Gradient** in Table S1 below.

Table S1. Gradient for HPLC analyses

Time (min)	Flow (mL/min)	H_2O + 0.1% TFA	MeCN + 0.1% TFA
0	0.800	100	0
15	0.800	70	30
18	0.800	0	100
19	0.800	0	100
19.5	0.800	100	0
22	0.800	100	0

Synthesis and characterization of new molecules

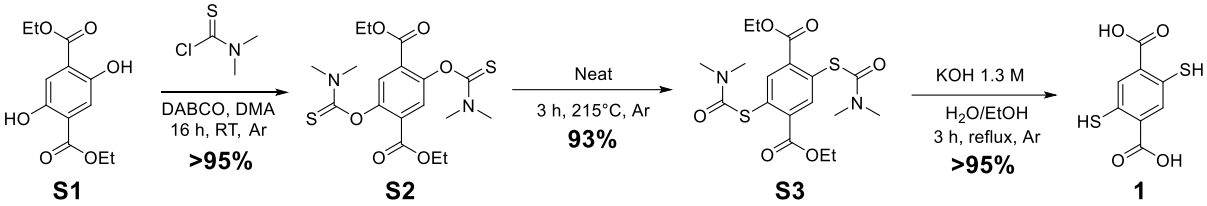

Diethyl 2,5-bis(dimethylthiocarbamoyloxy)terephthalate (S2)

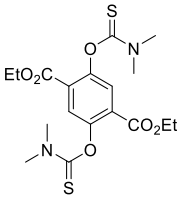

To a solution of **S1** diethyl 2,5-dihydroxyterephthalate (10 g, 39 mmol, 1 eq.) in dry DMA (100 mL) was added dropwise at 0°C a solution of dimethylthiocarbamoyl chloride (19 g, 157 mmol, 4 eq.) and DABCO (18 g, 157 mmol, 4 eq.) in dry DMA (50 mL). The mixture was stirred under nitrogen at room temperature for 24 h. The precipitate was filtrated and washed extensively with water (4×250 mL). The solid was dried under vacuum to give compound **S2** as a white powder (17 g, 38 mmol, >95%).

^{1}H NMR (300 MHz, $CDCl_3$) δ ppm = 7.74 (s, 2H, Ar), 4.31 (q, J = 7.2 Hz, 4H, CH_2), 3.47 (s, 6H, NCH_3), 3.41 (s, 6H, NCH_3), 1.34 (t, J = 7.2 Hz, 6H, CH_3)

The data were in agreement with the literature reference. *J. Am. Chem. Soc.*, **2006**, *128*, 10253-10257

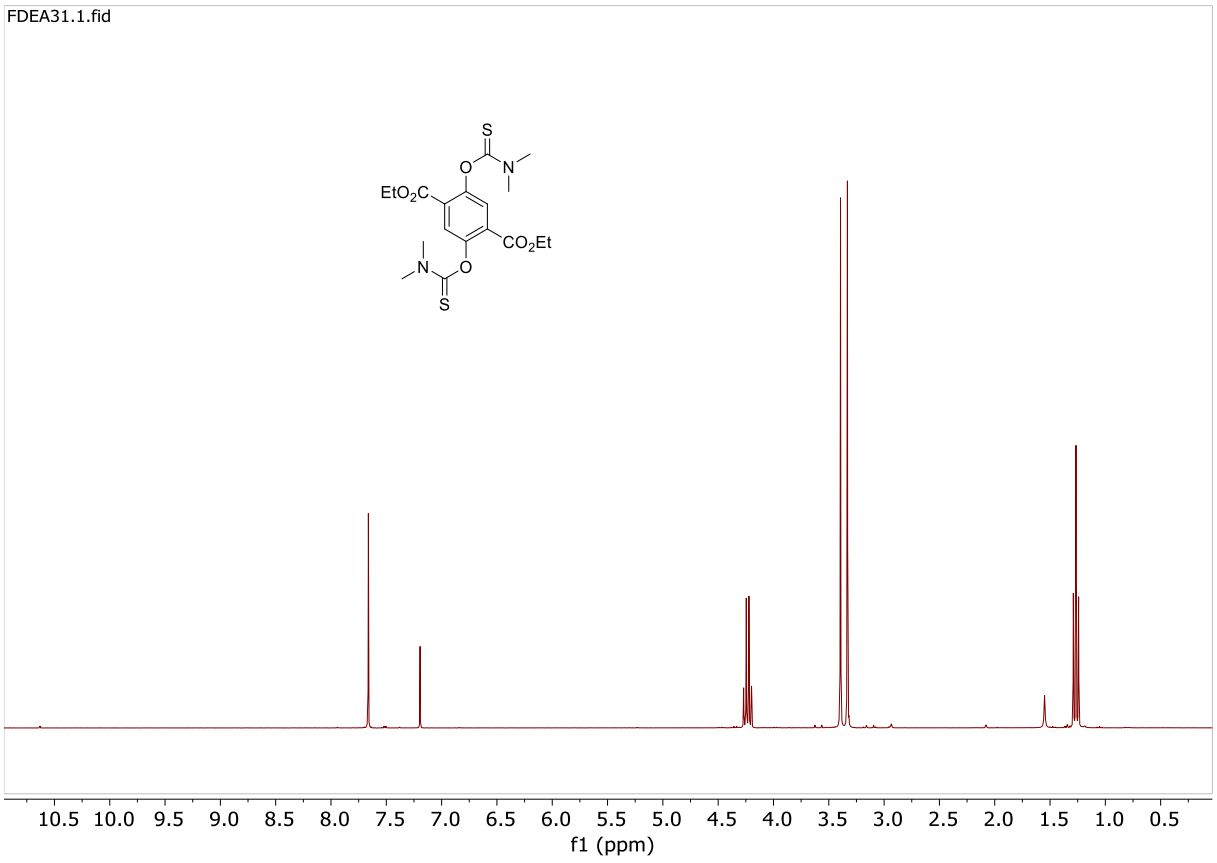

Diethyl 2,5-bis(dimethylcarbamoylsulfanyl)terephthalate (S3)

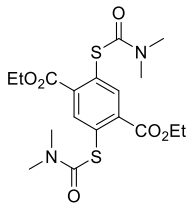

Diethyl 2,5-bis(dimethylthiocarbamoyloxy)terephthalate **S2** (3,6 g, 8.21 mmol) was heated under neat conditions at 210°C for 2 h. The solid was cooled at 90°C. Then, ethanol was added (120 mL) and the mixture was cooled at 0°C overnight. The precipitate was washed with cooled ethanol (2×45 mL) and dried under vacuum to give compound **S3** as a beige powder (3.3 g, 7.62 mmol, 93%).

^{1}H NMR (300 MHz, $CDCl_3$) δ ppm = 8.09 (s, 2H, Ar), 4.32 (q, J = 7.2 Hz, 4H, CH_2), 3.10 (brs, 6H, NCH_3), 2.99 (br s, 6H, NCH_3), 1.34 (t, J = 7.2 Hz, 6H, CH_3)

The data were in agreement with the literature reference. *J. Am. Chem. Soc.*, **2006**, *128*, 10253-10257

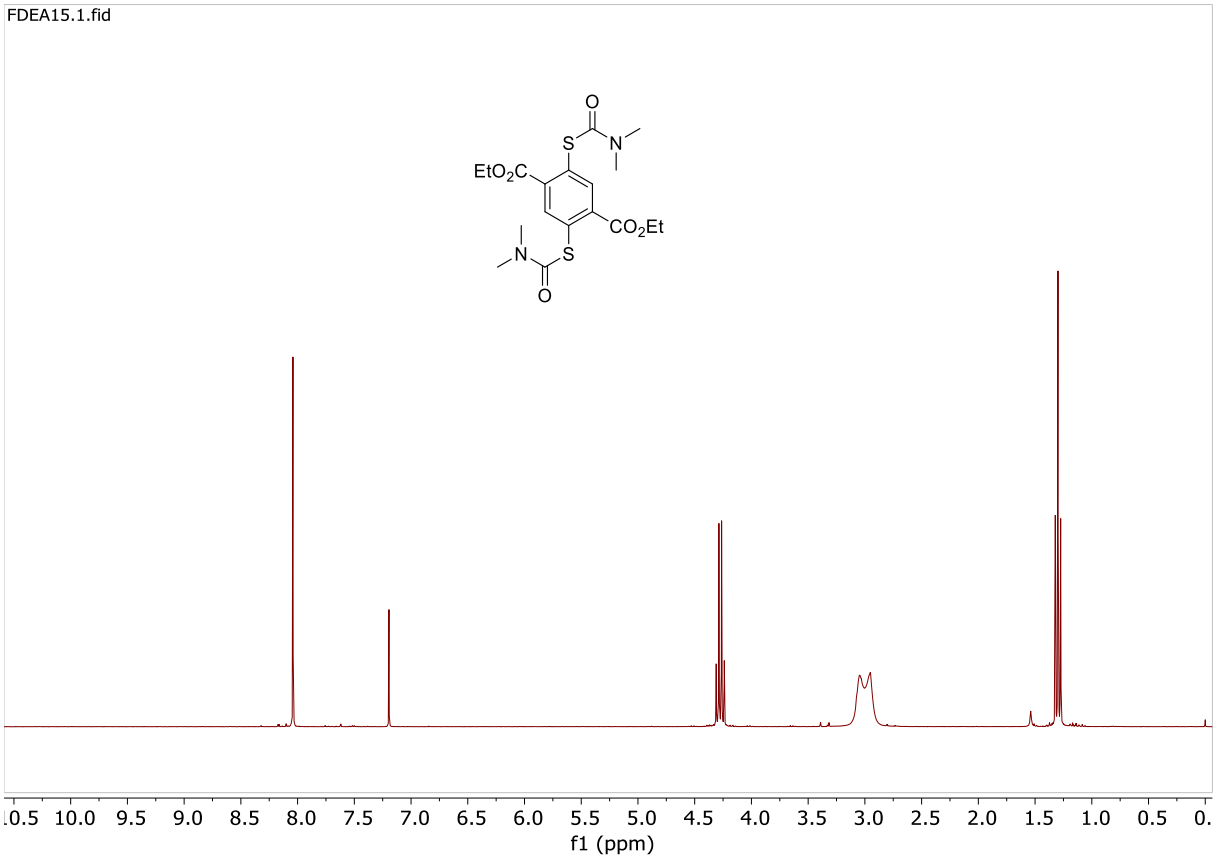

2,5-Dimercaptoterephthalic acid (1)

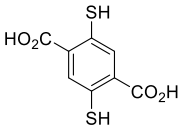

A solution of diethyl diethyl 2,5-bis(dimethylcarbamoylsulfanyl)terephthalate **S3** (2.9 g, 6.7 mmol, 1 eq.) in degassed 1.3 M KOH (7.3 g, 130.3 mmol, 17 eq.) in EtOH/H_2O (1:1, 100 mL) was heated under reflux under an inert atmosphere for 3 h. The reaction mixture was cooled in an ice-bath, and concentrated HCl (30 mL) was added until pH 1. A bright yellow precipitate was formed, filtered, and washed extensively with water, yielding compound **1** as a yellow solid (1.5 g, 6.6 mmol, >95%).

^{1}H NMR (300 MHz, CD_3OD) δ = 8.06 (s, 2H, Ar)

The data were in agreement with the literature reference. *J. Am. Chem. Soc*., **2006**, *128*, 10253-10257

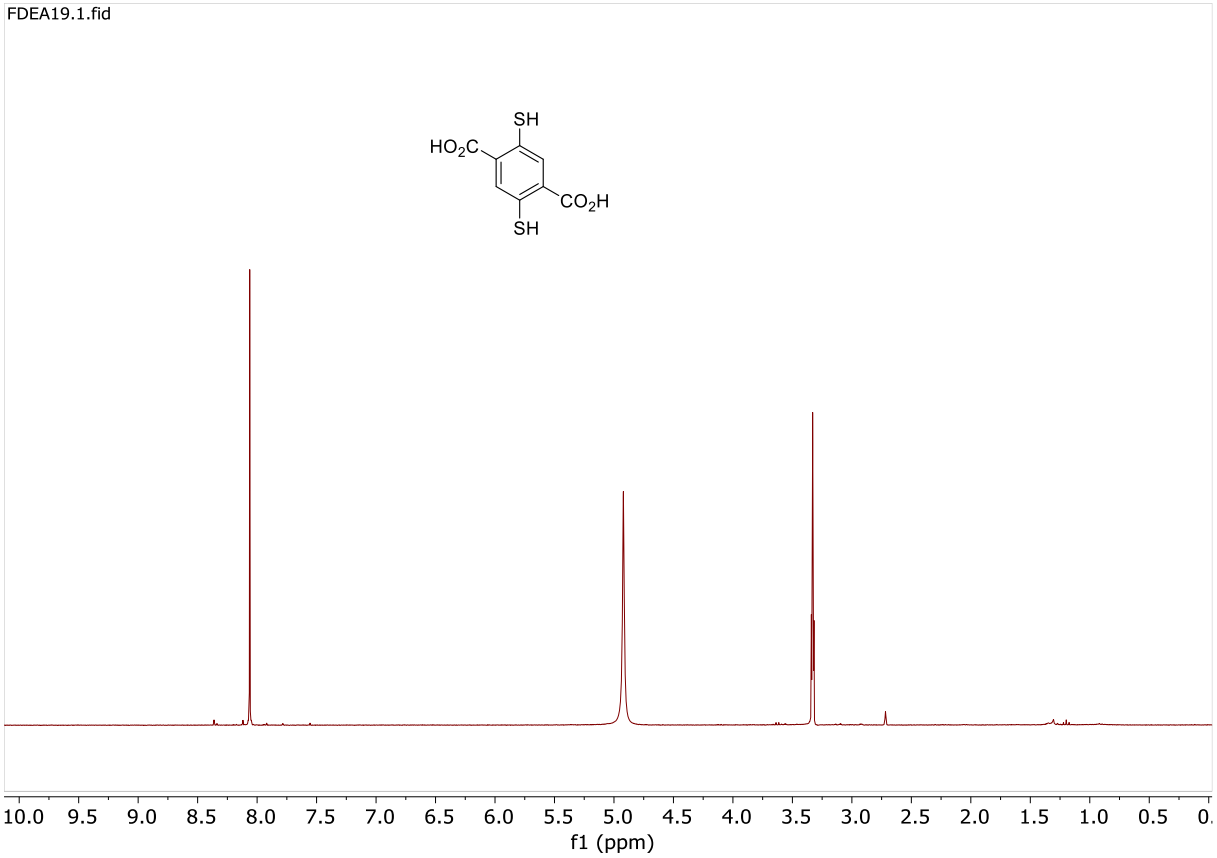

2,5-Di[(2-cyanoethyl)thio]terephthalic acid (2)

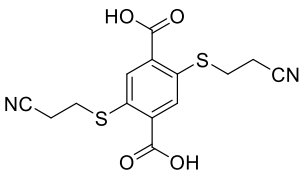

2,5-Dimercaptoterephthalic acid **1** (0.965 g, 4.2 mmol, 1 eq.) was dissolved in degassed THF (20 mL) and heated to 70°C. Then, resulting mixture was added on a suspension of NaH (60% in mineral oil, 1.047 g, 26.2 mmol, 6.2 eq.) in degassed anhydrous THF (10 mL). The suspension was stirred at r.t. during 1 h then 3-bromopropionitrile (4 mL, 48.2 mmol, 12 eq.) was added dropwise at r.t. The mixture was heated at 70°C for 16 h. The solvent was evaporated and the yellow solid crude residue was suspended in $CHCl_3$ (50 mL) then filtered off using a hydrophobic membrane (5 µm). The solid was dried under vacuum then poured into 1 M HCl (40 mL). The precipitate was filtered off using a hydrophilic membrane (5 µm) and washed with water (5×20 mL). The solid was dried under vacuum to afford 2,5-di[(2-cyanoethyl)thio]terephthalic acid **2** (1.417 g, 4.2 mmol, >95%) as a bright yellow amorphous solid.

^{1}H NMR (300 MHz, DMSO-d_6): 13.62 (bs, 2H, CO_2H), 7.80 (s, 2H, H_{ar}), 3.26 (t, *J* = 6.8 Hz, 4H, SCH_2), 2.87 (t, *J* = 6.8 Hz, 4H, CH_2CN)

^{13}C NMR (75 MHz, DMSO-d_6): 166.7 (CO_2H), 134.1 (CS), 132.9 (CCO_2H), 128.5 (CH_{ar}), 119.2 (CH_2CN), 27.1 (SCH_2), 16.5 (CH_2CN)

HR-ESI-MS (positive mode) *m/z* : calcd. for $C_{14}H_{12}N_2NaO_4S_2$ $[M+Na]^+$ 359.0131, found 359.0145

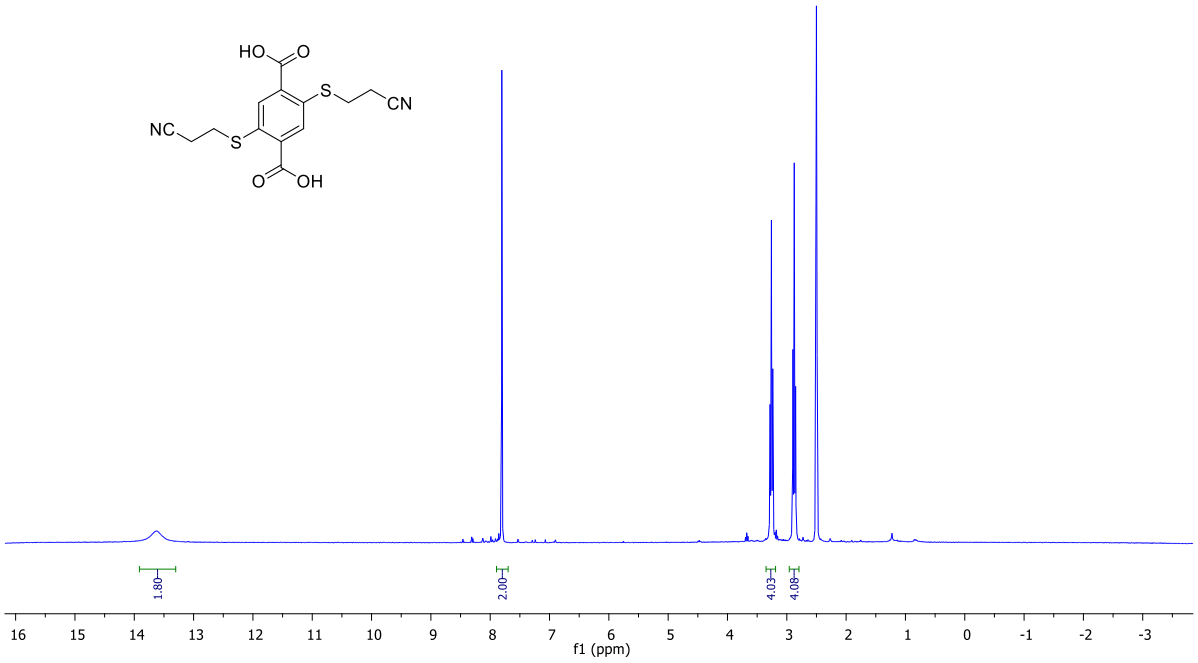
HO
O
S
CN
NC
S
O
OH
1.80
2.00
4.03
4.08
16 15 14 13 12 11 10 9 8 7 6 5 4 3 2 1 0 -1 -2 -3
f1 (ppm)

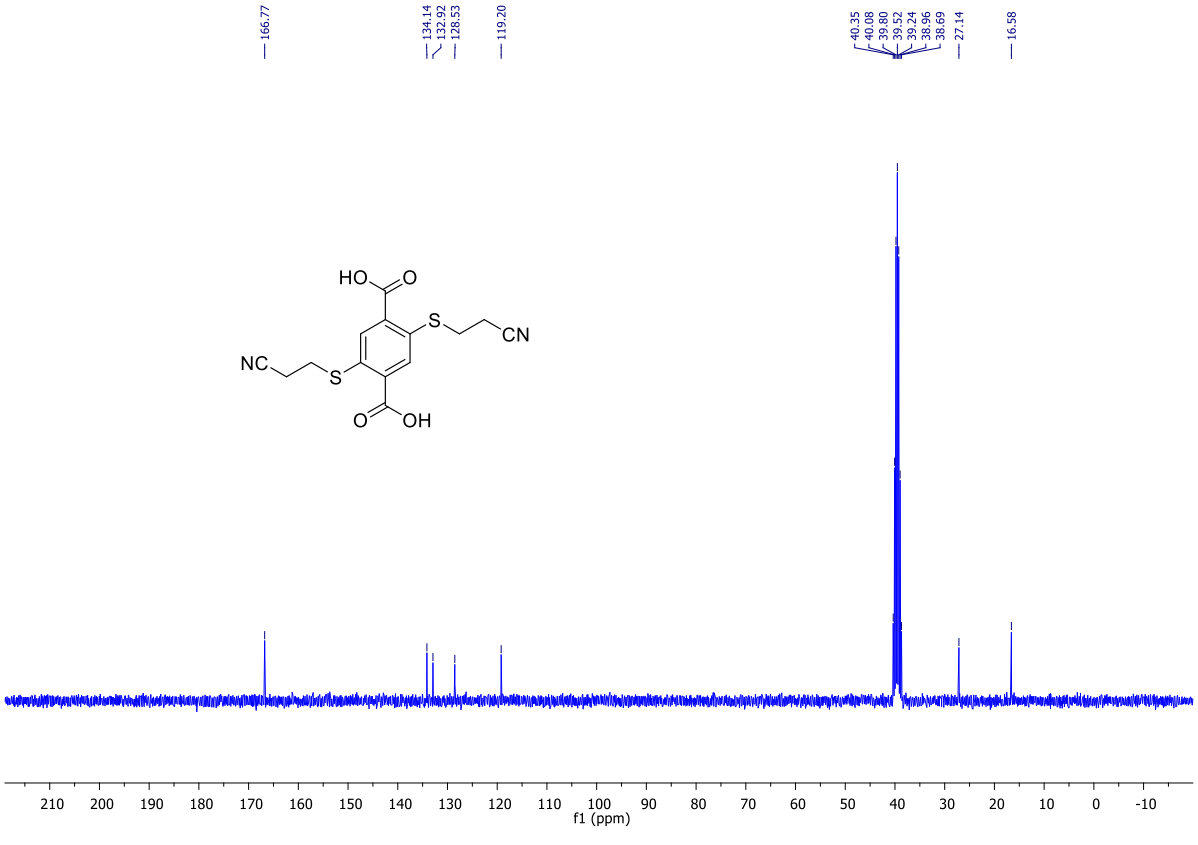
166.77
134.14
132.92
128.53
119.20
40.35
40.08
39.80
39.52
39.24
38.96
38.69
27.14
16.58
HO
O
S
CN
NC
S
O
OH
210 200 190 180 170 160 150 140 130 120 110 100 90 80 70 60 50 40 30 20 10 0 -10
f1 (ppm)

1-Ammonium-3,6-dioxaoct-8-yl 2,3,4,6-tetra-O-acetyl-α-D-mannopyranoside *p*-toluenesulfonate (4-Man)

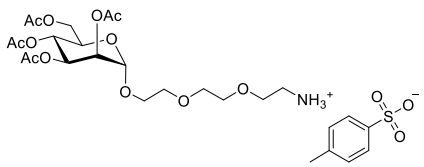

A solution of azide **3-Man** (13.56 g, 26.83 mmol, 1 eq.) and *p*TsOH (4.77 g, 27.70 mmol, 1 eq.) in dry MeOH (500 mL) with Pd/C 10% (1.4 g, 10%w) was placed under H_2 atmosphere (1 bar). The reaction was monitored by TLC and stirred until completion. After 45 min, the mixture was filtered on a pad of celite and washed with MeOH and the solvent was evaporated to afford the desired product ammonium **4-Man** *p*TsOH salt (16.15 g, 24.78 mmol, 92%) as a green amorphous solid.

^{1}H NMR (300 MHz, CD_3OD): 7.67 (d, *J* = 8.1 Hz, 2H, CH_{Ar}), 7.20 (d, *J* = 7.8 Hz, 2H, CH_{Ar}), 5.23 (dd, *J* = 7.8, 2.1 Hz, 3H, H_2, H_3, H_4), 4.86 (d, *J* = 1.2 Hz, 1H, H_1), 4.19 (m, 1H, H_5), 4.08 (m, 2H, H_6), 3.87-3.78 (m, 2H, CH_2OMan), 3.70-3.63 (m, 8H, 4xCH_2O), 3.14 (br, 2H, CH_2N), 2.33 (s, 3H, $C_{Ar}CH_3$), 2.10, 2.04, 1.99, 1.92 (s, 4x3H, $COCH_3$).

^{13}C NMR (300 MHz, CD_3OD): 171.0, 172.3, 171.9, 170.1 (4x*C*OCH_3), 142.2 ($C_{Ar}CH_3$), 140.3 ($C_{Ar}SO_3$), 128.4 (2xC, C_{Ar}), 125.6 (2xC, C_{Ar}), 97.5 (C_1), 70.22, 69.8, 69.7 (3xCH_2O), 69.4 (C_2), 69.3 (C_3), 68.5 (C_5), 67.0 (CH_2O), 66.8 (CH_2OMan), 65.9 (C_4), 62.2 (C_6), 39.5 (CH_2N), 19.9, 19.30, 19.26, 19.2 (4xCO*C*H_3).

HR-ESI-MS (positive mode) *m/z*: calcd. for $C_{20}H_{34}NO_{12}$: $[M]^+$ = 480.2076, found 480.2074.

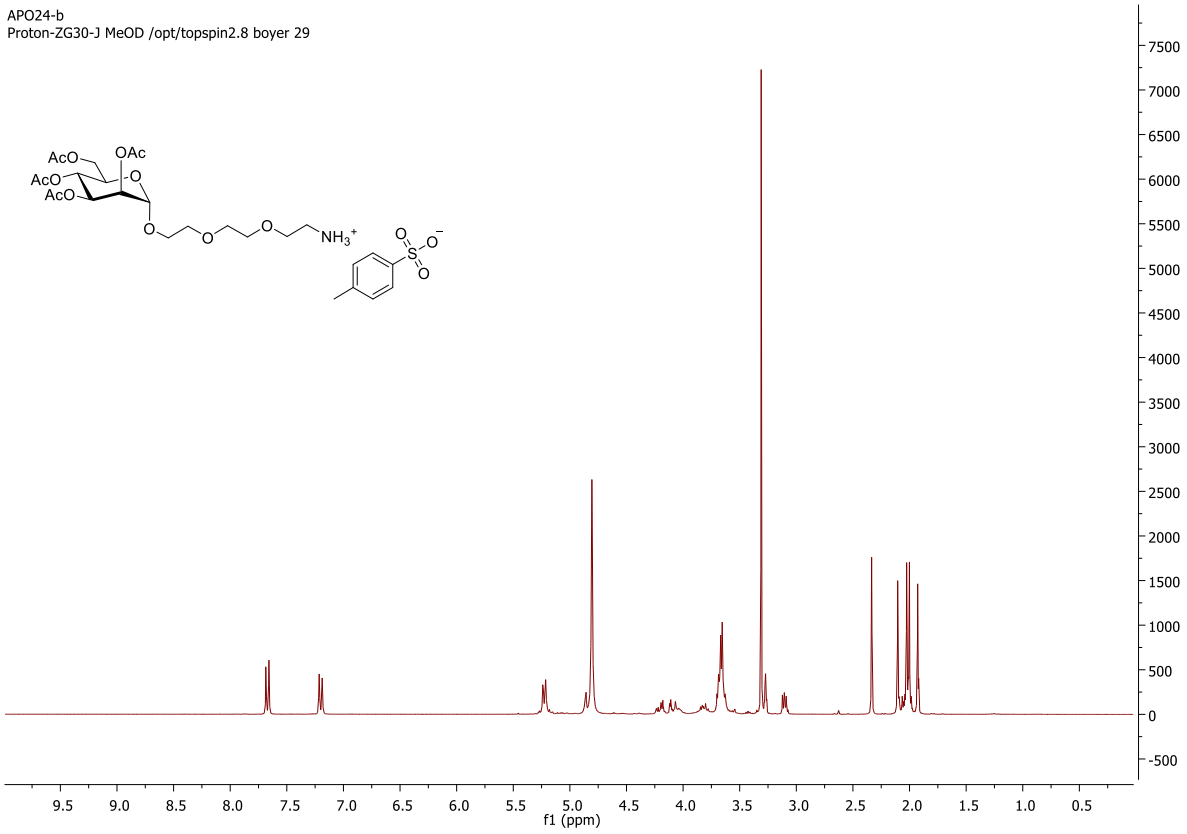
APO24-b
Proton-ZG30-J MeOD /opt/topspin2.8 boyer 29
AcO
OAc
AcO
O
AcO
O
O
O
NH3+
O
S
O
O
O
7500
7000
6500
6000
5500
5000
4500
4000
3500
3000
2500
2000
1500
1000
500
0
-500
9.5
9.0
8.5
8.0
7.5
7.0
6.5
6.0
5.5
5.0
4.5
4.0
3.5
3.0
2.5
2.0
1.5
1.0
0.5
f1 (ppm)

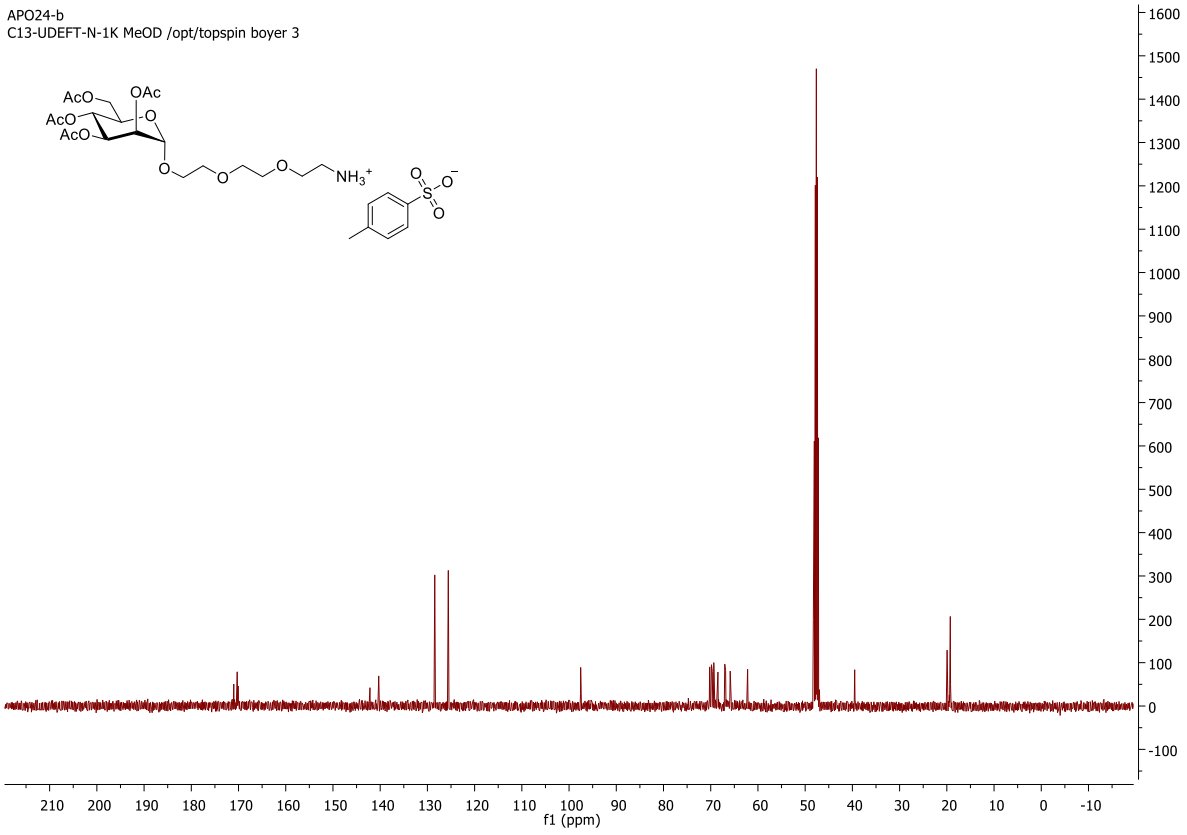
APO24-b
C13-UDEFT-N-1K MeOD /opt/topspin boyer 3
AcO
OAc
AcO
O
AcO
O
O
O
NH3+
O
S
O
O
O
1600
1500
1400
1300
1200
1100
1000
900
800
700
600
500
400
300
200
100
0
-100
210
200
190
180
170
160
150
140
130
120
110
100
90
80
70
60
50
40
30
20
10
0
-10
f1 (ppm)

1-Ammonium-3,6-dioxaoct-8-yl 2,3,4,6-tetra-*O*-acetyl-β-D-galactopyranoside *p*-toluenesulfonate (4-Gal)

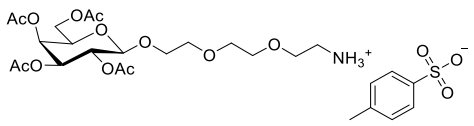

A solution of azide **3-Gal** (777 mg, 1.31 mmol, 1 eq.) and *p*TsOH (250 mg, 1.32 mmol, 1 eq.) in dry MeOH (65 mL) with Pd/C 10% (99 mg, 10%w) was placed under H_2 atmosphere (1 bar). The reaction was monitored by TLC and stirred until completion. After 20 min, the mixture was filtered on a pad of celite and washed with MeOH and the solvent was evaporated to afford the desired product ammonium **4-Gal** and *p*TsOH salt (850 mg, 1.3 mmol, >95%) as a green amorphous solid.

^{1}H NMR (400 MHz, CD_3OD): 7.71 (d, *J* = 8.2 Hz, 2H, CH_{Ar}), 7.25 (d, *J* = 8.2 Hz, 2H, CH_{Ar}), 5.39 (dd, *J* = 3.1, 1.0 Hz, 1H, H_4) 5.15-5.07 (m, 2H, H_2 + H_3), 4.69 (d, *J* = 7.3 Hz, 1H, H_1), 4.22-4.07 (m, 3H, H_6 + CH_2OGal), 4.01-3.91 (m, 1H, H_5), 3.78-3.63 (m, 9H, 4xCH_2O + CH_2OGal), 3.13 (bs, 2H, CH_2N), 2.37 (s, 3H, $C_{Ar}CH_3$), 2.14, 2.05, 2.03, 1.95 (s, 4x$COCH_3$)

^{13}C NMR (100 MHz, CD_3OD): 172.1, 171.9, 171.5, 171.4 (4xC, *C*OCH_3), 143.6 (*C*CH_3), 141.7 (*C*SO_3), 129.8 (2xC, C_{Ar}), 126.9 (2xC, C_{Ar}), 102.3 (C_1), 72.3, 71.8, 71.5, 71.3, 70.2 (5xC, CH_2O + CH_2OGal), 71.2 (C_5), 70.4, 68.8 (C_2 + C_3), 67.9 (C_4), 62.5 (C_6), 40.7 (CH_2N), 21.3, 20.8, 20.6, 20.5 (5xC, CO*C*H_3 + C*C*H_3).

HR-ESI-MS (positive mode) *m/z* : calcd. for $C_{20}H_{34}NO_{12}$: $[M]^+$ = 480.2076, found 480.2073.

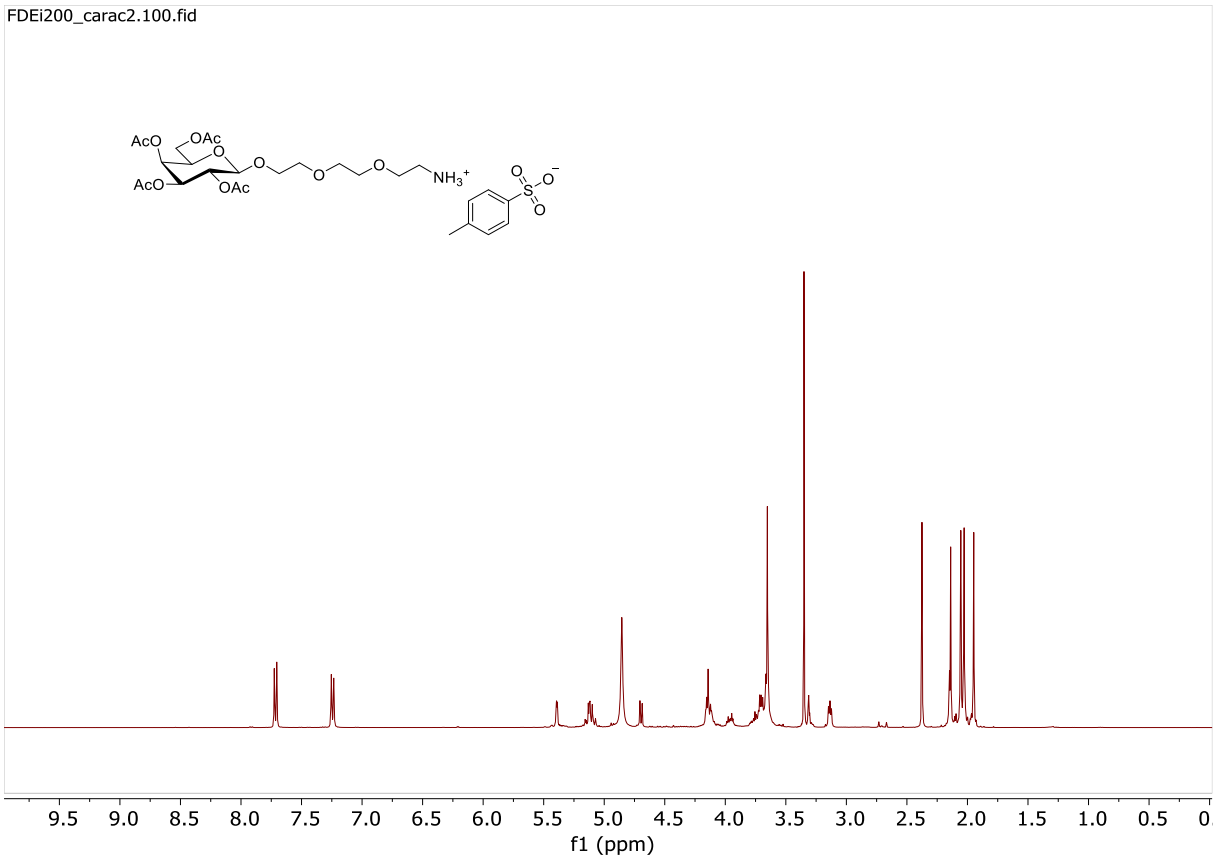
FDEi200_carac2.100.fid
AcO
OAc
AcO
OAc
NH3+
9.5 9.0 8.5 8.0 7.5 7.0 6.5 6.0 5.5 5.0 4.5 4.0 3.5 3.0 2.5 2.0 1.5 1.0 0.5 0
f1 (ppm)

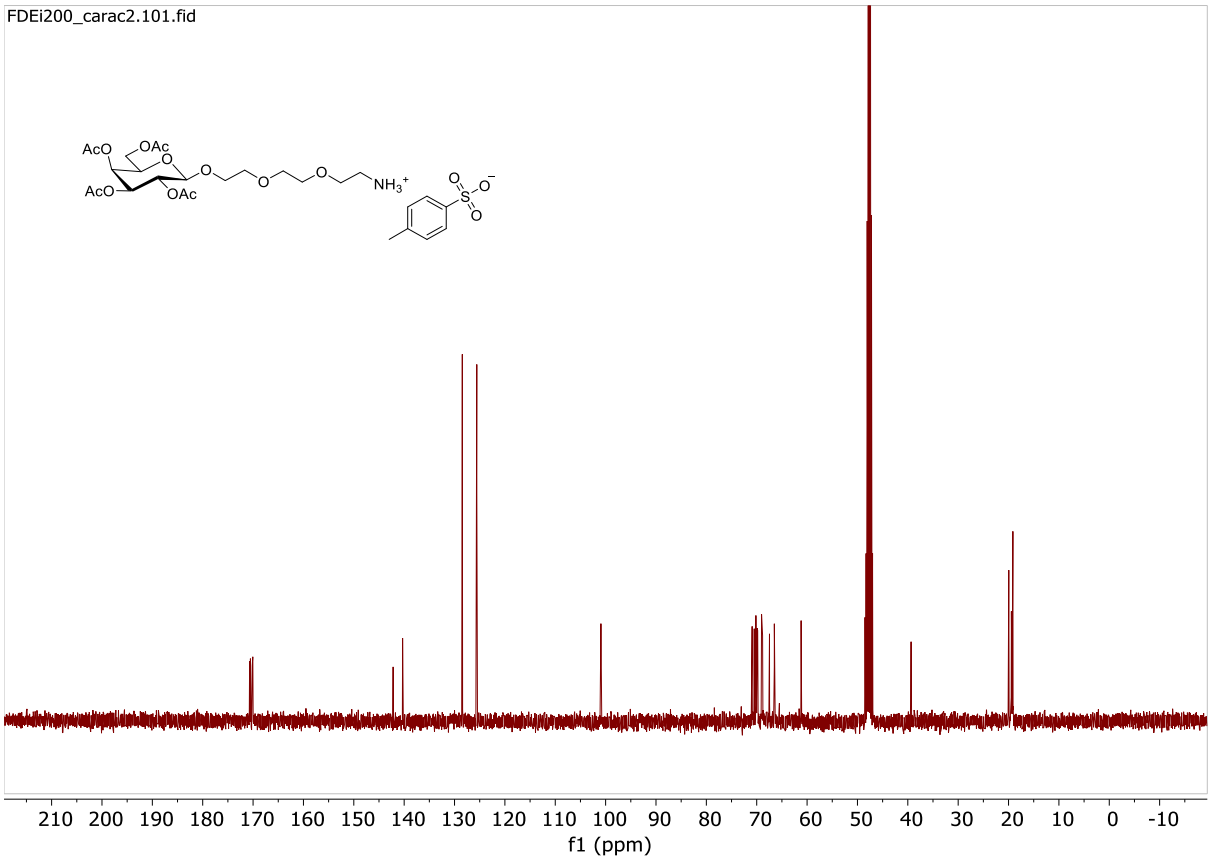
FDEi200_carac2.101.fid
AcO
OAc
AcO
OAc
NH3+
210 200 190 180 170 160 150 140 130 120 110 100 90 80 70 60 50 40 30 20 10 0 -10
f1 (ppm)

1-Ammonium-3,6-dioxaoct-8-yl 2,3,4-tri-*O*-acetyl-α-L-fucopyranoside *p*-toluenesulfonate (4-Fuc)

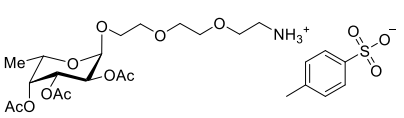

A solution of azide **3-Fuc** (1.014 g, 2.27 mmol, 1 eq.) and *p*TsOH (0.433 g, 2.28 mmol, 1 eq.) in dry MeOH (100 mL) with Pd/C 10% (79 mg, 10%w) was placed under H_2 atmosphere (1 bar). The reaction was monitored by TLC and stirred until completion. After 25 min, the mixture was filtered on a pad of celite and washed with MeOH and the solvent was evaporated to afford the desired product ammonium **4-Fuc** *p*TsOH salt (1.279 g, 2.15 mmol, 95%) as a green amorphous solid.

^{1}H NMR (400 MHz, CD_3OD): 7.71 (d, *J* = 8.2 Hz, 2H, CH_{Ar}), 7.24 (d, *J* = 8.2 Hz, 2H, CH_{Ar}), 5.35 (dd, *J* = 10.7, 3.4 Hz, 1H, H_3) 5.27 (dd, *J* = 3.5, 1.4 Hz, 1H, H_2), 5.11-5.04 (m, 2H, H_1 + H_2) 4.27 (qd, *J* = 6.5, 1.4 Hz, 1H, H_5), 3.84-3.80 (m, 1H, CH_2OFuc), 3.72-3.66 (m, 9H, 4xCH_2O + CH_2OFuc), 3.14 (bs, 2H, CH_2N), 2.37 (s, 3H, $C_{Ar}CH_3$), 2.15, 2.05, 1.96 (s, 4x$COCH_3$)

^{13}C NMR (100 MHz, CD_3OD): 172.3, 172.0, 171.8 (3xC, *C*OCH_3), 143.6 ($C_{Ar}CH_3$), 141.7 ($C_{Ar}SO_3$), 129.8 (2xC_{Ar}), 127.0 (2xC_{Ar}), 97.5 (C_1), 72.6 (C_4), 71.6, 71.4, 71.3 (3xCH_2), 69.5 (C_3), 69.4 (C_2), 68.2 (FucO*C*H_2CH_2), 67.9 (FucOCH_2*C*H_2), 65.7 (C_5), 40.7 (CH_2N), 21.3 ($C_{Ar}CH_3$), 20.7, 20.6, 20.5 (3xCO*C*H_3), 16.2 (C_6).

HR-ESI-MS (positive mode) *m/z* : calcd. for $C_{18}H_{32}NO_{10}$: $[M]^+$ = 422.2021, found 422.2014.

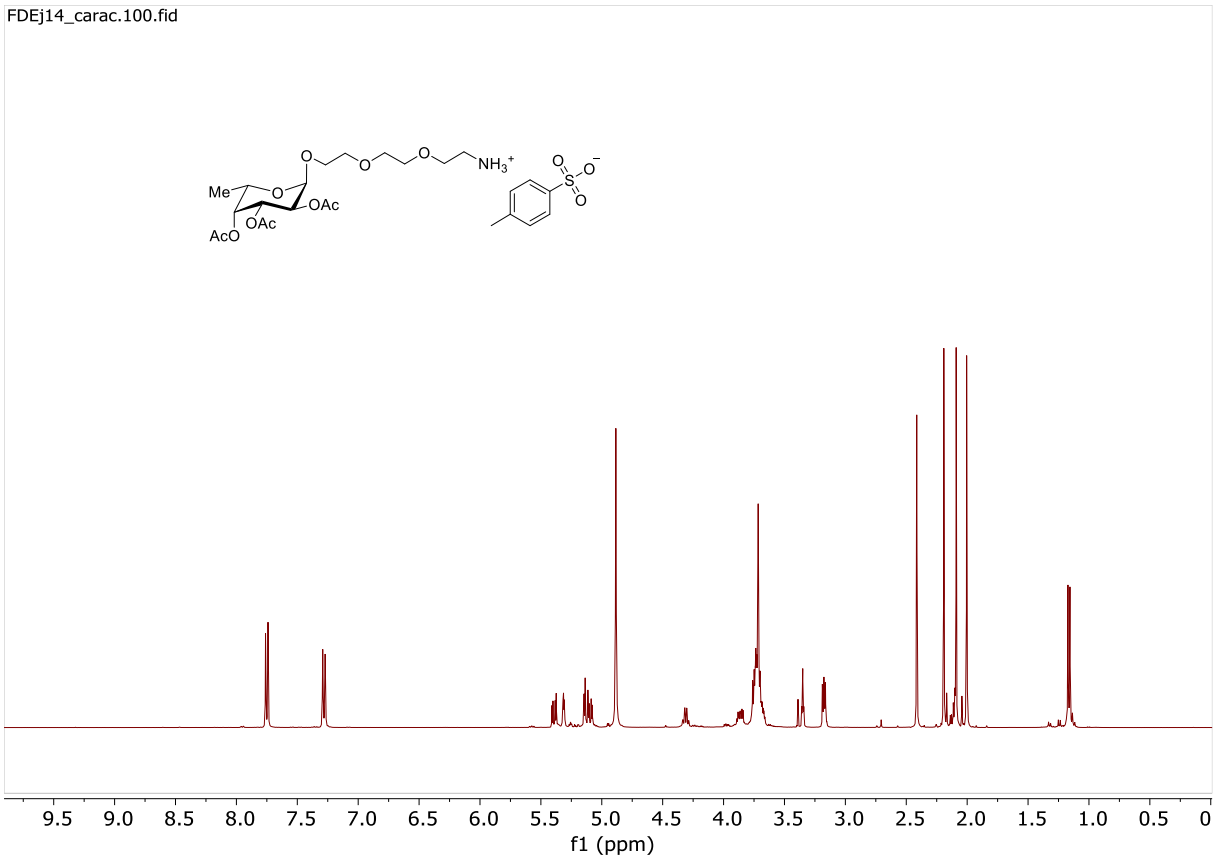
FDEj14_carac.100.fid
Me
O
OAc
AcO
OAc
O
O
O
NH3+
O
S
O
O
9.5 9.0 8.5 8.0 7.5 7.0 6.5 6.0 5.5 5.0 4.5 4.0 3.5 3.0 2.5 2.0 1.5 1.0 0.5 0
f1 (ppm)

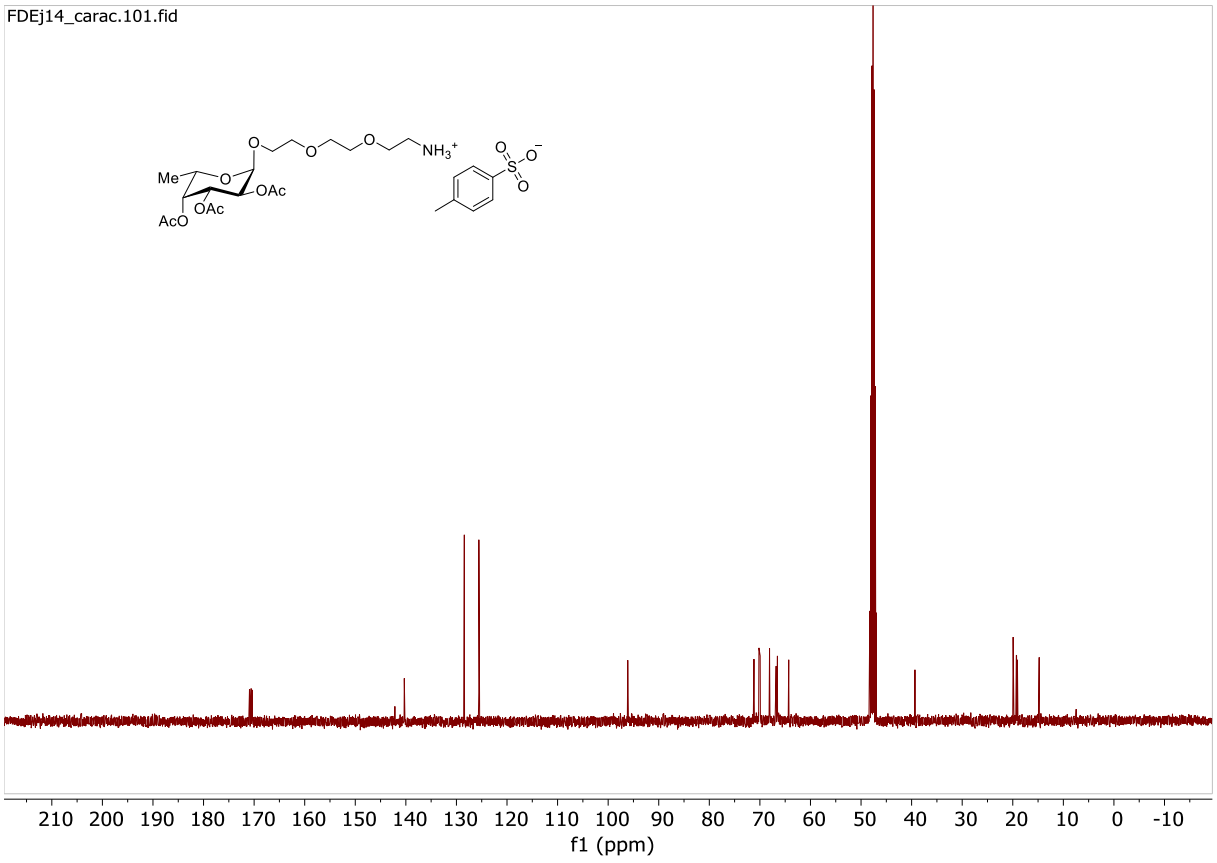
FDEj14_carac.101.fid
Me
O
OAc
AcO
OAc
O
O
O
NH3+
O
S
O
O
210 200 190 180 170 160 150 140 130 120 110 100 90 80 70 60 50 40 30 20 10 0 -10
f1 (ppm)

General procedure for the formation of amides

2,5-Di[(2-cyanoethyl)thio]terephthalic acid **2** (1 eq.), HOBt•H_2O (2.6 eq.) and EDCI•HCl or EDCI (2.6 eq.) were suspended under inert atmosphere (Ar) in dry CH_2Cl_2 affording a heterogeneous yellow solution. Amine **4** (2.6 eq.) dissolved in dry CH_2Cl_2 was added dropwise, *i*Pr_2NEt (2.6 eq.) was then added and the stirring was continued during 18 h. The solvent was evaporated off and the crude residue was purified by flash silica gel column chromatography (CH_2Cl_2/MeOH 97:3) to afford the desired amide **5**.

2,5-Di[(2-cyanoethyl)thio]-*N*,*N*-di[3,6-dioxa-8-(2,3,4,6-tetra-*O*-acetyl-β-D-galactopyranosyloxy)-oct-1-yl]terephthalamide (5-Gal)

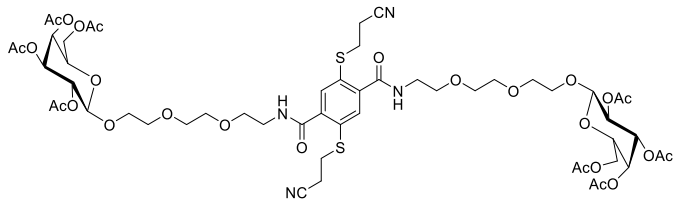

Prepared according to the general procedure from diacid **2** (614 mg, 1.827 mmol, 1 eq.), HOBt•H_2O (728 mg, 4.727 mmol, 2.6 eq.), EDCI (840 µL, 4.727 mmol, 2.6 eq.) in CH_2Cl_2 (100 mL), *i*Pr_2NEt (840 µL, 4.822 mmol, 2.7 eq.) and amine **4-Gal** (3.100 g, 4.757 mmol, 2.6 eq.) in CH_2Cl_2 (50 mL) affording compound **5-Gal** (1.244 g, 54%) as a brown oil.

Rf = 0.5 ($CHCl_3$/MeOH, 19:1)

^{1}H NMR (400 MHz, $CDCl_3$): 7.69 (s, 2H, H_{ar}), 7.16 (t, *J* = 5.2 Hz, 2H, NH), 5.37 (d, *J* = 3.4 Hz, 2H, H_4), 5.17 (dd, *J* = 7.9; 10.5 Hz, 2H, H_2), 5.00 (dd, *J* = 3.4; 10.5 Hz, 2H, H_3), 4.51 (d, *J*= 7.9 Hz, 2H, H_1), 4.18-4.05 (m, 4H, H_6 + $H_{6'}$), 3.98-3.88 (m, 4H, CH_2OGal + H_5), 3.75-3.60 (m, 22H, CH_2OGal + 4×OCH_2 + NHCH_2), 3.19 (t, *J* = 7.0 Hz, 4H, SCH_2), 2.68 (t, *J* = 7.0 Hz, 4H, CH_2CN), 2.14; 2.05; 2.04; 1.98 (4×6H, $COCH_3$)

^{13}C NMR (100 MHz, $CDCl_3$): 170.6; 170.4; 170.3; 169.7 (4×*C*OCH_3), 166.7 (CONH), 140.3 (*C*CONH), 132.3 (CH_{ar}), 131.9 (CS), 118.1 (CN), 101.4 (C_1), 70.9 (C_3), 70.80; 70.4; 70.3; 69.7 (4×C, OCH_2), 70.79 (C_5), 69.2 (CH_2OGal), 68.9 (C_2), 67.1 (C_4), 61.3 (C_6), 40.1 ($NHCH_2$), 30.4 (SCH_2), 21.0; 20.85; 20.84; 20.7 (4×CO*C*H_3), 18.3 (*C*H_2*C*N)

HR-ESI-MS (positive mode) *m*/*z*: calcd. for $C_{54}H_{74}N_4Na_2O_{26}S_2$ $[M+2Na]^{2+}$ = 652.1909, found 652.1909.

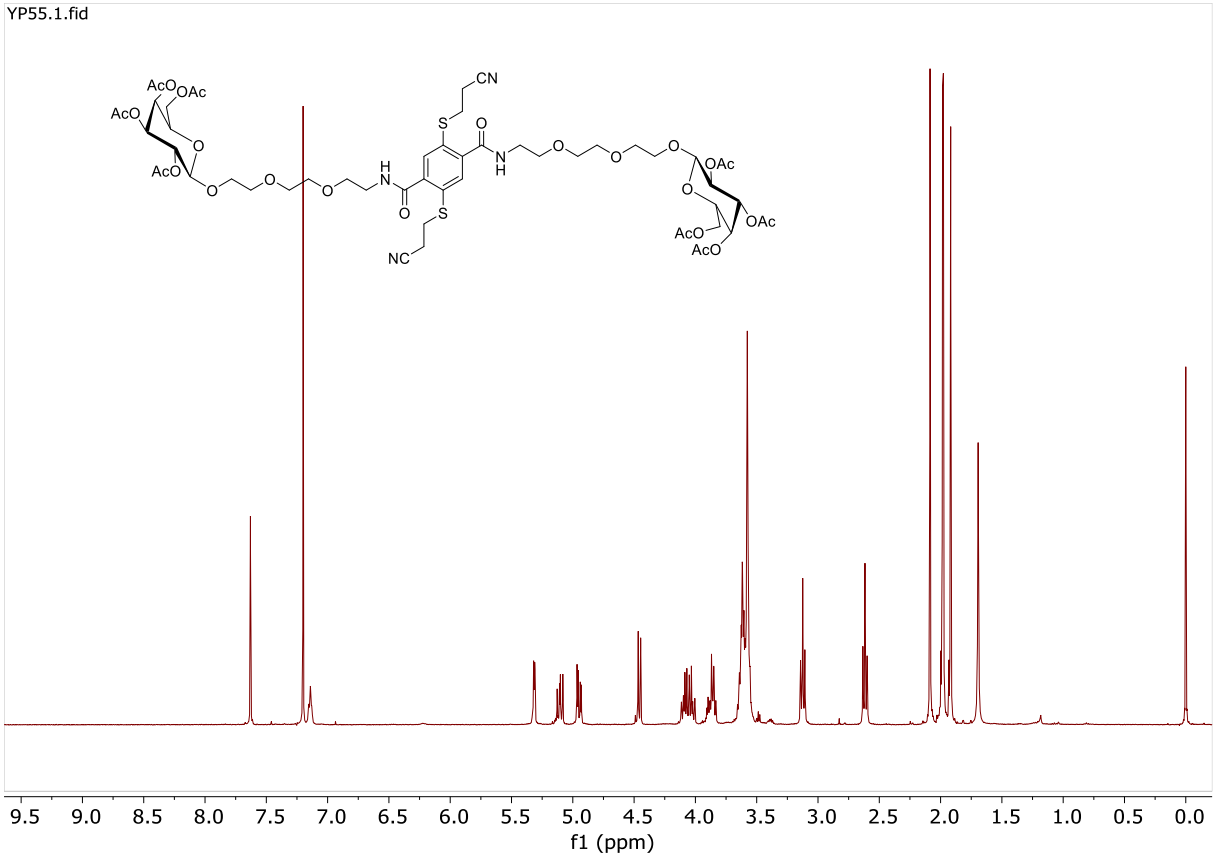
YP55.1.fid
9.5 9.0 8.5 8.0 7.5 7.0 6.5 6.0 5.5 5.0 4.5 4.0 3.5 3.0 2.5 2.0 1.5 1.0 0.5 0.0
f1 (ppm)

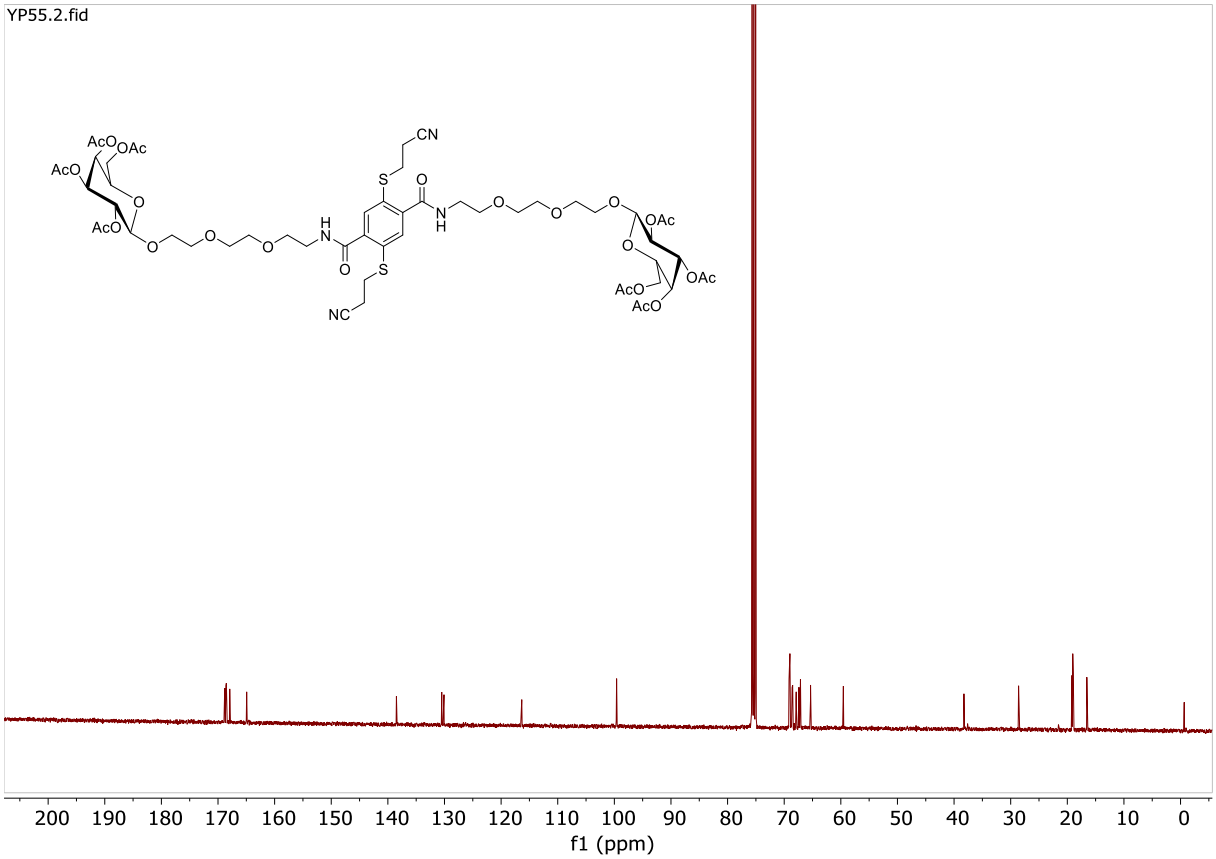
YP55.2.fid
200 190 180 170 160 150 140 130 120 110 100 90 80 70 60 50 40 30 20 10 0
f1 (ppm)

2,5-Di[(2-cyanoethyl)thio]-*N*,*N*-di[3,6-dioxa-8-(2,3,4-tri-*O*-acetyl-α-L-fucopyranosyloxy)-oct-1-yl]terephthalamide (5-Fuc)

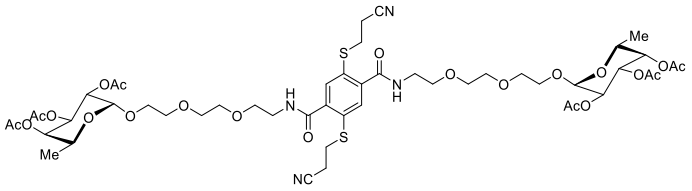

Prepared according to the general procedure from diacid **2** (312 mg, 0.926 mmol, 1 eq.), HOBt•H_20 (370 mg, 2.42 mmol, 2.6 eq.), EDCI (430 µL, 2.42 mmol, 2.6 eq.) in CH_2Cl_2 (25 mL), *i*Pr_2Net (420 µL, 2.42 mmol, 2.6 eq.) and amine **4-Fuc** (1.405 g, 2.36 mmol, 2.5 eq.) in CH_2Cl_2 (25 mL) affording the desired product **5-Fuc** (584 mg, 55%) as a brown oil.

Rf = 0.5 ($CHCl_3$/MeOH, 19:1)

^{1}H NMR (300 MHz, $CDCl_3$): 7.62 (s, 2H, H_{ar}), 7.25 (br, 2H, NH), 5.33-5.26 (m, 2H), 5.22 (m, 2H), 5.09-5.00 (m, 4H), 4.17 (q, *J* = 6.6 Hz, 2H, H_5), 3.75-3.67 (m, 2H, CH_2OFuc), 3.67-3.55 (m, 22H, CH_2OFuc + 4×OCH_2 + NHCH_2), 3.14 (t, *J* = 7.0 Hz, 4H, SCH_2), 2.64 (t, *J* = 7.0 Hz, 4H, CH_2CN), 2.12; 2.01; 1.92 (3×6H, $COCH_3$), 1.08 (d, *J* = 6.6 Hz, H_6).

^{13}C NMR (75 MHz, $CDCl_3$): 170.7; 170.5; 170.3 (3×*C*OCH_3), 166.7 (CONH), 140.3 (*C*CONH), 132.0 (CH_{ar}), 131.7 (CS), 118.1 (CN), 96.2 (C_1), 71.2 (C_4), 70.7; 70.4; 70.1; 69.6 (4×OCH_2), 68.2 (C_2 or C_3), 68.0 (C_2 or C_3), 67.3 (CH_2OFuc), 64.4 (C_5), 40.0 (NHCH_2), 30.2 (SCH_2), 20.9; 20.76; 20.70 (3×*C*OCH_3), 18.2 (*C*H_2*C*N), 15.9 (C_6).

HR-ESI-MS (positive mode) *m/z* : calcd. for $C_{50}H_{71}N_4O_{22}S_2$ $[M+H]^+$ = 785.2835, found 785.2831.

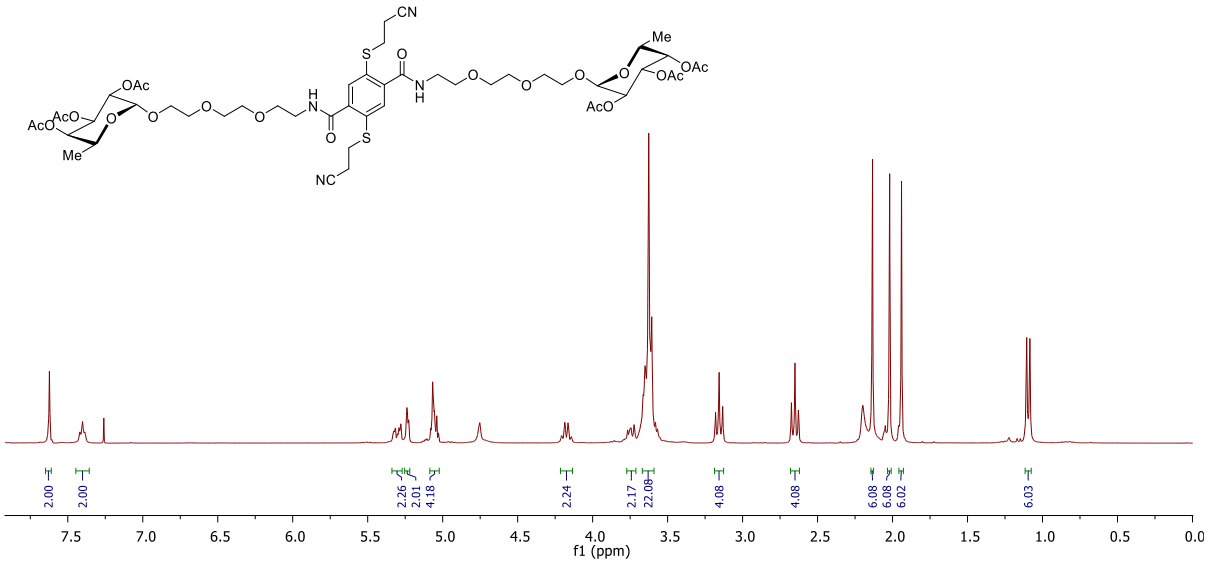
CN
S
O
N
H
OAc
AcO
AcO
O
O
O
O
O
O
O
Me
OAc
OAc
AcO
Me
O
O
S
NC
2.00
2.00
2.26
2.01
4.18
2.24
2.17
22.08
4.08
4.08
6.08
6.08
6.02
6.03
7.5
7.0
6.5
6.0
5.5
5.0
4.5
4.0
3.5
3.0
2.5
2.0
1.5
1.0
0.5
0.0
f1 (ppm)

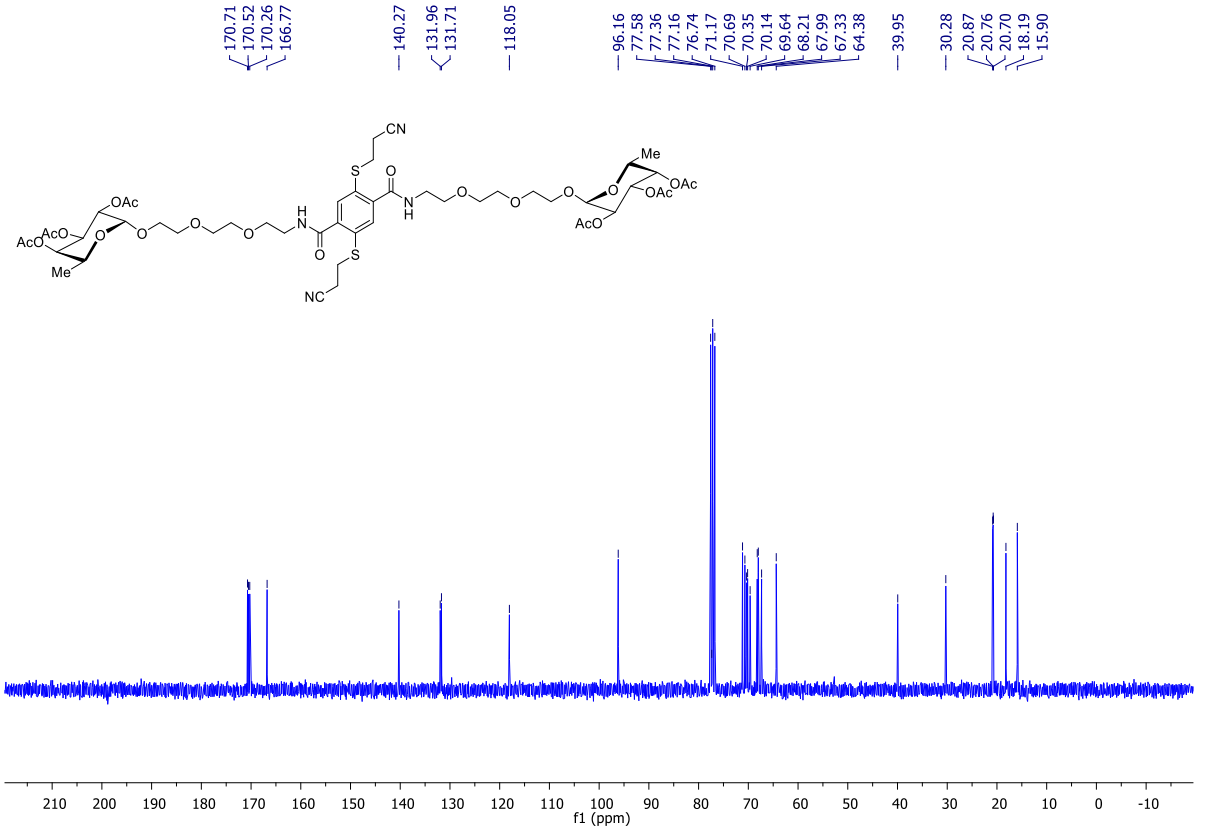
170.71
170.52
170.26
166.77
140.27
131.96
131.71
118.05
96.16
77.58
77.36
77.16
76.74
71.17
70.69
70.35
70.14
69.64
68.21
67.99
67.33
64.38
39.95
30.28
20.87
20.76
20.70
18.19
15.90
CN
S
O
N
H
OAc
AcO
AcO
O
O
O
O
O
O
O
Me
OAc
OAc
AcO
Me
O
O
S
NC
210
200
190
180
170
160
150
140
130
120
110
100
90
80
70
60
50
40
30
20
10
0
-10
f1 (ppm)

2,5-Di[(2-cyanoethyl)thio]-*N*,*N*-di[3,6-dioxa-8-(2,3,4,6-tetra-*O*-acetyl-α-D-mannopyranosyloxy)-oct-1-yl]terephthalamide (5-Man)

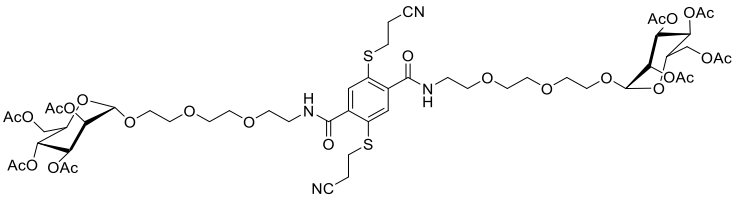

Prepared according to the general procedure from diacid **2** (291 mg, 0.87 mmol, 1 eq.), HOBt monohydrate (354 mg, 2.31 mmol, 2.6 eq.), EDCI•HCl (400 µL, 2.26 mmol, 2.6 eq.) in CH_2Cl_2 (40 mL) , *i*Pr_2NEt (350 µL, 2.01, 2.3 eq.) and amine **4-Man** (1.398 g, 2.35 mmol, 2.7 eq.) in CH_2Cl_2 (35 mL) affording the desired product **5-Man** (598 mg, 55%) as a brown oil.

Rf = 0.5 ($CHCl_3$/MeOH, 19:1)

^{1}H NMR (300 MHz, $CDCl_3$): 7.67 (s, 2H, CH_{ar}), 7.14 (br, 2H, NH), 5.33-5.25 (m, 4H, H_3 + H_4), 5.22 (dd, *J* = 1.6; 3.0 Hz, 2H, H_2), 4.85 (d, *J* = 1.6 Hz, 2H, H_1), 4.25 (dd, *J* = 4.9; 12.1 Hz, 2H, H_6), 4.10-3.95 (m, 4H, H_5 + $H_{6'}$), 3.83-3.73 (m, 2H, CH_2OMan), 3.73-3.59 (m, 22H, CH_2OMan + 4×OCH_2 + NHCH_2), 3.17 (t, *J*= 7.0 Hz, 4H, SCH_2), 2.66 (t, *J* = 7.0 Hz, 4H, CH_2CN), 2.13; 2.07; 2.02; 1.96 (4×6H, $COCH_3$).

^{13}C NMR (75 MHz, $CDCl_3$): 170.8; 170.3; 170.2; 169.8 (4×C, *C*OCH_3), 166.8 (CONH), 140.4 (*C*CONH), 132.2 (CH_{ar}), 131.7 (CS), 118.1 (CN), 97.7 (C_1), 70.7; 70.4; 70.0; 69.7 (4×C, OCH_2), 69.6 (C_2), 69.2 (C_3 or C_4), 68.5 (C_5), 67.3 (CH_2OMan), 66.1 (C_3 or C_4), 62.5 (C_6), 40.0 ($NHCH_2$), 30.4 (SCH_2), 21.0; 20.88; 20.84; 20.82 (4×C, CO*C*H_3), 18.3 (*C*H_2*C*N).

HR-ESI-MS (positive mode) *m*/*z*: calcd. for $C_{54}H_{74}N_4NaO_{26}S_2$ $[M+Na]^+$ = 1281.3925, found 1281.3927.

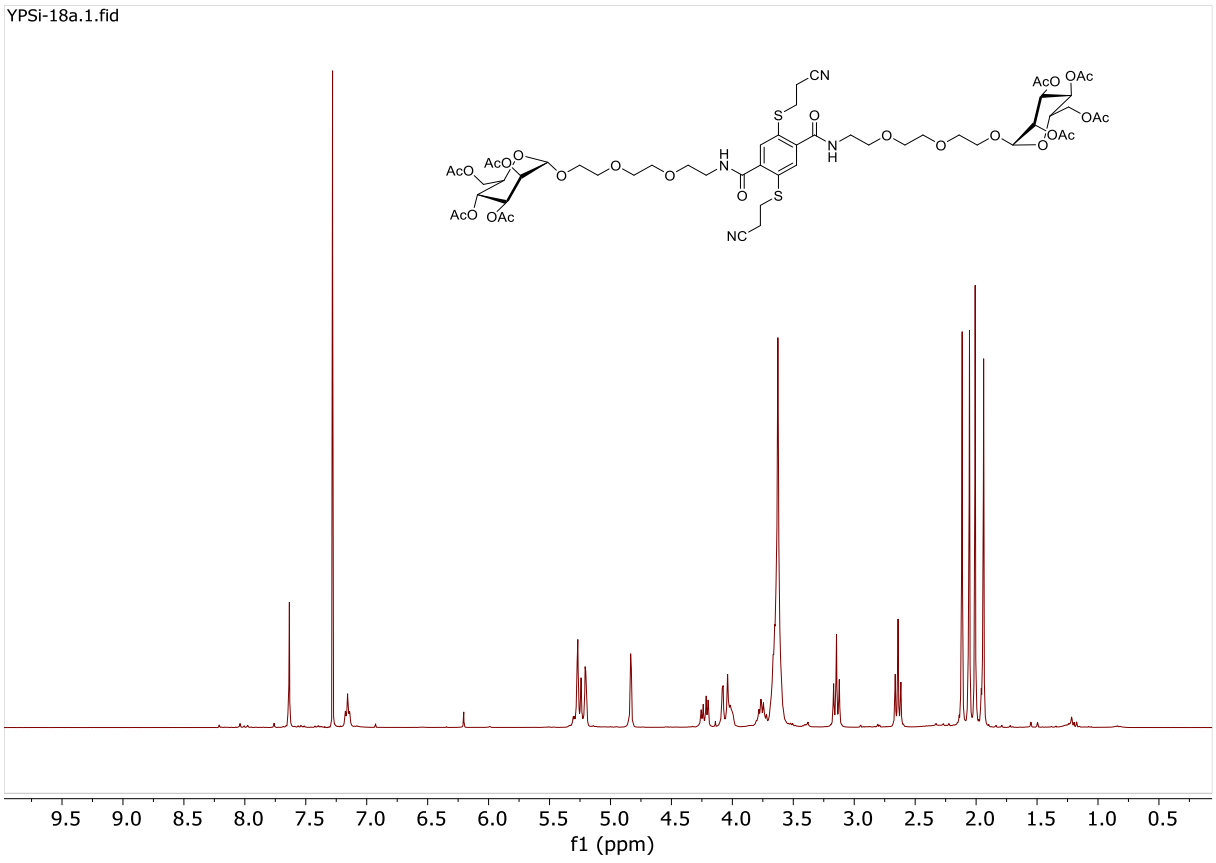
YPSi-18a.1.fid
9.5 9.0 8.5 8.0 7.5 7.0 6.5 6.0 5.5 5.0 4.5 4.0 3.5 3.0 2.5 2.0 1.5 1.0 0.5
f1 (ppm)

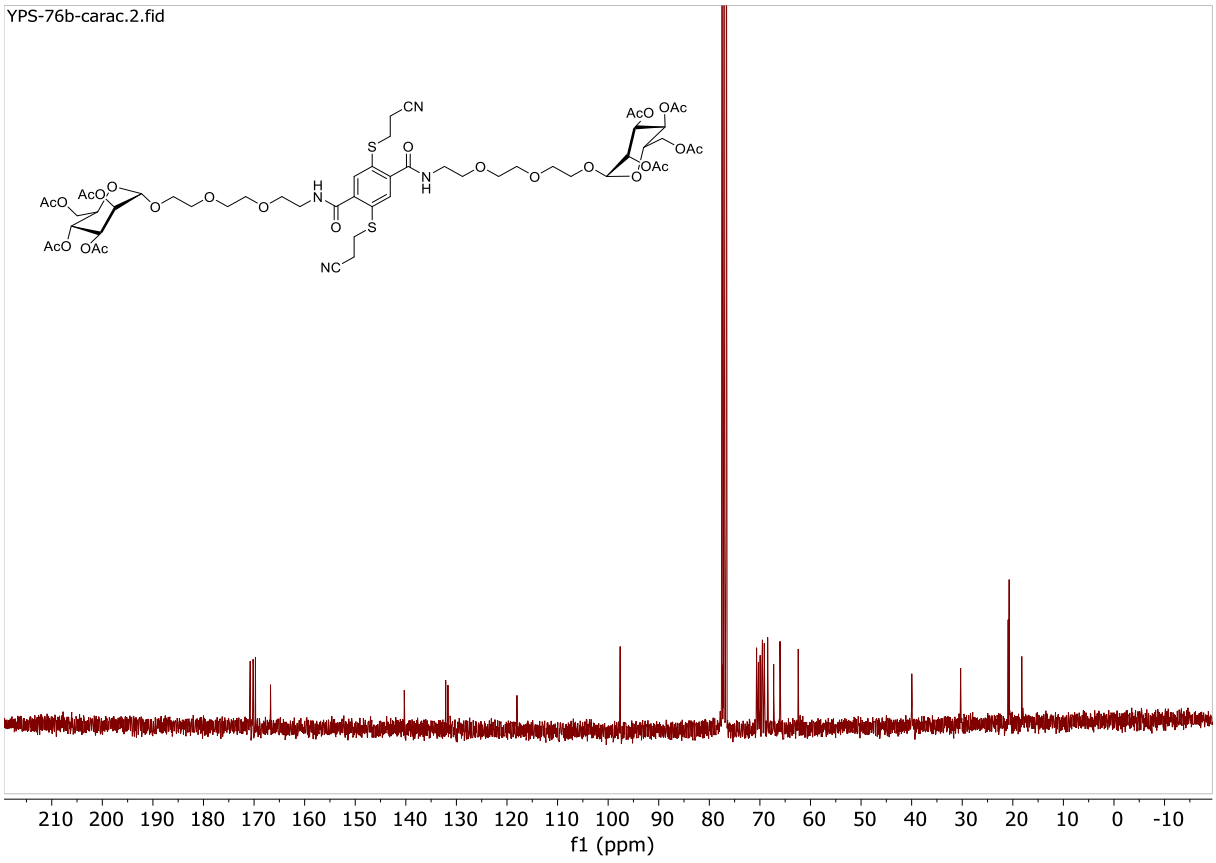
YPS-76b-carac.2.fid
210 200 190 180 170 160 150 140 130 120 110 100 90 80 70 60 50 40 30 20 10 0 -10
f1 (ppm)

General procedure for deprotection of 2-cyanoethyl and acetate

Protected 1,4-dithiophenol **5** (1 eq.) and CsOH•H_2O (20 eq.) were dissolved in degassed THF/MeOH (1:1, 10 mL) under inert atmosphere. The mixture was stirred at r.t. for 3 h then HCl 2 N was carefully added until pH 4. Solvent was evaporated. The residue was purified by a 4 g C18 silica gel column chromatography (Gradient: 4 CV 100% H_2O + 0.25 % TFA, 10 CV 100 % MeOH + 0.25 % TFA, 4 CV 100 % MeOH + 0.25 % TFA, 4 CV 100 % H_2O + 0.25% TFA). Methanol was removed via a rotary evaporator and the remaining water was removed using a freeze-dryer affording the desired unprotected product **6**.

2,5-Mercapto-*N*,*N*-di[3,6-dioxa-8-(β-D-galactopyranosyloxy)-oct-1-yl]terephthalamide (6-Gal)

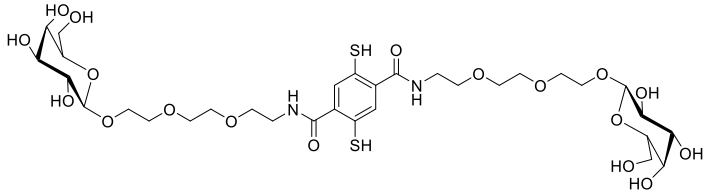

Prepared according to the general procedure from compound **5-Gal** (360 mg, 0.286 mmol, 1 eq.) and CsOH•H_2O (868 mg, 2.47 mmol, 8.6 eq.) in THF/MeOH (1:1, 30 mL) affording the desired 1,4-dithiophenol **6-Gal** (189 mg, 80%) as a white foam.

^{1}H NMR (400 MHz, D_2O + εTFA): 7.50 (s, 2H, CH_{ar}), 4.33 (d, *J* =7.8 Hz, 2H, H_1), 4.05-3.97 (m, 2H, CH_2OGal), 3.87 (d, *J* = 3.5 Hz, 2H, H_4), 3.80-3.64 (m, 22 H), 3.63-3.55 (m, 8H), 3.47 (dd, *J* = 7.8; 9.9 Hz, 2H, H_2).

^{13}C NMR (100 MHz, D_2O + εTFA): 169.7 (CONH), 135.7 (*C*CONH), 130.0 (CH_{ar}), 128.0 (CS), 102.8 (C_1), 75.0; 72.6; 70.7; 68.5 (4×C, C_2 or C_3 or C_4 or C_5), 69.69; 69.60; 69.3; 68.6; 68.5 (5×C, CH_2), 60.8 (C_6), 39.3 ($NHCH_2$).

HR-ESI-MS (positive mode) *m/z* : calcd. for $C_{32}H_{52}N_2NaO_{18}S_2$ $[M+Na]^+$ = 839.2549, found 839.2552.

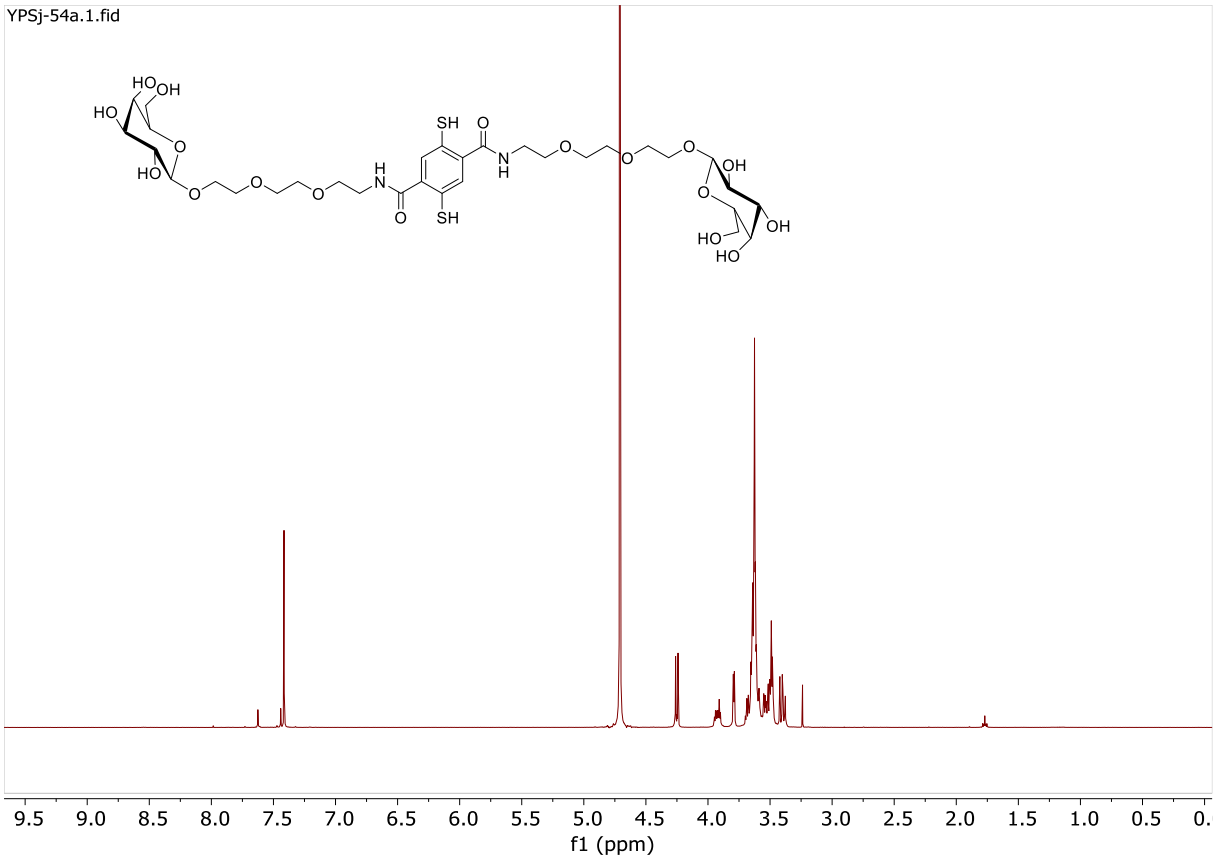
YPSj-54a.1.fid
9.5 9.0 8.5 8.0 7.5 7.0 6.5 6.0 5.5 5.0 4.5 4.0 3.5 3.0 2.5 2.0 1.5 1.0 0.5 0.
f1 (ppm)

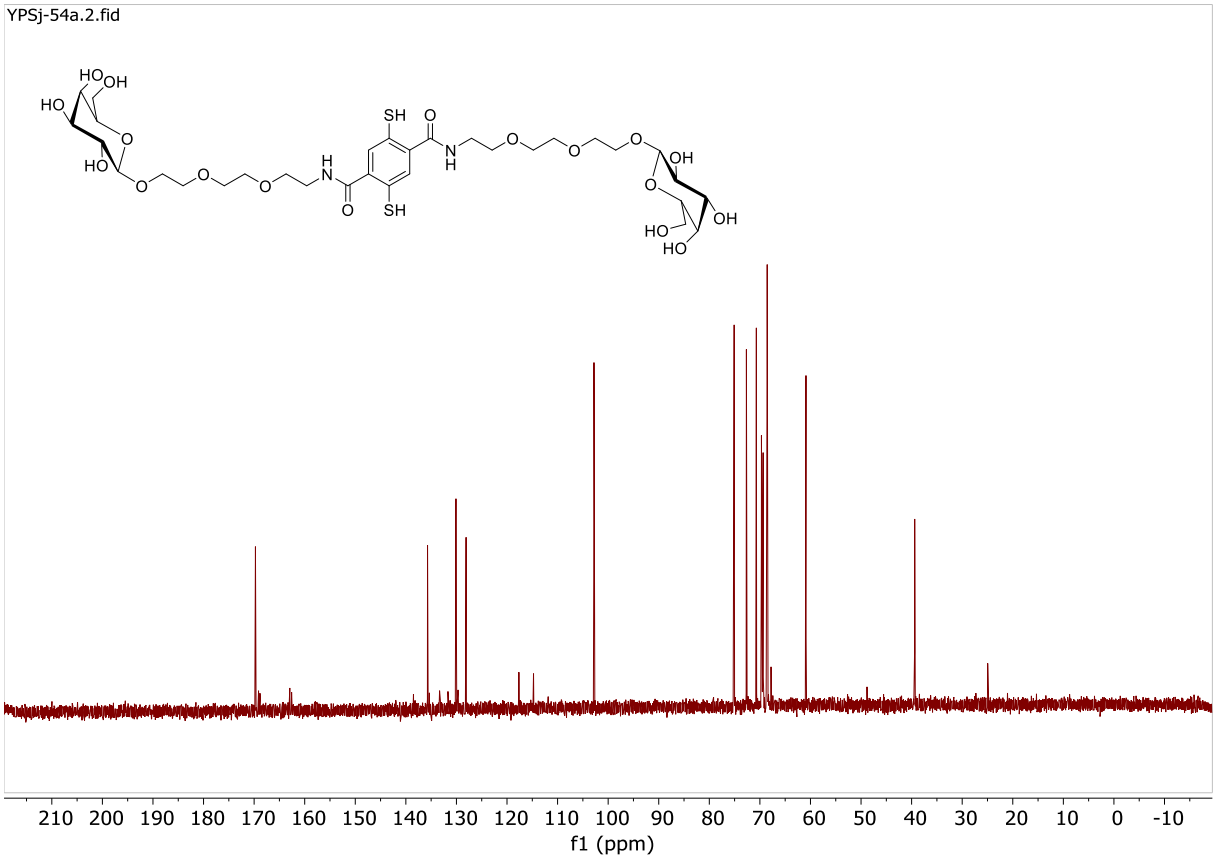
YPSj-54a.2.fid
210 200 190 180 170 160 150 140 130 120 110 100 90 80 70 60 50 40 30 20 10 0 -10
f1 (ppm)

2,5-Mercapto-*N*,*N*-di[3,6-dioxa-8-(α-L-fucopyranosyloxy)-oct-1-yl]terephthalamide (6-Fuc)

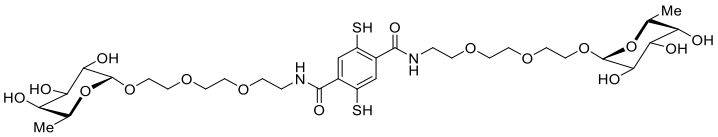

Prepared according to the general procedure from compound **5-Fuc** (115 mg, 0.1 mmo, 1 eq.) and CsOH•H_2O (311 mg, 1.85 mmol, 18.5 eq.) in THF/MeOH (1:1, 9 mL) affording the desired 1,4-dithiophenol **6-Fuc** (54 mg, 68%).

^{1}H NMR (400 MHz, D_2O + εTFA): 7.50 (s, 2H, CH_{ar}), 4.84 (d, *J* = 3.9 Hz, 2H, H_1), 4.0.2 (q, *J* = 6.6 Hz, 2H, H_5), 3.82-3.64 (m, 24 H, H_2 + H_3 + H_4 + CH_2OFuc + 4×CH_2O), 3.64-3.53 (m, 6H, CH_2OFuc + NHCH_2), 1.16 (d, *J* = 6.6 Hz, 6H, H_6).

^{13}C NMR (100 MHz, D_2O + εTFA): 169.7 (CONH), 135.7 (*C*CONH), 130.1 (CH_{ar}), 128.2 (CS), 98.6 (C_1), 71.8; 69.5; 68.0 (C_2 or C_3 or C_4), 69.7; 69.6; 69.4; 68.7 (4×CH_2O), 66.8 (CH_2OFuc), 66.6 (C_5), 39.3 (NHCH_2), 15.3 (C_6).

HR-ESI-MS (positive mode) *m*/*z*: calcd. for $C_{32}H_{53}N_2O_{16}S_2$ $[M+H]^+$ = 785.2831, found 785.2835.

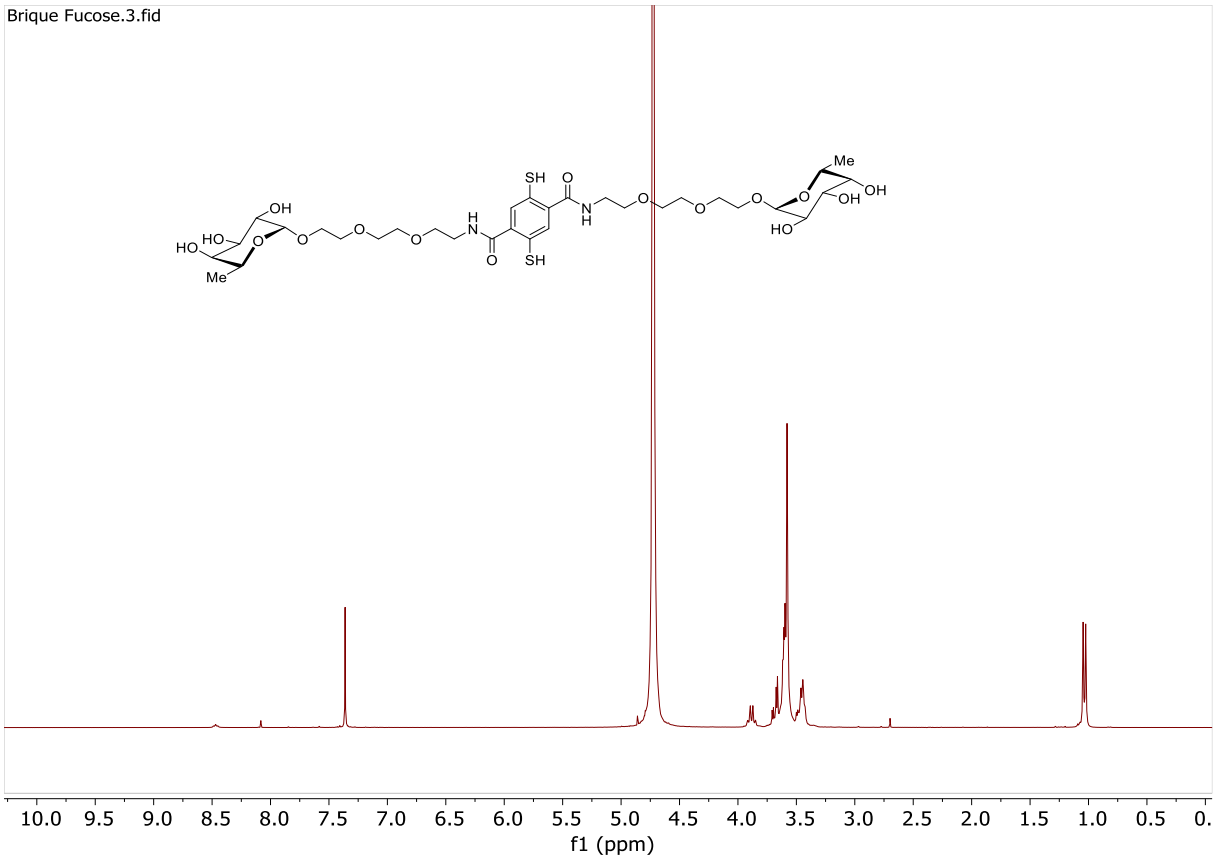
Brique Fucose.3.fid
10.0 9.5 9.0 8.5 8.0 7.5 7.0 6.5 6.0 5.5 5.0 4.5 4.0 3.5 3.0 2.5 2.0 1.5 1.0 0.5 0.
f1 (ppm)

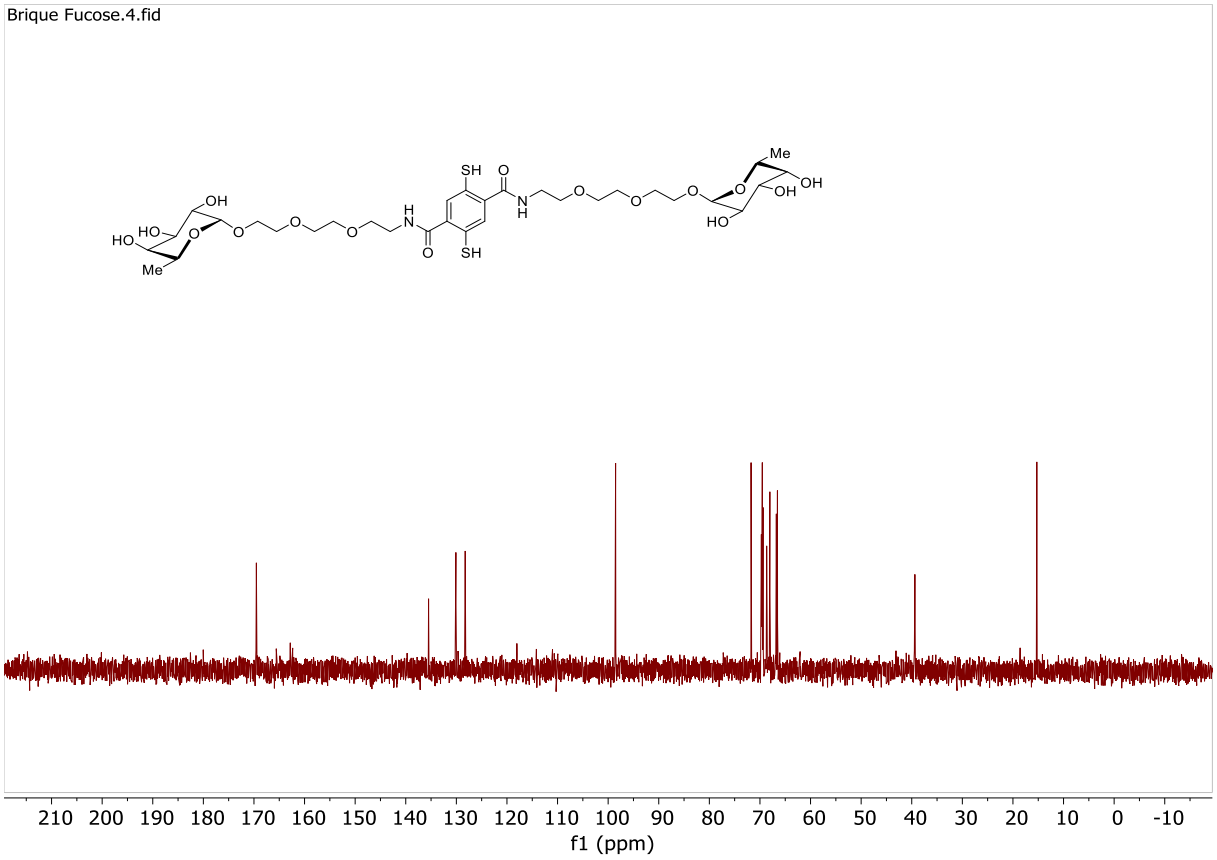
Brique Fucose.4.fid
210 200 190 180 170 160 150 140 130 120 110 100 90 80 70 60 50 40 30 20 10 0 -10
f1 (ppm)

2,5-Mercapto-*N*,*N*-di[3,6-dioxa-8-(α-D-mannopyranosyloxy)-oct-1-yl]terephthalamide (6-Man)

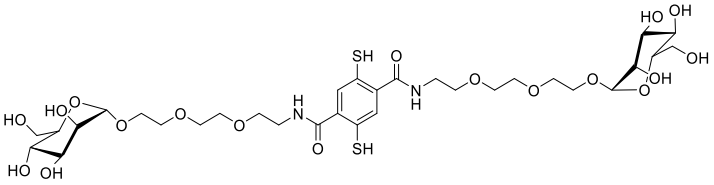

Prepared according to the general procedure from compound **5-Man** (58 mg, 0.046 mmol, 1 eq.) and $CsOH•H_2O$ (157 mg, 0.935 mmol, 18.5 eq.) in THF/MeOH (1:1, 6 mL) affording the desired 1,4-dithiophenol **6-Man** (25 mg, 67%) as a white foam.

^{1}H NMR (400 MHz, D_2O + εTFA): 7.94 (s, 2H, CH_{ar}), 4.82 (d, *J* = 1.7 Hz, 2H, H_1), 3.90 (dd, *J* = 1.7 Hz, 2H, H_2), 3.87-3.53 (m, 34 H).

^{13}C NMR (100 MHz, D_2O + εTFA): 169.7 (CONH), 135.6 (*C*CONH), 130.0 (CH_{ar}), 128.0 (CS), 99.8 (C_1), 72.6; 70.4; 69.9; 66.6 (4×C, C_1 or C_2 or C_3 or C_4), 69.6; 69.47; 69.44; 68.6; 66.2 (5×C, OCH_2), 60.8 (C_6), 39.4 (CH_2NH).

HR-ESI-MS (positive mode) *m*/*z* : calcd. for $C_{32}H_{52}N_2NaO_{18}S_2$ $[M+Na]^+$ = 839.2549, found 839.2552.

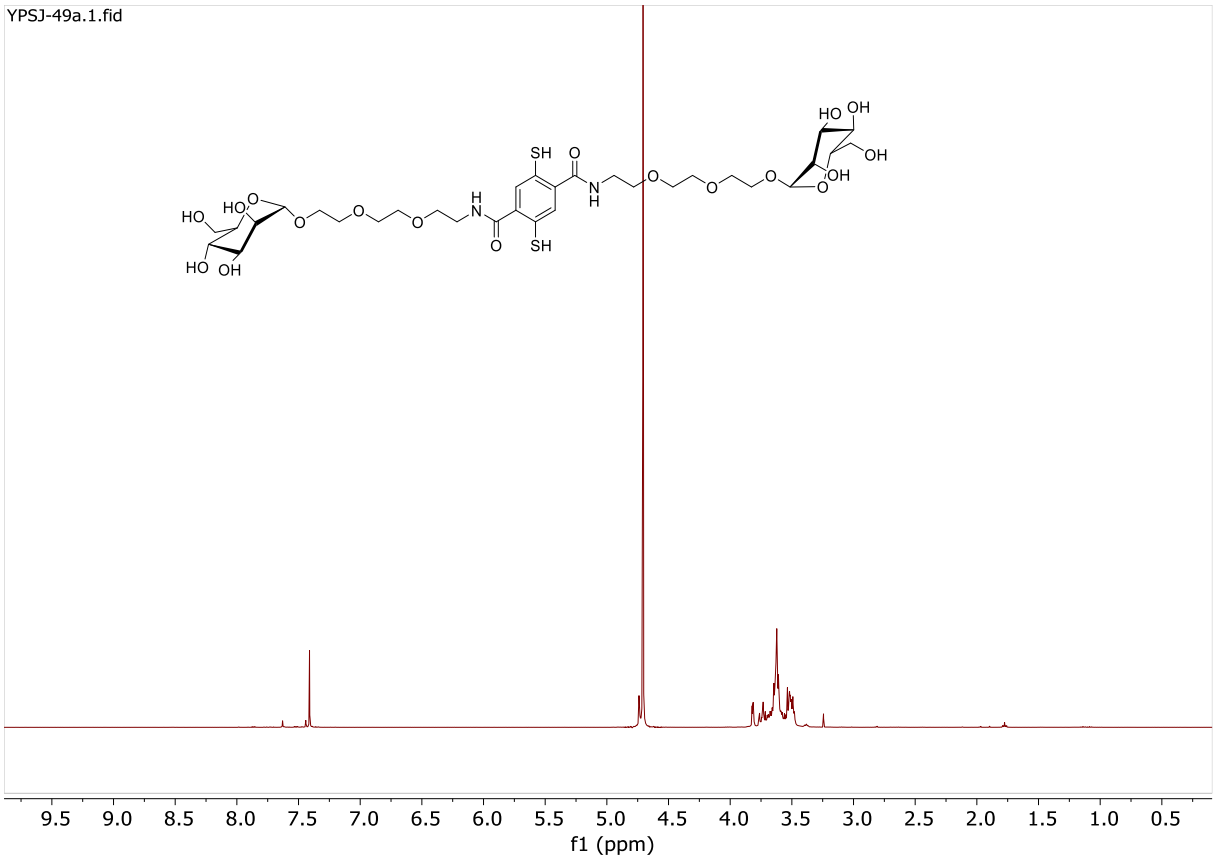
YPSJ-49a.1.fid
9.5 9.0 8.5 8.0 7.5 7.0 6.5 6.0 5.5 5.0 4.5 4.0 3.5 3.0 2.5 2.0 1.5 1.0 0.5
f1 (ppm)

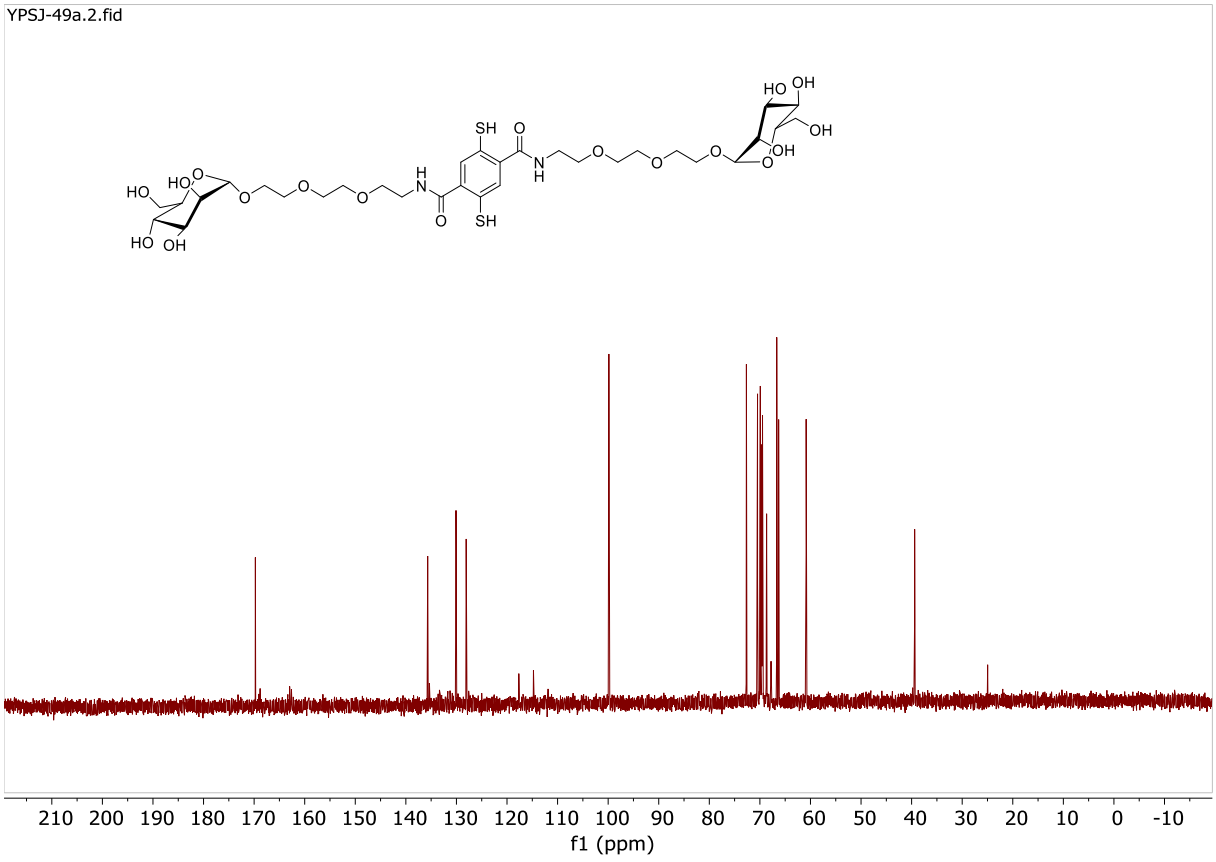
YPSJ-49a.2.fid
210 200 190 180 170 160 150 140 130 120 110 100 90 80 70 60 50 40 30 20 10 0 -10
f1 (ppm)

Equilibration and purification of glycosylated dyn[3,4]arenes M_3/M_4, G_3/G_4 and F_3/F_4

1,4-Dithiophenol **6** (100 mg, 4 mM) was dissolved in Tris buffer (Tris 200 mM, $NaCl_2$ 100 mM, $CaCl_2$ 100 µM) and was equilibrated at RT with stirring in a closed vial during 48 to 72 h. Progress of the reaction was monitored by UHPLC. The equilibrated DCL was then freeze-dried and the crude product was purified by reversed phase silica gel column chromatography (40-g C18 cartridge, Gradient: 4 CV 100% H_2O + 0.1% TFA, 15 CV to increase from 0 to 100% MeOH + 0.1% TFA, 4 CV 100% MeOH + 0.1% TFA). The fractions of the column were analysed one-by-one by UHPLC and combined accordingly. Methanol was evaporated off with the heating bath set at a maximum of 25°C. The remaining water was removed using a freeze-dryer affording the desired glycosylated dyn[3,4]arenes.

Preparation of M_3/M_4

Prepared according the general procedure from **6-Man** (151 mg, 4 mM) and affording **M_3/M_4** (63 mg, 42%) as a slightly yellow powder.

Preparation of G_3/G_4

Prepared according the general procedure from **6-Gal** (236 mg, 4 mM) and affording **G_3/G_4** (70 mg, 30%) as a slightly yellow powder.

Preparation of F_3/F_4

Prepared according the general procedure from **6-Fuc** (316 mg, 4 mM) and affording **F_3/F_4** (238 mg, 75%) as a very slightly yellow powder.

Dynamic combinatorial libraries

General procedure for the preparation of DCLs without lectin

In a typical experiment, the 1,4-dithiophenols (4 mM overall) were dissolved in TRIS buffer (200 mM, NaCl 100 mM, $CaCl_2$ 100 µM, pH 7.4). The mixture was allowed to equilibrate by stirring (400 rpm) in an open vial at r.t. The reaction was monitored by HPLC by injection of 4 µL of the DCL solution. UV absorbance was recorded at 210 and 254 nm.

General procedure for the preparation of DCLs without multiple lectins:

In a typical experiment, 1,4-dithiophenols **6** (4 mM overall) were suspended in TRIS buffer (200 mM, NaCl 100 mM, $CaCl_2$ 100 µM, pH 7.4). The mixture was equilibrated by stirring in an open vial at room temperature (Figure S8). After 24 h, four DCLs were prepared in open vials. In the first one (Ref), the original DCL was diluted 10 times with buffer solution affording a library composed of 1,4-thiophenols (0.4 mM overall). The other ones were diluted ten times with buffer and lectin (LecA, LecB or AFL) was added resulting in a library composed of 1,4-dithiophenols **6** (0.4 mM overall) and lectin (0.4 mM). After 24 h, the Ref DCL was diluted 2× with 1M HCl and analyzed by UHPLC (**Sample 1**) by injection of 25 µL of the sample. Meanwhile, the DCLs were centrifuged (2 min, 10 000 rpm). The supernatants were collected and diluted 2× with 1M HCl and analyzed by HPLC (**Sample 2**, **Sample 4** and **Sample 6**) by injection of 25 µL of the sample. The precipitates were diluted in buffer and 1M HCl (1:1 v/v) to afford the same volume as the Ref DCL and analyzed by HPLC (**Sample 3**, **Sample 5** and **Sample 7**) by injection of 25 µL of the sample.

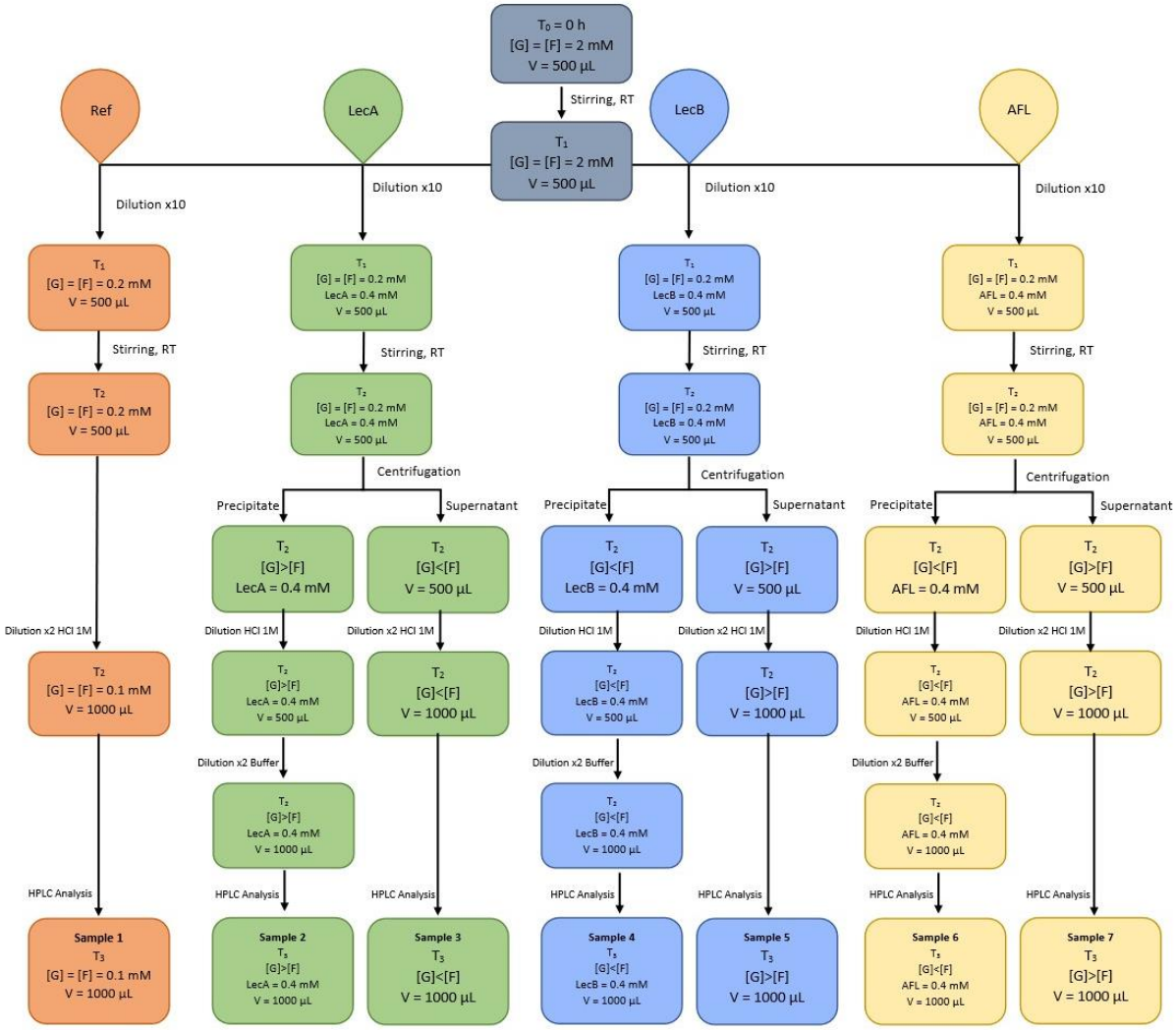

Figure S8. Protocol for DCL of **G**/**F** with and without lectin: reference (orange), LecA (green), LecB (blue) and AFL (yellow)

Isothermal Titration Calorimetry (raw data)

ITC experiments were performed with a microcal calorimeter Malvern ITC200. Temperature was set to 298 K. In every experiment, the host solution is at concentration [Host] in a Tris buffer (200 mM, NaCl 100 mM, $CaCl_2$ 100 µM, pH 7.4) and placed in the cell (200 µL), while the guest at the concentration [Guest] and is placed in the syringe (40 µL). Then, successive aliquots of guest solution were added thanks to a computer-automated injector with 2 min intervals. Heat changes were recorded after each addition. The first injection was discarded from each dataset to remove effect of guest diffusion across the syringe tip during the equilibration process. For the following tables, thermodynamic parameters were obtained from binding model of the MicroCal ITC Origin software. n is for stoichiometry. Raw data are converted from kcal to kJ applying a factor of 4.184.

ConA vs **M_3/M_4**

Table S2. ITC data for the binding properties of **M_3/M_4** towards ConA

	[ConA] mM	[**M_3/M_4**] mM	n	Kd (nM)	ΔH (kj/mol)	-TΔS (kJ/mol)	ΔG (kJ/mol)
ConA vs **M_3/M_4** #1	0.12	0.2	0.09	250	-123	7.2	-37.6
ConA vs **M_3/M_4** #2	0.12	0.2	0.066	279	-70.6	2.8	-37.4
ConA vs **M_3/M_4** #3	0.12	0.2	0.112	250	-110	6.1	-37.6
ConA vs **M_3/M_4** #4	0.12	0.2	0.112	397	-122.6	7.2	-36.5
Average			0.09	294	-106.6	5.8	-37.3

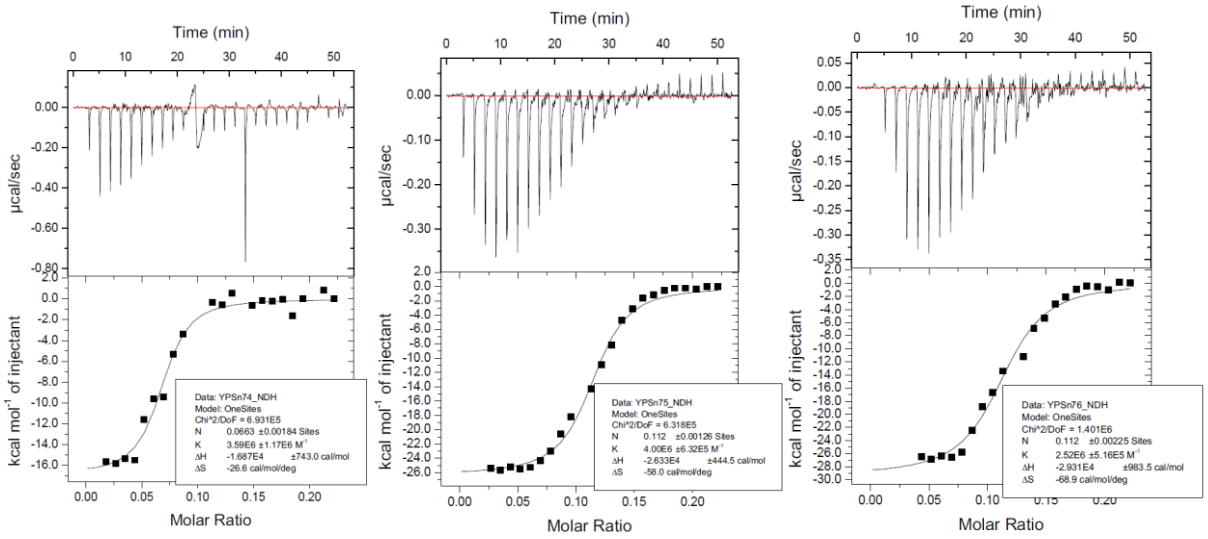

Figure S9. Isothermal titration microcalorimetry (ITC) analysis of the binding properties toward ConA (0.12 mM) for **M_3/M_4** (0.2 mM, top panels) and the association titration curve obtained with a 1:1 binding model (bottom panels).

LecA vs **G_3/G_4**

Table S3. ITC data for the binding properties of **G_3/G_4** towards LecA

	[LecA] mM	[**G_3/G_4**] mM	n	Kd (nM)	ΔH (kj/mol)	-TΔS (kJ/mol)	ΔG (kJ/mol)
LecA vs **G_3/G_4** #1	0.049	0.4	0.12	214	-167	129	-38.1
LecA vs **G_3/G_4** #2	0.049	0.4	0.08	174	-150	111	-38.6
LecA vs **G_3/G_4** #3	0.049	0.4	0.10	168	-158	119	-38.7
Average			0.10	185	-158.3	119.7	-38.5

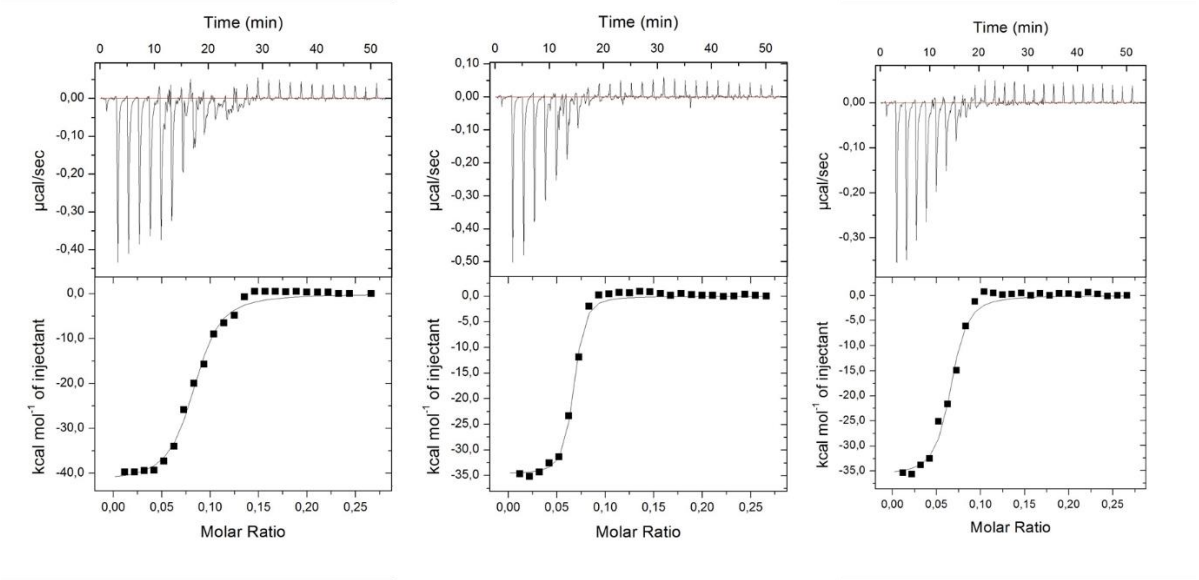

Figure S10. Isothermal titration microcalorimetry (ITC) analysis of the binding properties toward LecA (0.049 mM) for **G_3/G_4** (0.4 mM, top panels) and the association titration curve obtained with a 1:1 binding model (bottom panels).

LecB vs **F_3/F_4**

Table S4. ITC data for the binding properties of **F_3/F_4** towards LecB

	[LecB] mM	[**F_3/F_4**] mM	n	Kd (nM)	ΔH (kj/mol)	-TΔS (kJ/mol)	ΔG (kJ/mol)
LecB vs **F_3/F_4** #1	0.0829	0.145	0.12	8	-218.6	-172.0	-46.3
LecB vs **F_3/F_4** #2	0.0829	0.145	0.10	155	-230.8	-192.0	-38.8
LecB vs **F3/F4** #3	0.0829	0.145	0.08	108	-227.8	-188.3	-39.7
Average			0.10	90	-225.8	-184.1	-41.6

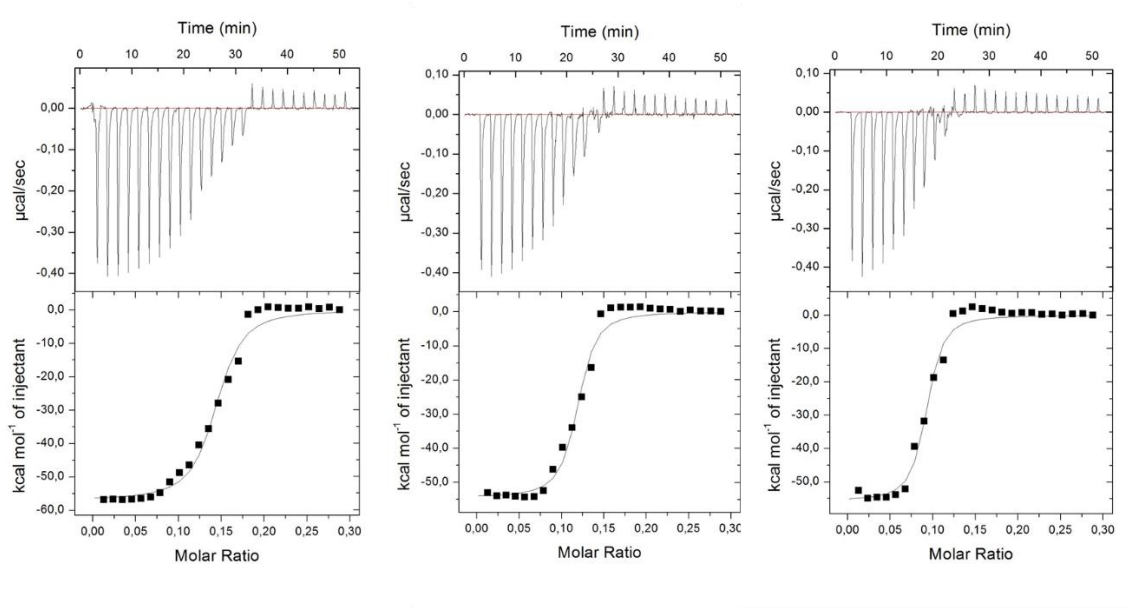

Figure S11. Isothermal titration microcalorimetry (ITC) analysis of the binding properties toward LecB (0.0829 mM) for **F_3/F_4** (0.145 mM, top panels) and the association titration curve obtained with a 1:1 binding model (bottom panels).

AFL vs **αFucOMe**

Table S5. ITC data for the binding properties of **αFucOMe** towards AFL

	[AFL] mM	[αFucOMe] mM	n	Kd (nM)	ΔH (kj/mol)	-TΔS (kJ/mol)	ΔG (kJ/mol)
AFL vs αFucOMe	0.05	3.00	2.98	40300	-32.8	7.7	-25.1

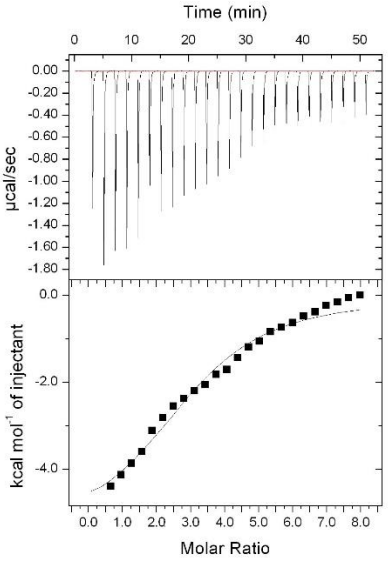

Figure S12. Isothermal titration microcalorimetry (ITC) analysis of the binding properties toward AFL (0.05 mM) for **αFucOMe** (3 mM, top panel) and the association titration curve obtained with a 1:1 binding model (bottom panel).

AFL vs **F_3/F_4**

Table S6. ITC data for the binding properties of **F_3/F_4** towards AFL

	[AFL] mM	[**F_3/F_4**] mM	n	Kd (nM)	ΔH (kj/mol)	-TΔS (kJ/mol)	ΔG (kJ/mol)
AFL vs **F_3/F_4** #1	0.01	0.023	0.08	30	-335.0	292	-43.0
AFL vs **F_3/F_4** #2	0.02	0.076	0.14	46	-335.0	293	-41.9
Average			0.11	38	-335.0	292.5	-42.4

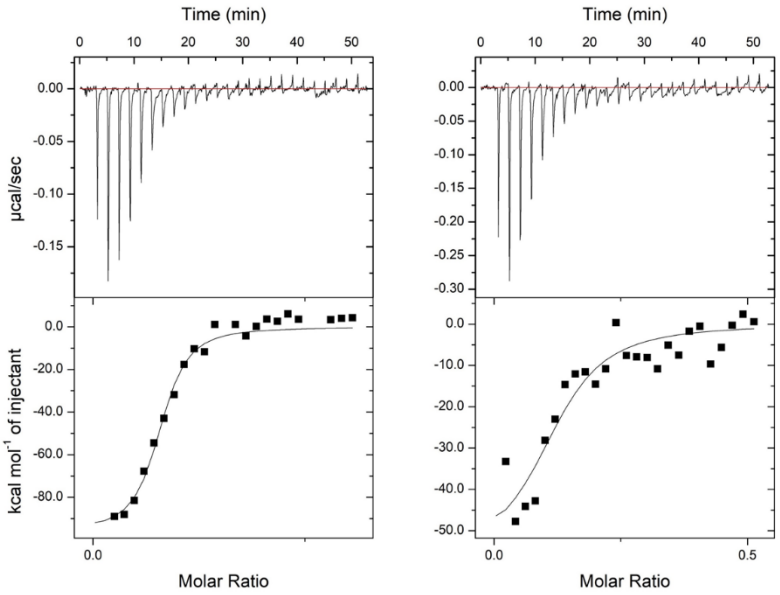

Figure S13. Isothermal titration microcalorimetry (ITC) analysis of the binding properties toward AFL (0.01 mM) for **F_3/F_4** (0.023 and 0.076 mM, top panels) and the association titration curve obtained with a 1:1 binding model (bottom panels).

Toxicity assays on PAO1

P. aeruginosa strain PAO1 (the main strain model used in virulence analyses) was grown in Luria-Bertani Broth overnight at 37°C with an orbital shaker. Growing cells at OD_{600} of 0.3 – 0.6 (beginning of the exponential growth phase) were washed three times with a PBS solution (pH 7.3), and used in the following assays.

These *P. aeruginosa* cells were swabbed over the surface of Muller-Hinton II agar plates and exposed to dynarene concentrations ranging from 100 µM to 10 mM (using 10 µL solutions spotted over the growing cells). These plated cells did not show any inhibition zones due to exposure to these dynarene spotted concentrations.

Live-Dead assays monitoring dead cells (permeable to propidium iodide - PI) in PBS: *P. aeruginosa* cells exposed to the dynarene glycoclusters generated in this study further confirmed this absence of toxicity over more than 4 h incubation time.

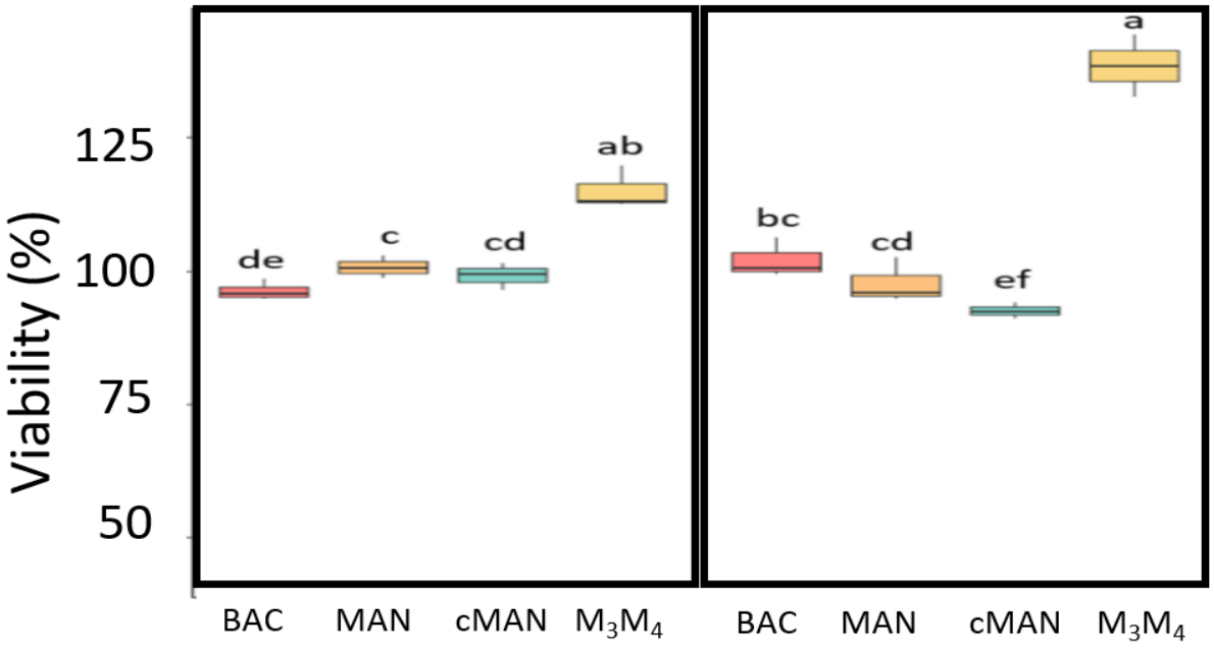

Figure S14. Boxplot analysis of the relation between the relative viability of *P. aeruginosa* PAO1 cell suspensions exposed to mannosylated glycoconjugates (BAC = PAO1 alone, MAN = methyl α-D-mannopyranoside, cMAN = mannosylated calixarene-based glycoclusters, see Figure S1). The G/R ratios obtained from TECAN fluorescence microplate monitoring after 15 min, 1 h, 4 h and 24 h. Samples were prepared and stained as indicated in the LIVE/DEAD® BacLight™ Bacterial Viability Kits. The integrated intensities of the green (535 ± 25 nm) and red (620 ± 10 nm) emission of suspensions excited at 485 ± 20 nm were acquired, and the green/red fluorescence ratios (RatioG/R) were calculated for each proportion of live/dead P. aeruginosa cells. Each point represents the mean of twelve measurements replicated three times using independent bacterial broths. Boxplots with distinct letter codes showed significant differences (p-values < 0.05 using Kruskal-Wallis (KW) Dunn tests)

Toxicity on A549 epithelial cells

A549 Cell lines (ATCC, Massanas, VA, USA) used in the assays were grown in flasks with a culture media Dulbecco's Modified Eagle's Medium (DMEM) with 4.5 g/L glucose (HG), 10% (v/v) fetal calf serum (FCS) (DMEM-calf high glucose) and a 1% penicillin/streptomycin mixture (Sigma Aldrich, Saint-Quentin Fallavier, France). These flasks were incubated at 37°C with 5% (v/v) CO_2. The cell culture growth media was changed every 2-3 days. A549 cells were treated with 0.05% (m/v) trypsin-EDTA (Thermo Fisher Scientific, New Hampshire, USA) and cells in suspension were counted using a Scepter cell counter (Merk Millipore), diluted in culture media then seeded into E96-microtiter plates.

Realtime cell analyses (RTCA) on A549 cell monolayers were performed after 48-72 h cell growth until at least 80% confluency. These cells were then exposed to PAO1 cells pre-treated during 15 min with 1 mM of $\mathbf{X_3}$/$\mathbf{X_4}$ dynarene glycoclusters and diluted 10% in cell culture media without antibiotics (Multiplicity of infection MOI 10).

RTCA of A549 cell adhesion were performed with epithelial cells in suspension in culture media without antibiotics pre-incubated with 4.13 μM $\mathbf{X_3}$/$\mathbf{X_4}$ dynarene glycoclusters or with PAO1 cells pre-treated during 15 min with 1 mM of $\mathbf{X_3}$/$\mathbf{X_4}$ dynarene glycoclusters (MOI10) before loading onto microtiter plates.

RTCA were performed onto an xCELLigence SP station (ACEA Biosciences, San Diego, USA) using RTCA software 2.1. Data are expressed as Delta Cell Indexes (DCI). For each well the DCI at a given time is the difference between a reference DCI value (time of treatment t0) and the Cell index at Delta time ($DCI_{ti} = CI + (1- DCI_{ti-t0}$). At the end of experiments, A549 cells were fixed with formalin 5% for cell imaging. Experiments were performed in Ibidi glass dishes (Cliniscience, Nanterre, France) for Nanolive (Nanolive SA, Lausanne, Switzerland) 3D-cell imaging and 96-wells plates for x4 imaging and automated cell counts using a Cytation 3 platform (BioteK Instruments Winooski, VT, USA). A549 cells were labeled with Dapi (10 ng/mL, Sigma Aldrich), Phalloïdin-TRITC 7.5 μM, (Sigma Aldrich) and/or Dihydrorhodamine-123 2.5 μg/mL (DHR, Applied Bioprobes, ThermoFisher Scientific) in PBS 0.1% Triton and washed twice in PBS before cell imaging.

Aggregation bacterial cell assays

Multivalent $\mathbf{X_3}$/$\mathbf{X_4}$ dynarenes (galactose, fucose et mannose) were dissolved in a PBS solution (25 mM stock solutions). PBS has an osmolarity of 315 mOs, and is physiologically compatible with living cells and proteins. *P. aeruginosa* cells and ligands were mixed (short vortexing and spinning) in order to obtain 100 μM to 1 mM final concentrations of $\mathbf{X_3}$/$\mathbf{X_4}$ dynarenes at OD_{600} of 1 (using exponential phase cells OD_{600} 0.4-0.6 cell cultures) in 1 mL of final reaction volume of PBS. These reaction mixtures were kept at room temperature (22-23°C) for 15 minutes at slow agitation (30 rpm), and then analysed in a small size Malvern glass support containing 6 mL PBS.